SZENT ISTVÁN UNIVERSITY

Adhesive and tribological behaviour of cold atmospheric plasma-treated polymer surfaces

PhD Dissertation

By

Hayder Lateef Radhi Al-Maliki

Gödöllő
2018

Doctoral school

Denomination: Mechanical Engineering PhD School

Science: Polymer Tribology and Machine Elements

Leader: Prof. Dr. István Farkas
Dr. of Technical Sciences
Faculty of Mechanical Engineering
Szent István University, Gödöllő, Hungary

Supervisor: Prof. Dr. Gábor Kalácska
Dr. of Technical Sciences
Institute for Mechanical Engineering Technology
Faculty of Mechanical Engineering
Szent István University, Gödöllő, Hungary

…… ……

Affirmation of supervisor Affirmation of head of school

CONTENTS

NOMENCLATURE AND ABBREVIATIONS

a	Precise contact area, area of attached spot
A_o	Apparent contact area, μm^2
At.-%	Atomic ratio, %
C1s	Characteristic peaks of carbon atoms from XPS, at.-%
E	Young's modulus
F_a	Adhesion component of friction force, N
F_d	Deformation component of friction force, N
F_f	Friction force, N
F_s	Destructive shearing force, N
h	Hight of droplet, mm
K	Constants which depend on the material properties
n	Number of attached spots
$N1_S$	Characteristic peaks of nitrogen atoms from XPS, at.-%
nF/nC	The ratio between the fluorine and carbon contents
nO/nC	The ratio between the oxygen and carbon contents
O1s	Characteristic peaks of oxygen atoms from XPS, at.-%
P	Normal load, N
pv	Pressure-velocity factor
r	Radius of droplet, mm
R_a	Surface average roughness, μm
RCA	The real contact area, μm^2
Sa	3D surface roughness parameter indicates to average roughness, μm
Sku	3D surface roughness parameter indicates to kurtosis
Ssk	3D surface roughness parameter indicates to skewness
Sz	3D surface roughness parameter indicates to maximum height, μm
T_e	Plasma's electrons temperature, K
T_g	Glass transition temperature, °C
T_h	Plasma's heavy particles temperature, K
T_m	Melting temperature, °C
v	Poisson's ratio
W_a	Work of adhesion, J/m^2
WCA	Water contact angle, deg°

Greek symbols

τ	The shear strength at the interface
σ	Tensile strength, MPa
σ%	σ%: statistical deviation or spread
σ_S	The surface energy of the solid surface
σ_S^P	The polar component of the surface energy of the solid surface
σ_S^D	The dispersive component of the surface energy of the solid surface

σ_L	The surface energy of the liquid
σ_L^D	The dispersive component of the surface energy of the liquid
σ_L^P	The polar component of the surface energy of the liquid
μ	Coefficient of friction, N/mm^2
α	Thermal expansion coefficient
γ_{disp}	Dispersive of surface energy, mJ/m^2
γ_{pol}	Polar component of surface energy, mJ/m^2
γ_{LG}	Energy of liquid-air interface, mJ/m^2
γ_{SG}	Energy of the solid-air interface, mJ/m^2
γ_{SL}	Energy of solid-liquid interface, mJ/m^2
γ_{tot}	Total of surface energy, mJ/m^2
θ	Droplet contact angle, deg°
θ_{CH2I2}	Contact angle of diiodomethane, deg°
θ_w	Contact angle of water, deg°

Abbreviations

AFM	Atomic force microscopy
AKI	Institute of Materials and Environmental Chemistry
APG	Atmospheric pressure plasma glow
APPJ	Atmospheric pressure plasma jet
CCI	Coherence Correlation Interferometry
DBD	Dielectric Barrier Discharge source
DP	Degree of polymerisation
HDT	Heat deflection temperature
H PIII	Hydrogen plasma immersion ion implantation
He PIII	Helium plasma immersion ion implantation
LTE	Local thermal equilibrium plasma
MTA	Hungarian Academy of Sciences
non-LTE	Plasma is not in local thermal equilibrium
N PBII	Nitrogen plasma-based ion implantation
N PII	Nitrogen plasma ion implantation
N PIII	Nitrogen plasma immersion ion implantation
PA6-E	Polyamide 6 Extruded
PBII	Plasma-based ion implantation
PBII&D	Plasma-based ion implantation and deposition
PC	Polycarbonates
PE	Polyethylene
PEEK	Polyether etherketone
PET	Polyethylene terephthalate
PFA	Perfluoroalkoxy alkanes
PIL	Plasma-induced luminescence
PLLA	Polylactic acid
PMMA	Polymethyl methacrylate

POM-C	Polyoxymethylene Copolymer
PP	Polypropylene
PS	Polystyrene
PTFCE	Polychlorotrifluoroethylene
PTFE	Polytetrafluoroethylene
PVC	Polyvinyl chloride
PVDC	Polyvinylidene chloride
SEE	Surface Energy Evaluation
SEM	Scanning electron microscopy
SDBD	Surface diffuse barrier discharge
UHMW-PE HD1000	Ultra High Molecular Weight Polyethylene High Density 1000
UHMW-PE HD500	Ultra High Molecular Weight Polyethylene High Density 500
XPS	X-ray photoelectron spectroscopy

1. INTRODUCTION, OBJECTIVES

In this chapter, the importance of the research topic is presented along with the objectives of this research.

1.1. Introduction

Non-polar materials and polymers, in particular, have low surface energy, thus low adhesion force. A hydrophilic surface is required to obtain adequate adhesion to other material types. On the other hand, the superhydrophobic surface is required for several applications. The development in the testing of sticking technologies of machine parts made of engineering plastics comes into the foreground rather continually (Ebnesajjad, 2015). Vehicle industry is an excellent example of importance to explore quick high strengths and elastic component contacts (Keresztes, 2016), this made the surface treatment required to promote surface properties. Many different methods have been developed for polymer modification, such as chemical vapour deposition, soft lithographic imprinting, sol-gel method, etc. However, there are many current and emerging wetting and adhesion issues which require an additional surface processing to enhance interfacial surface properties (Wolf and Sparavigna, 2010). Plasma treatment has become the best method to improve the surface wettability of polymers (Takahashi et al., 2011). Among studies have been extensively investigated low-pressure plasma techniques (plasma immersion ion implantation) and their effects on the surface modification of various polymers (Kalácska et al., 2012). Recently, atmospheric-pressure plasma has been rising interest to use for surface modification of polymeric materials instead of low-pressure plasma in the academic research and industrial applications, due to its vacuum less system as it is operated at atmospheric pressure and its effects of ablation, crosslinking and activation which improve the tribological and adhesive properties.

The prevailing belief is that corrosion and fatigue are the underlying failure mechanisms. Indeed, friction and wear are essential mechanisms that should be taken into consideration as well, especially, in the moving machine elements failure studies (Zsidái et al., 2002). Due to proven corrosion resistance and self-lubricating ability, engineering polymers are chosen for the construction of moving parts in specific applications of microelectronics, mechatronics and industrial equipment. The interest of polymers came from them high strength, stiffness, and functional dimensions' stability. However, they often experience difficulties in glueing (Pandiyaraj et al., 2008), and instability or overload during sliding (Samyn et al., 2005). Some issues can be resolved by filling solid lubricants into the polymer (Samyn et al., 2006). However, they also weaken the initial bulk properties. Therefore, it is worth investigating what surface modification can bring in further controlling the polymer performance simultaneously related to adhesion and sliding. Thus, recently have been using several technologies for polymer surface treatment. In addition, several studies have been discussed some of different plasmas on the polymer surface tribology and adhesion properties (Kalácska et al., 2009; Kalácska et al., 2012; Samad et al., 2010).

The present research deals with testing the reliability of polymer surfaces modified with Dielectric Barrier Discharge (DBD) source, atmospheric cold plasma process in polymer-polymer and polymer-metal contact-systems through revealing adhesive and tribological characteristics. The named process is suitable to modify the physical and chemical structures of polymer surfaces efficiently and thus change their surface characteristics including their adhesive and tribological properties.

Two groups of polymers had been selected: the first is engineering polymers including PEEK, PET, PA6-E, and POM-C. The second is Polyolefin polymers and Fluorine polymer include PP, UHMW-PE (HD1000 and HD500), and PTFE due to the importance of these groups in sticking technique application also in industrial and medical applications, etc. In contrast, (S235-construction steel) has been utilised as the main metallic counterpart. We characterise the untreated, treated, contacted and tribologically tested samples by complex surface analytical, adhesive and tribological tests. The primary target is to find relationships between the parameters of plasma treatment and the induced surface chemical and physical changes as well as links between the adhesive and tribological characteristics that can form the basis of producing structures with reliable polymer-polymer and polymer-metal bonding.

1.2. Objectives

The main aim of the research to describe (or/and find) the relation and useful data between the surface properties and the tribological behaviour of engineering polymers due to the effect of the DBD atmospheric plasma treatment. The objectives of this work are:

- Description of the sliding friction measurements of the different polymer/steel pairs using pin-on-disc tribometer apparatus under dry and lubricated conditions with treated and virgin polymer surfaces.
- Comparison of friction and wear behaviour of the selected engineering polymers in connection with their plasma treated surface. Surface energies, chemical composition, and surface topography are taken into consideration.
- Investigate the adhesive behaviour of the virgin, and DBD plasma treated polymers. Change in surface energies (polar and dispersive components); wettability is investigated. Adhesive bonding tests are performed with typical glueing materials selected for engineering polymers.
- Giving general connection between virgin and DBD plasma treated polymers concerning surface characterisation and tribological behaviour.
- Set the optimal condition and possibilities of DBD plasma treatment advantageous for the selected engineering polymers.

2. LITERATURE REVIEW

In this chapter, scientific entrance and the critical literature which related to the research topic going to be reviewed, in addition to identifying the gap in the literature. Implying the progressive development of polymer adhesive, tribology and surface treatment to give obviously perception about the obstacles encountered by former researchers and the solutions they have reached which is considered the base and catalyst that forced us to launch this research.

2.1. Introduction to polymers

The word plastic came mainly from the Greek word Plastikos, meaning "able to be shaped and moulded" (Nptel, 2016). The name polymer drove from the ancient Greek word πολύς (polus) meaning "many or much" and μέρος "meros" for parts (Wikipedia: Polymer, 2017). We can define polymer is a group of atoms in the molecule, the bonds among themselves are very strong, but weaker bonds to adjacent molecules. Polymers can be considered as large structures and monomers like the bricks that enter into them. The double bond and active functional groups act as the driving force, repeatedly, to add monomer molecule to the other to configure a polymer molecule. This process is known as polymerisation. The number of so activated that a chain reaction of self-addition of ethylene molecules is generated, resulting in the mer, in a polymer chain, is called the degree of polymerisation (DP) (Kumar and Gupta, 2003; Chanda and Roy, 2006). For example, ethylene, the prototype monomer molecule, due to the double bond that it has, it is very reactive. Under several conditions influence like heat, light, or chemical agents this bond becomes the production of a high-molecular weight material, almost identical in chemical composition to ethylene, known as polyethylene or the polymer of ethylene as shown in Fig. 2.1.

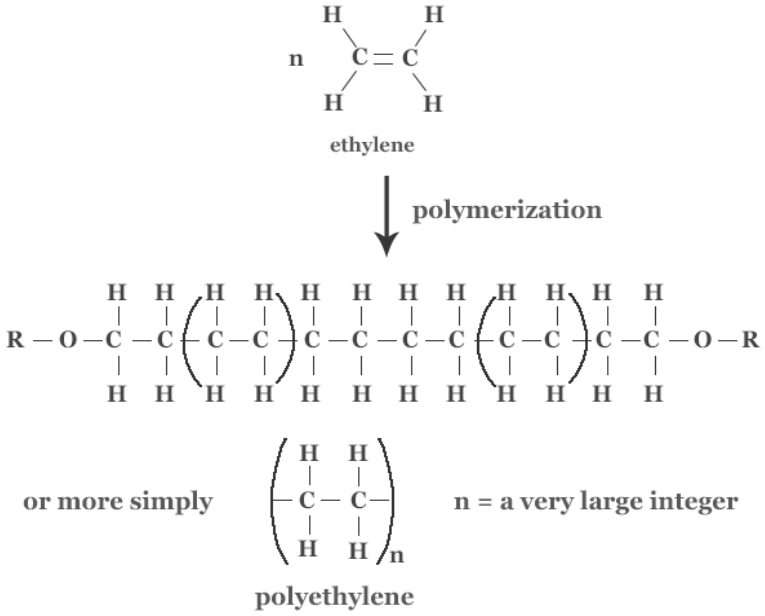

Fig. 2.1. Intermediate steps during formation of polyethylene (Tutorvista, 2017)

2.2. Polymer structure

The structure of polymer depends on the formulation of its molecular chains during a chemical reaction. There are two different types of chemical reactions of polymer formulation: polyaddition and polycondensation. Polyaddition is bonding monomers with each other without loss atoms. In

polycondensation, the two different monomers loss atoms during combining to form a single molecule, which in turn can be classified into four categories depending on structure plastics: linear structure, branched structure, cross-linked structure, and network structure (Fig. 2.2) (Frank and Biederbick, 1984).

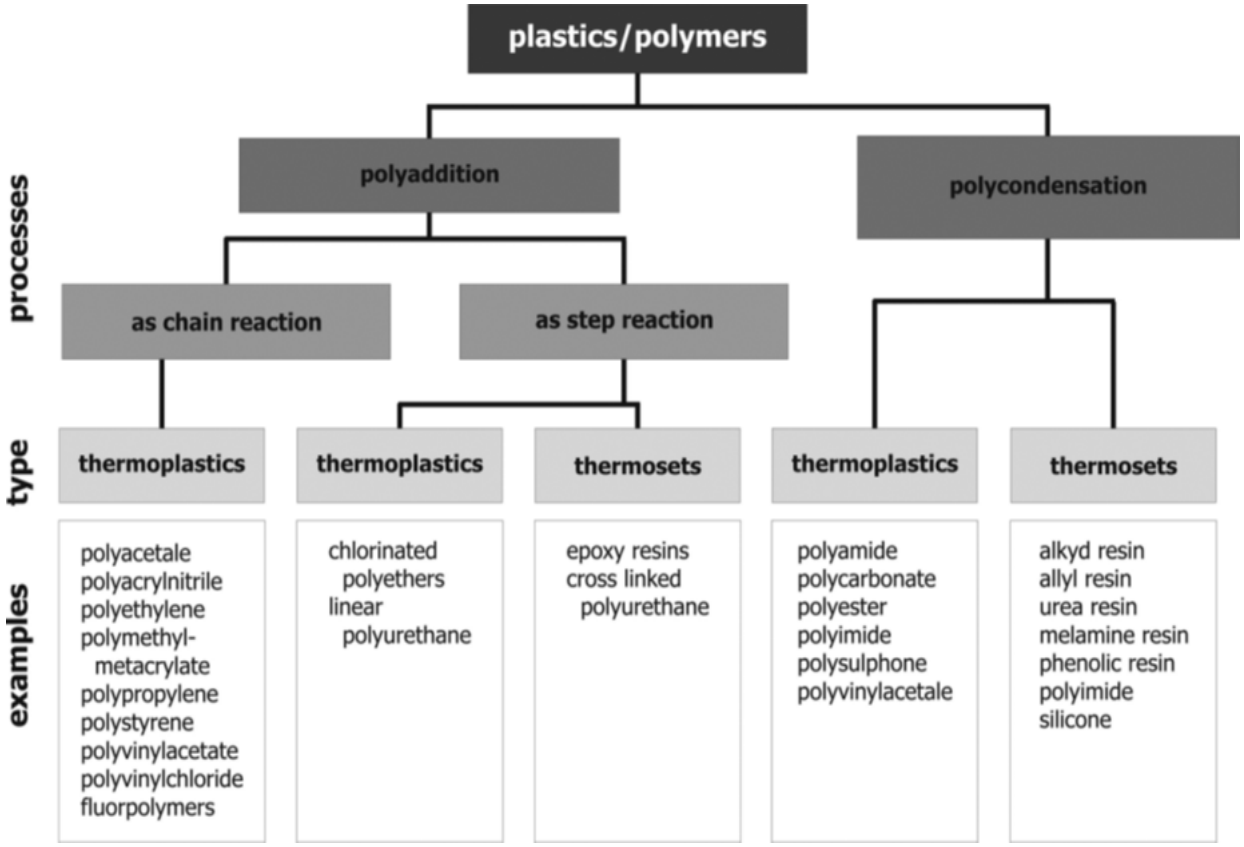

Fig. 2.2. Processes for plastics generating and examples (Frank and Biederbick, 1984)

The polymer molecular structure is responsible for many of the physical properties which are essential for their various applications. As mentioned polymers are composed of large molecules which consist of smaller units, called monomers, tightly bonded together with strong covalent bonds, as shown in Fig. 2.3, in the case of a linear polymer chain. The chemical formula is of the type $-(A)_n-$ where the monomer and the integer number *n*, called the degree of polymerisation or polymerisation index, is the number of monomers installing the chain. The polymer chain length and the molar mass is proportional to n. Polymer architecture at the molecular scale can be somewhat varied. In Fig. 2.4 it can be seen a depiction of three possible molecule architectures, leaving out the atomic-scale chemical details and representing them with lines (Hall, 1989).

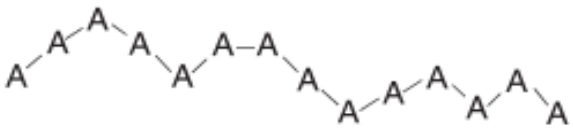

Fig. 2.3. A polymer chain where (A) is a monomer unit and (–) represents a covalent bond (Koutsos, 2009)

a) b) c)

Fig. 2.4. Types of molecular architectures a) linear chain b) branched molecule c) cross-linked network; molecules are linked through covalent bonds, the network extends over the whole sample forming a giant macromolecule (Koutsos, 2009)

A linear polymer consists of a long linear chain of monomers. A branched polymer comprises a long backbone chain with some shorter side chain branches attached covalently. Cross-linked polymers have monomers of one long or short chain bonded covalently with monomers of another short or long chain. Cross-linking results in a three-dimensional molecular network; the whole polymer is a giant macromolecule. Polymers are classified based on the chemical type of the monomers to homopolymers consist of the same type of monomers, and copolymers which have different repeating units as Fig. 2.5 shows. Also, depending on the arrangement of the monomers' types in the chain of the polymer to random copolymer, alternating copolymers, block copolymers, graft copolymers. It is worth mentioning that elastomers or rubbers have lightly cross-linked networks while thermosets are densely cross-linked networks (Koutsos, 2009; Mark, 1945).

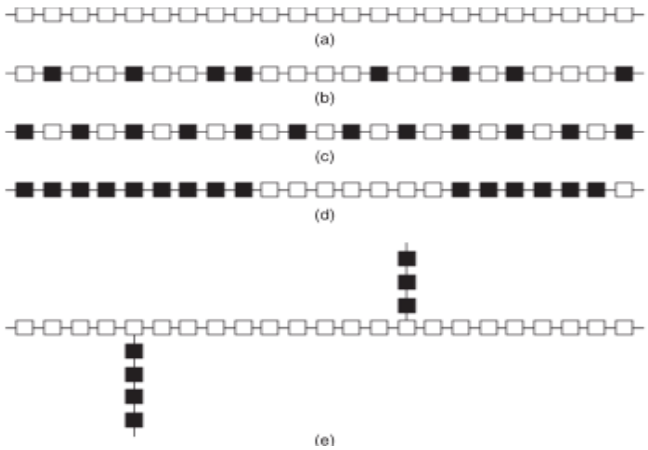

Fig. 2.5. a) Homopolymer; b) random copolymer; c) alternating copolymer; d) block copolymer; e) graft copolymer (Koutsos, 2009)

In my further research, I will examine thermoplastic homo and co-polymers as well.

2.3. General classifications of engineering plastics

The chemical structure can classify engineering plastics into thermosets having cross-linked molecular chains and thermoplastics which consist of linear molecular chains. There are two types of thermoplastic polymers: crystalline and amorphous. The microscopic arrangement of polymer molecules organises many properties of polymeric materials. Polymers can have an Amorphous which is disordered or Semi-crystalline which is partially crystalline and partially ordered structure as Fig. 2.6 illustrates. Furthermore, it is possible to classify polymers according to their application areas: plastics for structural components, packaging, elastomers for damping or high friction,

fibres for reinforcement, coatings for protection of materials surfaces and adhesives for joining of structural components (Chanda and Roy, 2006; Sęk, 1988).

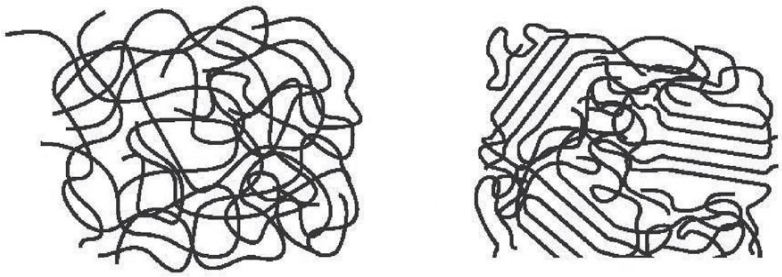

a) b)

Fig. 2.6. a) Amorphous polymer and b) simplified model of a Semi-crystalline polymer (Koutsos, 2009)

Eight types of Semi-crystalline thermoplastics will be uilized in the present reasearch.

2.3.1. Thermoplastics

Thermoplastics are the materials that get softer when the influence of heat above the glass transition temperature or melting temperature and becomes hard after the disappearance of the effect of heat (cooling). Thermoplastics can be melted and solidified for limited several times without deterioration in the mechanical properties, but the colour of thermoplastics can be degraded by increasing the number of recycling, thus affecting their appearance and properties. They are liquids in the molten state and glassy in the mushy state or partially crystalline. The molecules consist a series of long chains by joined end-to-end, every chain is independent of the other. The crystalline structure disappears, and the long chain becomes randomly scattered above the melting temperature. Fig. 2.7 shows the molecular structure of thermoplastic. The essential properties of the thermoplastics are high strength, high toughness, good hardness, chemical resistance, durability, self-lubrication, transparency and waterproofing (Kumar and Gupta,, 2003; Sęk, 1988).

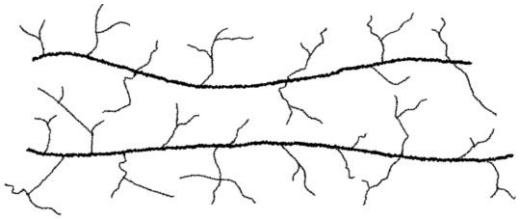

Fig. 2.7. Molecular of thermoplastics (Nptel, 2016)

2.3.2. Temperature resistance of thermoplastics

The thermoplastics temperature resistance can be measured by several methods. These methods include heat deflection temperatures (HDT), where usually the melt temperature T_m and glass transition temperature T_g of thermoplastic are measured under a load of 1.82 or 0.46 MPa. As it can be seen in Fig. 2.8 that thermoplastics pyramid divided into three major groups according to T_g are high-performance plastics, engineering plastics, and commodity plastics (All Seals, 2017).

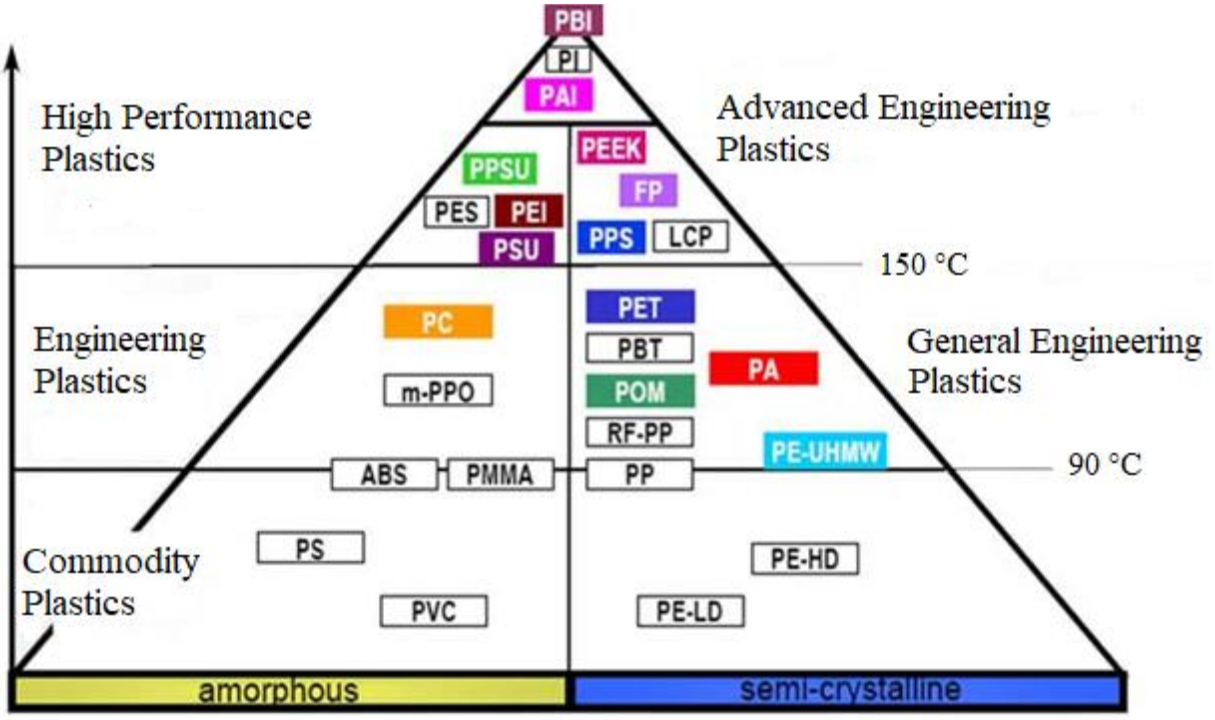

Fig. 2.8. Different groups of thermoplastics and their T_g (Thai Polymer supply, 2017)

In the conventional configurations of polymers, such as polyethylene (PE) is crystallised, but it is still partly amorphous, even when the temperature (T) is much lower than their melting point (T_m). Moreover, polymers with random configurations, such as atactic polystyrene (aPS), often exhibit little crystallinity at various values of (T) and consequently classified as ‘‘amorphous’’. A large proportion of a polymer becomes glassy when $T < T_g$, therefore, the glass transition has a significant effect on polymer properties. In many low molar mass, polymers have obvious physical results if solidification is connected with extremely rapid cooling rates. Fig. 2.9 shows the effect of (T) under the low strain mechanical behaviour of various types of polymer along with the principal regimes of behaviour (Meyer and Keurentjes, 2005; Crawford, 1998).

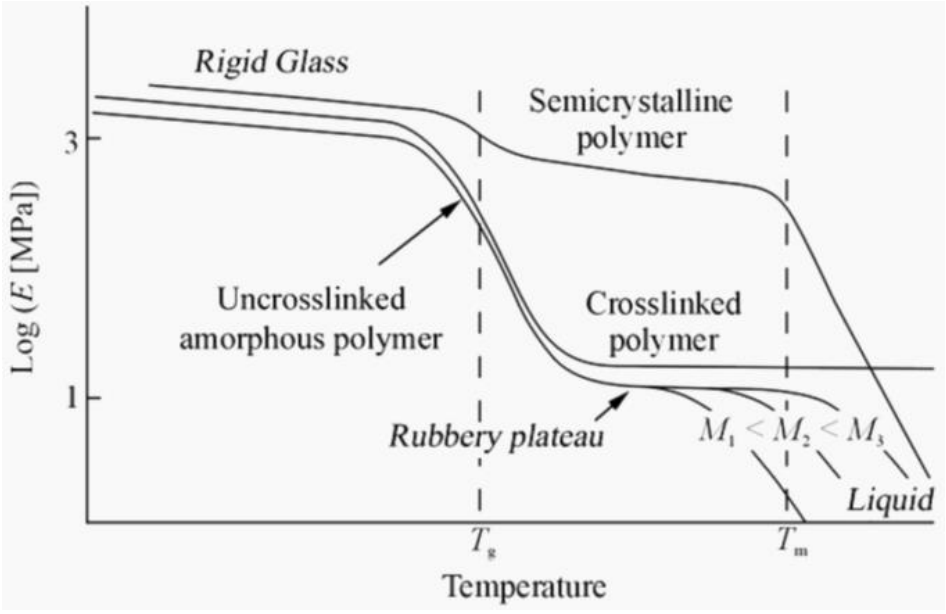

Fig. 2.9. The low strain mechanical response of various types of polymer (Meyer and Keurentjes, 2005)

2.4. Plasma modification of plastic surfaces

Plasma can be defined as chemically active media. Plasmas are varied depending on the way they are generated and their working power. Plasmas could create either low or very high temperature, and according to the generated heat, they can be termed as cold or thermal plasmas. Thermal plasmas are especially arc plasmas were widely industrialised in particular by aeronautic sector. Cold plasma technologies have been evolved in the microelectronics, but they have limited use due to their vacuum equipment. There are many efforts have tried to transpose plasmas to work under atmospheric pressure without the need for vacuum. The research has led to various sources that are described in (Tendero et al., 2006). One of the known facts that plasma is the fourth state of matter and it is more or less ionised gas constitutes about 99% of the universe. Plasma consists electrons, ions and neutrals; these contents may have the fundamental or excited states. From a laboratory point of view, plasma is electrically neutral. Whereas, it contains some free charge carriers thus is electrically conductive (Lieberman and Lichtenberg, 1994; Chapman, 1980). Plasma ionisation degree can range from small values, e.g. 10^{-4}–10^{-6} partially ionised gases to 100% fully ionised gases. In a laboratory, two types of plasma can be generated; the first is high-temperature plasmas which also called fusion plasmas, the second is low-temperature plasmas or gas discharges (Conrads and Schmidt, 2000).

2.4.1. Plasmas classification

Plasmas distinguish into different groups depending on the energy supply, and the amount of transferred energy to them. The properties of the plasma change depending on electronic density and temperature as Fig. 2.10 presents (Tenderoet al., 2006). There are two major plasma groups: the first is thermal equilibrium plasmas and the second is plasmas are not in thermal equilibrium. Plasmas those have an equal temperature of all particles (electrons, ions, and neutral species) is known as thermal equilibrium, for instance, stars and fusion plasmas. Usually, they are termed as "local thermal equilibrium" which shortened to (LTE). To obtain the equilibrium plasmas require high temperature typically ranging from 4.000 K to 20.000 K. Otherwise, plasmas are not in thermal equilibrium will be formed in short called (non-LTE) for example interstellar plasma matter (Lieberman and Lichtenberg, 1994). The (LTE and non-LTE plasmas) can distinguish depending on the pressure gas in the plasma as a subdivision. The high gas pressure indicates many collisions in the plasma, and it is intuitive that just a few collisions could happen in the plasma whether the gas pressure is low for example dielectric barrier discharge and atmospheric pressure glow discharge plasmas (Kalácska et al., 2015).

2.4.2. Atmospheric pressure plasmas

The plasma pressure directly effects on the transition of plasma from a glow discharge ($T_e > T_h$) to an arc discharge as Fig. 2.11 illustrated. Low-pressure plasmas under pressure range (10^{-4} to 10^{-2} kPa) are non-LTE. The light particles (electrons) temperature is higher than heavy particles. The inelastic collisions between electrons and heavy particles do not rise the heavy particles temperature because they are excitatory or ionising (Tendero et al., 2006).

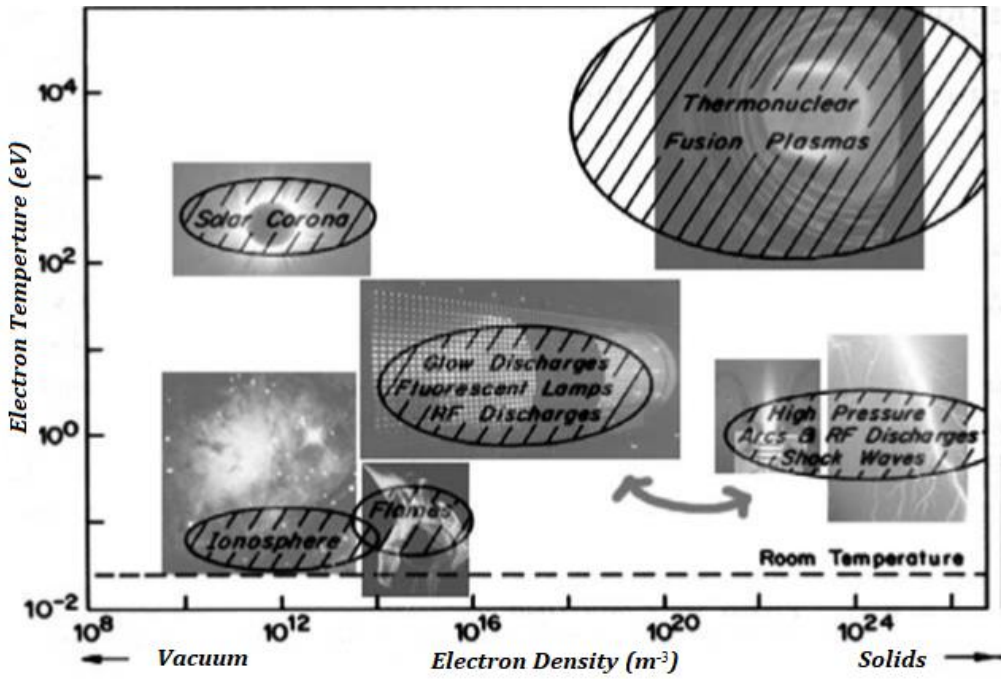

Fig. 2.10. 2D classification of plasmas (electrons temperature versus electrons density) (Boulos et al., 1994)

Atmospheric plasma jet contains two zones:

- A central zone or plasma core which is LTE,
- A peripheral zone which is non-LTE. In this zone, heavy particles temperature is much lower than electrons one.

For a free-burning argon arc, to generate an LTE state in the central zone the operating conditions have to be (a pressure of 300 kPa, currents of 300 to 400 A) (Griem, 1963). These operating conditions lead to an electron density of 1024 m^{-3} in the core. LTE may occur in the outer zones of these arcs where the electron density is lower than 1024 m^{-3}. Thereby, the local thermodynamic equilibrium is the influencing factor in determining plasma temperature. Also, the kind of plasma source plays a prominent role in plasma temperature value (Tendero et al., 2006).

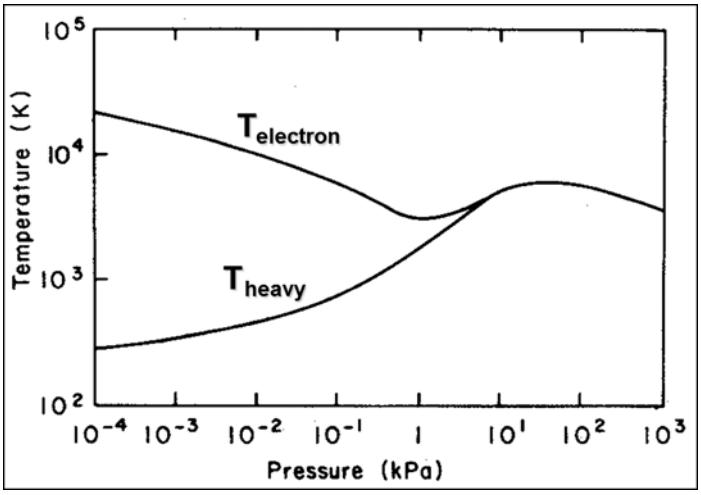

Fig. 2.11. Evolution of the plasma temperature (electrons and heavy particles) with the pressure in a mercury plasma arc (Boulos et al., 1994)

2.4.3. Atmospheric cold plasma for polymer surface treatment

The avoidance of expensive equipment required competing for vacuum-based plasma technologies is the main aim for cold plasma developments, for example, N PIII. There are several of applications where cannot replace the low-pressure plasmas. In spite of, there are many applications where non-equilibrium cold plasma at atmospheric and higher pressures represents a significant advantage (Kalácska et al., 2015).

Gas discharge plasma

Applying high potential difference between two electrodes placed in a gas, this encourages the gas to break down into positive ions and electrons, thereby rising in the gas discharge. The mechanism of gas breakdown is occurring when some electrons are released from the electrodes due to the effect of the omnipresent cosmic radiation. In the absence of a potential difference, the electrons released from the cathode cannot withstand the discharge. However, presenting a potential difference is accelerated the electrons by the electric field in front of the cathode and collide with the gas atoms. The essential collisions are leading to excitation and ionisation due to their inelastic mechanism. The excitation collisions when it is following by de-excitations with the emission of radiation is denoted “glow discharge”. The ionisation collisions produce new electrons and ions. “The electric field accelerates the ions toward the cathode, where they release new electrons by ion induced secondary electron emission. The electrons give rise to new ionisation collisions, creating new ions and electrons. These processes of electron emission at the cathode and ionisation in the plasma make the glow discharge self-sustaining plasma” (Fig. 2.12) (Bogaerts et al., 2002).

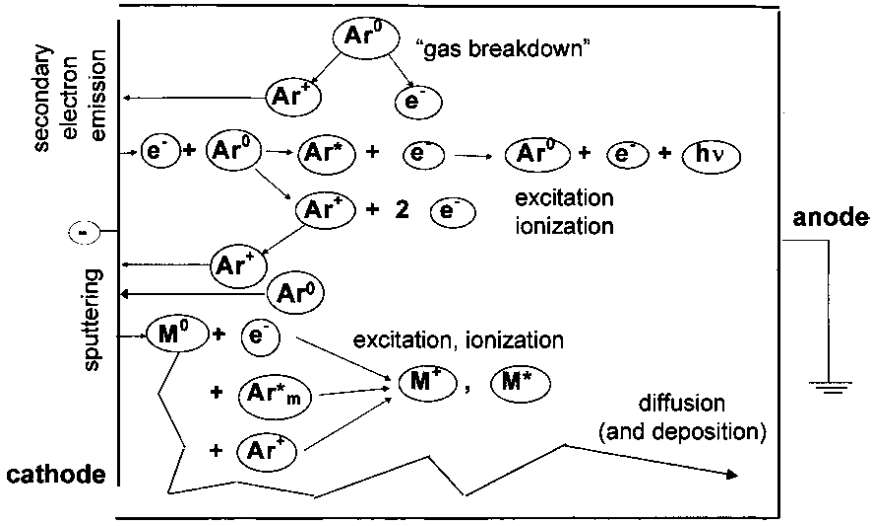

Fig. 2.12. Schematic of the fundamental plasma processes (Bogaerts et al., 2002)

Dielectric barrier discharge (DBD) source

DBD is one of the most common sources to generate “cold atmospheric plasma” (Kogelschatz, 2003; Sakai et al., 2005). A dielectric barrier at one or both electrodes can suppress and in combination with high-frequency power prevent streamers. To be appropriate for various applications, The DBD source constructions, electrode shapes, and dielectric are manufactured in different designs. Some of these systems are schematically shown in Fig. 2.13. A simple corona (not a DBD) arrangement with streamers is shown in Fig. 2.13 a) for comparison with DBD arrangements, Fig. 2.13 b). DBD systems for treatments of moving planar substrates are displayed

in Fig. 2.13 c) and d). For large-area treatments, multiple DBD arrangements can be used with a pair of grid-shaped electrodes covered by an alumina barrier, Fig. 2.13 e). In all DBD systems, the accumulated surface charges on dielectric barriers must be neutralised, e.g. by bipolar pulsed DC power in either static or flowing gas regimes (Bárdos and Baránková, 2010). Figs. (2.14 and 2.15) show the scheme and curves of voltage and current of DBD reactor which is typically utilised for flat surfaces.

The advantages:

- No vacuum is needed,
- Small contact times,
- Continuous in-line technology.

Typical cold atmospheric plasmas are appropriate for the fast and mass production of reactive radicals and plasma-activated reactions based on radical chemistry.

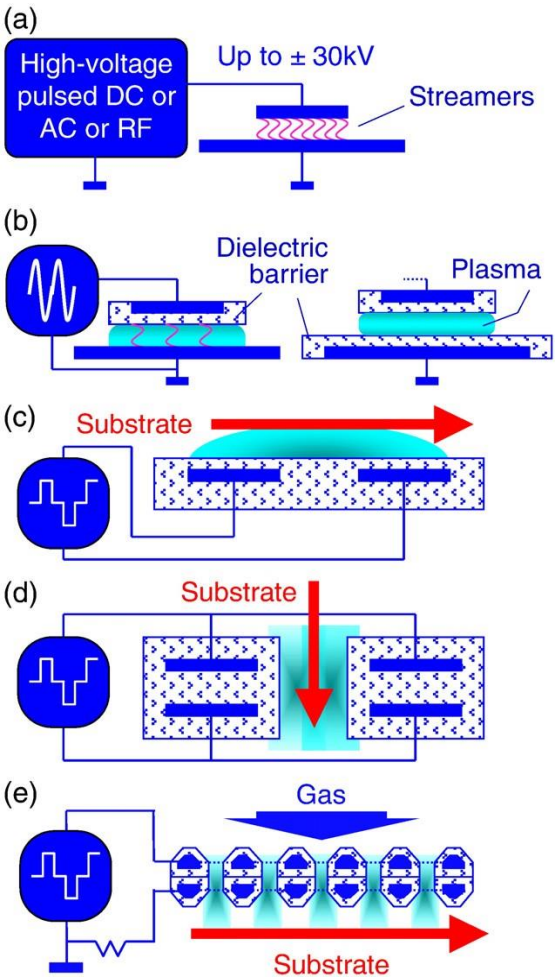

Fig. 2.13. Corona and dielectric barrier discharge (DBD) arrangements (Bárdos and Baránková, 2010):

a) Corona with streamers; b) dielectric barriers on electrodes; c) DBD arrangement for treatment of large-area planar substrates; d) DBD arrangement for two-sided treatments; and e) Multiple grid-type DBD arrangement (200 μm×200 μm windows). The arrows in c), d), and e) indicate the direction of substrate motion

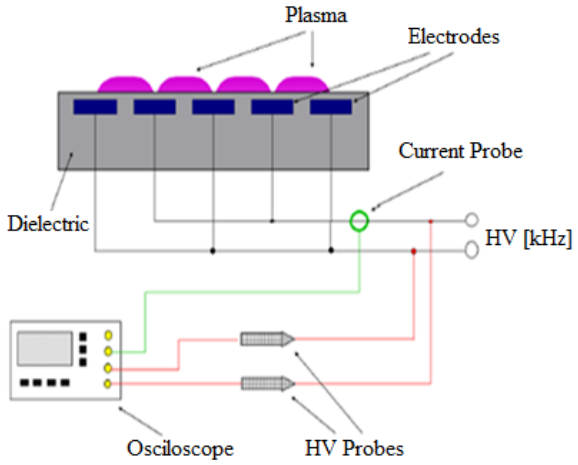

Fig. 2.14. Scheme of DBD reactor (Károly and Klébert, 2015)

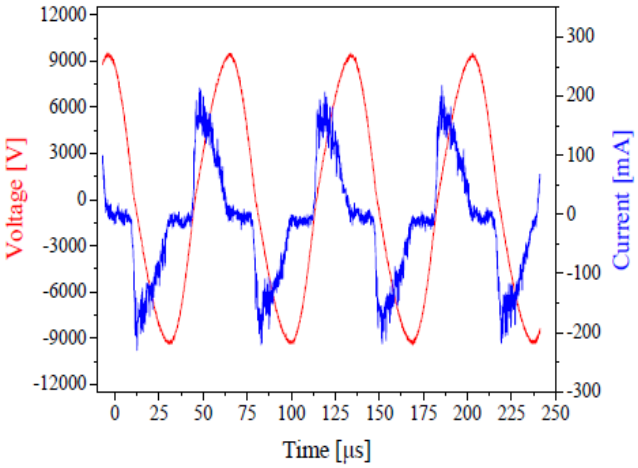

Fig. 2.15. Curves of voltage and current of DBD reactor (Károly and Klébert, 2015)

2.4.4. Influence of plasmas on polymer surface characteristics

Different types of plasma treatment have shown potential to improve the physical and chemical surface characteristics of polymers. The changes in wettability are a fundamental parameter to control adhesion, lubrication and/or interactions with molecules. The formation of polar groups at the surface after plasma treatment, such as, carbonyl, carboxyl and hydroxyl, will increase the surface energy. The enhancement of wettability after plasma treatment can be a combined effect of surface functionalization and increase in surface roughness. When surface grafting occurs relatively fast, the increase in roughness has mainly been observed after longer treatment time (Nastuta et al., 2008). Depending on the selection of adequate parameters, different types of plasma treatment are used for either enhancing as well as to decrease adhesion or surface hardness. The development of atmospheric (cold) plasma applications has been favoured over recent years for surface modification of polymers (Van Deynse et al., 2016), as it is a driving force to avoid expensive equipment for vacuum-based technologies and to simplify industrial applicability. Mainly for the surface modification of aromatic polymers by dielectric barrier discharge (DBD), the chemical functionalization of the polymer surface can be achieved efficiently by processing at relatively low or intermediate powers without introducing serious topographical damage (Upadhyay et al., 2005a). The surface modification of a PET film by atmospheric plasma in combination with different gas flows timely improved the hydrophilicity and was followed by hydrophobic recovery after longer times (Gotoh et al., 2012). In parallel, significant changes in surface morphology and reactivity of PET surfaces have been noticed (Esena et al., 2005; Rashed et al., 2009). While operating in air, the processing parameters such as discharge power, processing speed, processing duration, and electrode configurations affect the nature and scale of the surface changes. In general, longer duration (low processing speed and a high number of cycles) and high power induced greater changes in the surface wettability of the PET (Liu et al., 2006). Among the different studied environmental gases, air and oxygen gave the highest hydrophilicity, while argon and nitrogen yielded lower hydrophilicity of the PET surface (Onsuratoom et al., 2010). Cold atmospheric plasma (SDBD) improves the oxygen and nitrogen contents of PET (Novák et al., 2013).

In comparison to PET, the effects of plasma treatment on PEEK have been studied less frequently, but also led to hydrophilicity and better adhesion (Zhang et al., 2011) due to incorporation of functional groups and higher surface roughness after DBD (Luo et al., 2014). The hydrophilic property governed by oxygenation of PEEK after DBD in air also recovered after several months through loss of the structurally related functional groups, but it remained more stable than other non-aromatic polymers (Upadhyay et al., 2005b). PA6 is showing a reduction in the surface roughness and increase in O/C, and N/C atomic ratios due to DBD plasma treatment in two different gas flows (nitrogen and oxygen). The oxygen gas flow DBD plasma was more efficient to modify the surface compared to nitrogen one (Novák et al., 2014). Also, plasma treatment enhances the contact angle and alters the surface topography of PA66 (Labay et al., 2012). Plasma pre-treatment of biopolymer PLLA surface leads to the forming of pits consisting of crystalline phase with a mild increase of surface roughness (Slepicka et al., 2013).

The adhesion strength of PP and PFA has significantly enhanced due to atmospheric plasma treatment under several gas flows. The characteristics of the surface layer were introduced hydrophilic functional groups where the improvement level changed with time of treatment as Fig. 2.16 illustrates (Tsuchiya et al., 1998).

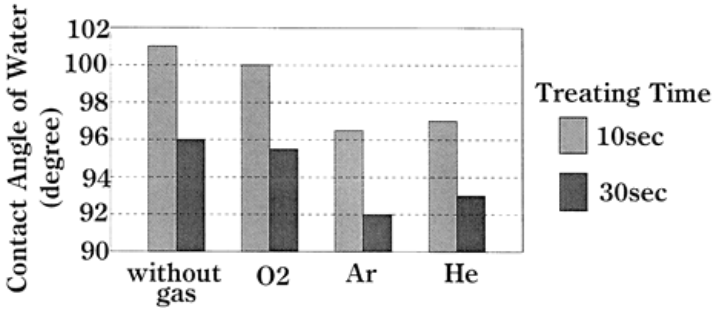

Fig. 2.16 Effect of gas blowing on wettability of PFA film (Tsuchiya et al., 1998)

Although atmospheric pressure plasma glow (APG) discharge treatment is moderate in energy characteristics, APG derived fluoro-polymers to similar surface properties under conventional low-pressure plasma (Prat et al., 2000). Treating metals and polymers by cold arc-plasma jet under atmospheric pressure leads to superficial hydrophilicity improvement and decreasing in the water contact angle of these materials as shown in Fig. 2.17 (Toshifuji et al., 2003).

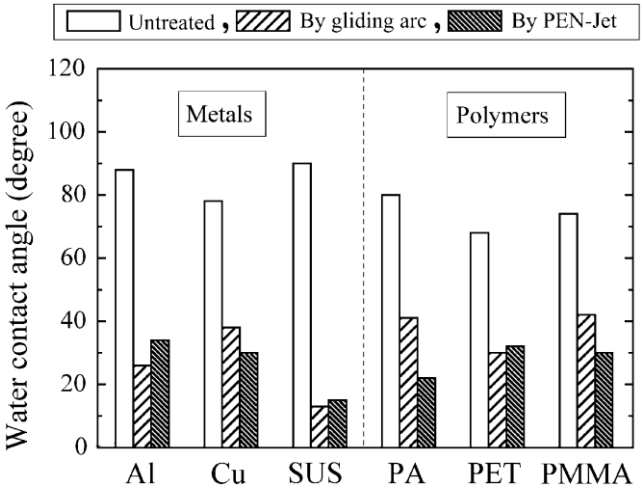

Fig. 2.17. Water contact-angles of various materials after treatment (Toshifuji et al., 2003)

Tóth et al. (2000) observed a significant improvement in the surface hardness of UHMW-PE after nitrogen plasma ion implanted treatment (N PII). The Hydrogen plasma immersion ion implantation (H PIII) treatment of UHMWP-E surface induces amelioration in the scratch resistance, temperature, surface mean roughness, O-content and hardness whereas surface slope and E modulus often decreased, but there is a possibility to increase upon treatment (Tóth et al., 2006a). In parallel, treating UHMW-PE by helium plasma immersion ion implantation (He PIII) are showed significant enhancing in the surface nanomechanical, chemical and wear properties. In the parameter ranges, the surface hardness displayed increasing up to six times, whereas the volume loss upon multipass is decreased up to about 2.5 times (Tóth et al., 2006b). In a related study, the influence of (N PIII) on UHMW-PE surface was investigated as well. The results exhibit a relatively increasing in hardness, macroscopic temperature and mean roughness, while volume loss decreased. However, Modulus decrease or maybe increase depending on the actual process parameter set applied. According to the parameter range which had been studied, researchers suggested that the reduction in the wear rate measurement significantly depending on thermal effects (Tóth et al., 2007). Tóth et al. (2010) in this statistical study which is revised the literature of engineering polymers treated by plasma based ion implantation (PBII) and plasma-based ion implantation and deposition (PBII&D), were concluded there is a rapidly trending in the number of related publications. As a consequence, the effect of nitrogen plasma based ion implantation (N PBII) on PTFE had been discovered by Kereszturi et al. (2010). The study achieved that the F/C atomic ratio is significantly decreased in an inverse relationship with voltage while the roughness is increased inversely with voltage and correlating directly with fluence. However, they could not see a clear relationship between wear volume and the main process parameters, but in general, it was improved across treatment with the increase of roughness and O/C atomic ratio. Further, the water contact angle recorded an increasing at low voltages and high fluences. The subjection of PP to plasma induced luminescence (PIL) shows that excitation mechanisms of PIL at ambient temperature becomes progressively controlled by tunnelling recombination mechanisms with the increase in the treatment duration (Duran et al., 2001).

Atmospheric DBD plasma enhances the wettability and the surface roughness of PP where this enhancement increase proportionally with increase the time of plasma exposure (Nishime et al., 2012). Also, PP roughness increases linearly with the atmospheric DBD plasma exposure time due to the polymer surface degradation and the formation of nodule-like features. These nodules are shaped by highly oxidised short polymer fragments which called in the literature a low molecular-weight oxidised materials (LMWOMs) (Kostov et al., 2013). In a subsequent study, Kostov et al. (2014a) inspected the surface modification of different engineering polymers, such as PET, PE and PP by atmospheric pressure plasma jet (APPJ). The primary aim of this research was to find the optimal treatment conditions as well as compare the effect of APPJ to another atmospheric pressure plasma source, e.g (DBD) on polymer surface characterisation. As a consequence of APPJ treatment the surface roughness increases as in Fig. 2.18. However, nodule-like structures were produced as well, but much smaller compared to that one which constituted in the previous study when the polymer was treated by DBD plasma. Researchers attributed that to the higher polymer degradation during the DBD processing.

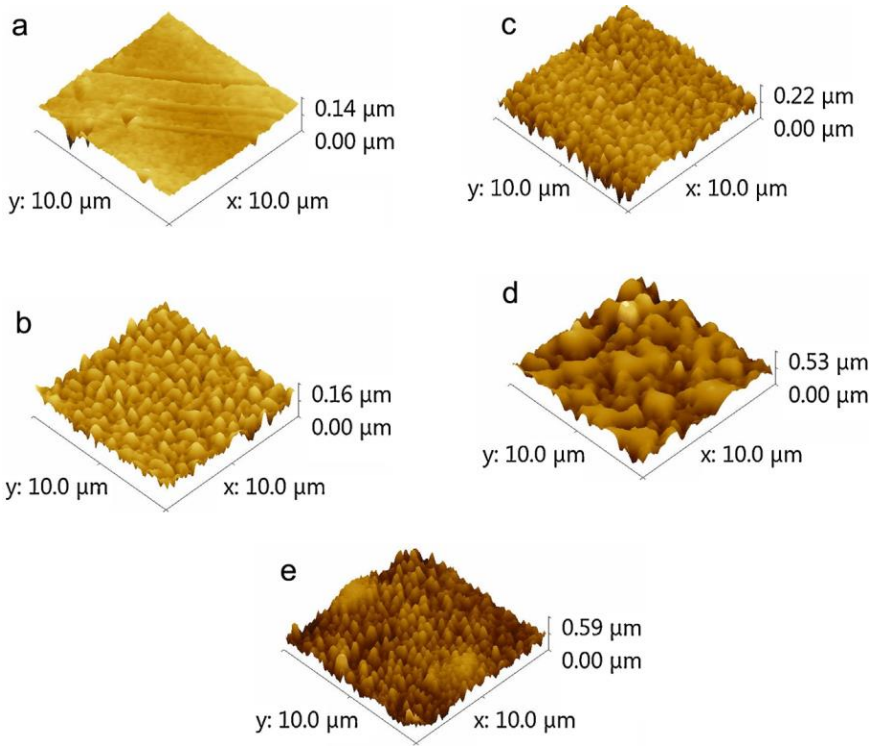

Fig. 2.18. AFM images of PP a) untreated, b) 30 s treated, c) 30 s treated and washed, d) 60 s treated, e) 60 s treated and washed. All treatments were conducted with sample reciprocations using signal amplitude 10 kV, frequency of 37 kHz and Ar flow of 1.3 l/min (Kostov et al., 2014a)

2.5. Adhesion of polymer

Adhesion is the interatomic and intermolecular interaction at the interface of two surfaces (Poisson et al., 2006). The adhesive bond is consisting of a couple of stages. The first stage is the molecules of polymer move towards the solid surface. The second stage of adhesion comprises of the direct interaction between the polymer and the solid surface, and it can be made up by different forces. When the distances between atoms and molecules do not exceed 0.5 nm, the covalent forces become predominant, while at farther distances; ionic and van der Waals forces are effective (between 1 and 100 nm approx.) (Deryagin et al., 1978). It is not easy to describe the mechanism of adhesion in simple phrases due to the complexity of the subject and evolving understanding (Qin and Schreiber, 1999). The objective of this section is to identify a single mechanism that explains phenomena adhesion (Kinloch, 1980; Pukánszky and Fekete, 1999).

Systems of polymer adhesion

"Adhesives and the associated adhesion mechanisms have been investigating for more than 60 years in the automotive and aerospace industries" (Awajaa et al., 2009). The low cost, good mechanical properties of polymers and bulk and surface advantageous is the motivated reason to investigate the adhesion of polymers and epoxy resins (Sargent, 2005; Hutchinson and Iglauer, 2006). The chemical characteristics of polymer interface are controlling the adhesion between the polymer surface and the paint substrate layer (Pijpers and Meier, 2001). For example, bumper bars are considerably made from (PP), and its adhesive system is a paint coating. The polymer is exposed poor surface adhesion properties in its reference state.

2.5.1. Adhesion mechanisms

There are three primary adhesion mechanisms: mechanical coupling, molecular bonding, and thermodynamic mechanism of adhesion.

Mechanical coupling

The mechanical coupling or interlocking (hook and eye) adhesion mechanism is based on the adhesive keying into the surface of the substrate (Basin, 1984; Fourche, 1995; Wake, 1976). This is similar to glue on wood (Akovali, 2012). Fig. 2.19 illustrates the interlocking concept. On one hand of the argument, it is believed that mechanical interlocking provides higher adhesion strength. On the other hand, some researchers believe that roughening of the surface is increasing the surface area for more molecular bonding interactions.

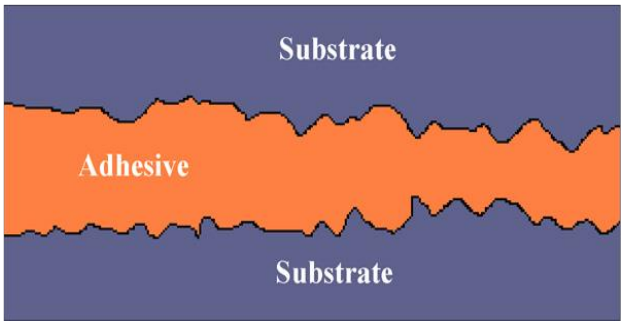

Fig. 2.19. Mechanical coupling between two substrates (Awajaa et al., 2009)

Molecular bonding

Molecular bonding is the best mechanism to explain the adhesion between two substrates in close local contact. Several intermolecular forces such as dipole-dipole interactions, van der Waals forces and chemical interactions can be developing between adhesive and substrate. This mechanism defines the strength of the adhesive joints by interfacial forces and by the presence of polar groups (Akovali, 2012). Molecular bonding mechanisms require a close local contact between the two substrates as shown in Fig. 2.20. However, close contact alone is virtually insufficient for excellent adhesion at the interface due to the presence some of the contact flaws such as cracks and air bubbles (Kinloch, 1980).

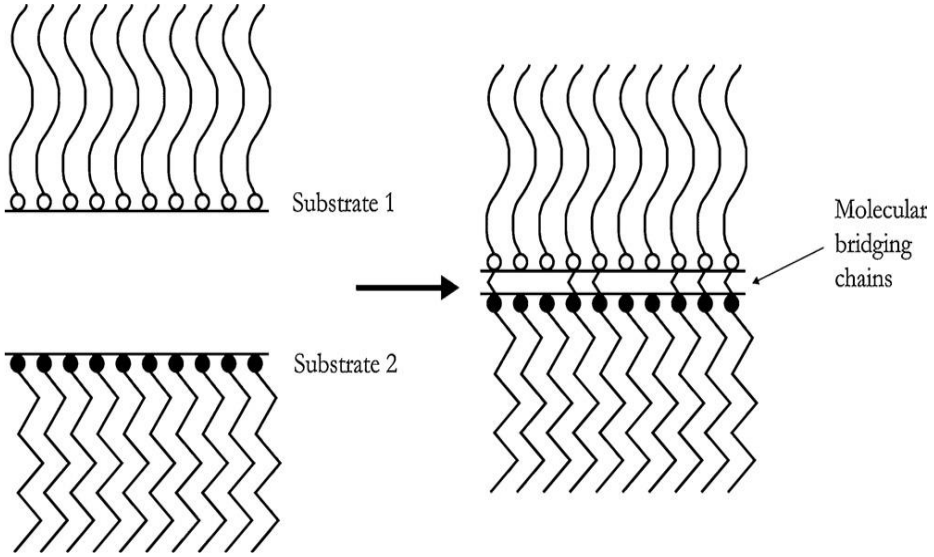

Fig. 2.20. The molecular bonding schematic between substrates (Awajaa et al., 2009)

Thermodynamic mechanism of adhesion

Young at the end of the 19th century imposed if liquid surface energy was known γ_L and contact with a simple solid, smooth, homogeneous, isotropic surface and non-deformable. The strength of adhesion of a system like the one shown in Fig. 2.21 can be estimated the adhesion work (W_a) by applying Eq. 2.1 (Awajaa et al., 2009):

$$W_a = \gamma_{SG} + \gamma_{LG} - \gamma_{SL}\ [J/m^2], \tag{2.1}$$

where γ_{SG}, γ_{LG}, and γ_{SL} represent the energy of the solid-air, liquid-air and solid-liquid interfaces respectively.

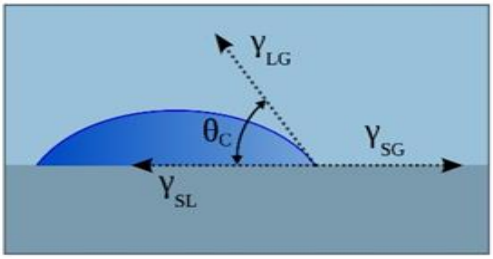

Fig. 2.21. Sessile drop on a surface indicating the contact angle and surface energies

The surface contact angle (θ) can be evaluated by utilising sessile drop method as shown in Fig. 2.22. Commonly, a small drop of double distilled, deionised water is put on the surface with a microsyringe. The height (h) and radius (r) values for the spherical segment can be determined by a special microscope where the contact angle (θ) calculated by applying Eq. 2.2:

$$\text{Contact angle } (\theta) = \arcsin \frac{2rh}{r^2+h^2}\ [\text{deg°}]. \tag{2.2}$$

In 1869, Dupre´ (1869) was observed that the surface contact angle could be connected to the thermodynamic adhesion work. He defined work of adhesion (W_a) is directly related to contact angle (surface energy) of the two substances which estimated from Eq. 2.3:

$$W_a = \gamma_L(1+\cos\theta)\ [J/m^2]. \tag{2.3}$$

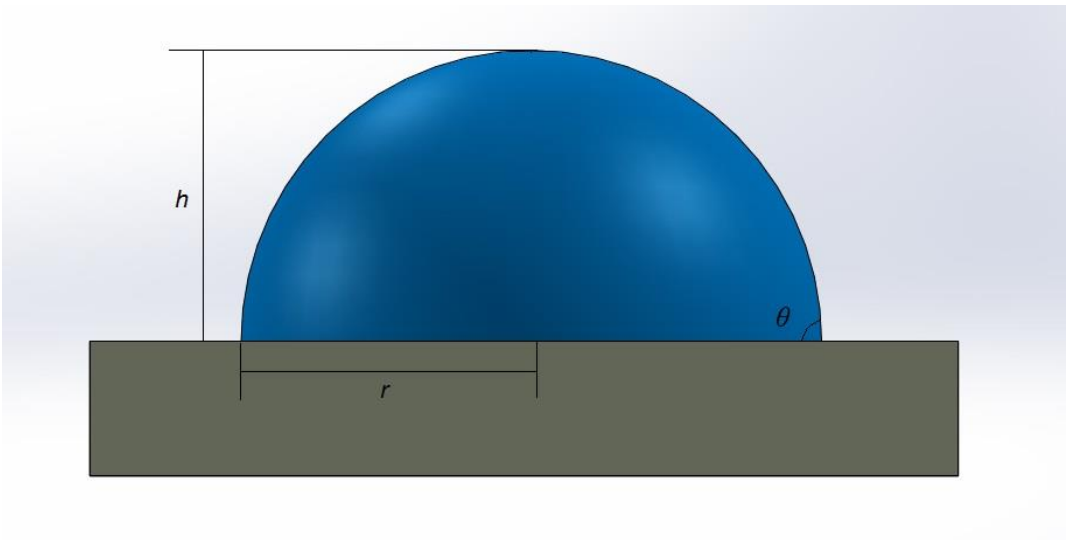

Fig. 2.22. Sessile drop method for calculation of contact angle (θ) extracted from (Baldan, 2012)

2.5.2. Adhesion of plasma treated polymers

Many theories have been introduced to describe and measure the surface tension of materials with applications to polymer systems (Mandolfino et al., 2014a). Hegemann et al. (2003) have been inspected the possibility to modify polymer surfaces by a plasma treatment in several ways (etching, cleaning, activation, cross-linking) to improve wetting properties, thus enhance the adhesion of plasma-deposited coatings. They could detect some adhesion enhancements of PC treated by nitrogen plasma for 5 min. Also, atmospheric pressure nitrogen plasma at a low temperature of gas improves the adhesion of polymer surface, especially for polypropylene (Choia et al., 2005). The emerging of new plasmas at that time such as atmospheric plasma forced Wolf and Sparavigna (2010) to examine its effect on the adhesion of polymers, they found that plasma substantially increases the wettability and adhesion of polymers. DBD plasma enhances the polymer's surface adhesion rate event after short time exposure (Ionita et al., 2010). The surface energy and the peel strength as well as of PET are substantially increased after SDBD plasma modification (Novák et al., 2013). Cold atmospheric plasma can enhance the efficiency of UHMW-PE surface in medical applications, where it is representing model material for bone. Preedy et al. (2014) used cold gas plasma with helium and helium /oxygen to treat UHMW-PE surface. The results showed that the surface properties and adhesion were improved, the hydrophilicity of treated polymer has introduced the possibility of proteins and cells adherence to the surface. On the same time, polyolefin (UHMW-PE and PP) exhibited increasing the surface energy and shear strength of adhesively bonded polymers after treatment by low-pressure plasma considering three plasma process parameters: exposure time, voltage and working gas. Fig. 2.23 shows the effect of low-pressure plasma on the lap-shear test (Mandolfino et al., 2014b).

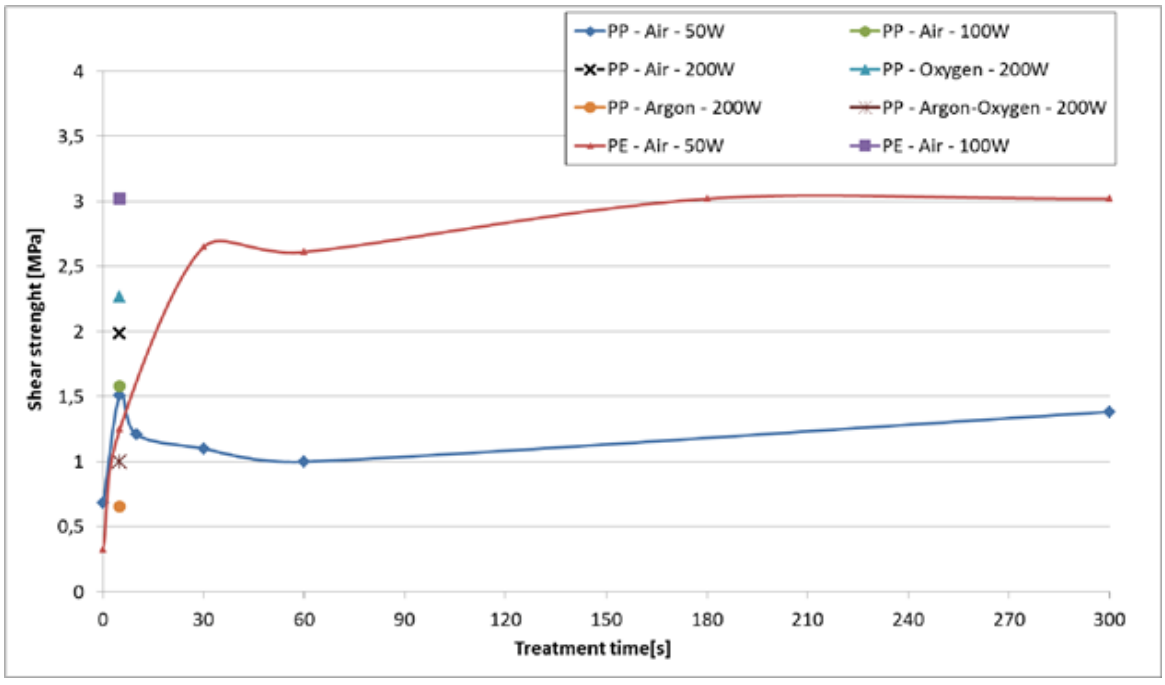

Fig. 2.23. Shear strength of PP joints with different parameters and working gas (Mandolfino et al., 2014b)

The structural adhesive bonding of PA6 composites treated by APPJ resulting that the bond strength reached the cohesive strength of adhesive, in case of multiple plasma treatments at 'low' intensity (Schäfer et al., 2015). In the field of aviation and space, polyimide surface has been

treated by atmospheric pressure plasma treatment to investigate its effect on PI adhesive bonding with titanium. The results point out that atmospheric pressure plasma treatment can improve the adhesive bonding of PI-titanium and PI-PI pairs as a consequence to increase the surface wettability due to forming of polar groups onto PI surface and enhancing the adhesion strength after treatment. The treatment introduces an alteration in the locus failure of bonded joints from an interfacial type failure for pristine joints to cohesive failure within adhesive for the treated joints (Akram et al., 2016; Akram et al., 2010).

2.6. Tribological aspects of plasma treated polymer surfaces

The phrase tribology drove from Greek roots, it consists of two words the first is τρίβω (tribo) which is a verb means "I rub"; and the second word is suffix logy drives from λογία (logia) which means "study of" or "knowledge of". This word was first time dubbed by the British scientists Frank Philip Bowden, David Tabor (1964) (Field, 2008), and Peter Jost in 1964 (Jost, 2017). The lubrication proficient Mitchell Luke (2012) was observed the problems of increasing friction on machines. Tribology is the science which studies the principles and applications of friction, lubrication and wear (Wikipedia: Tribology, 2017). Friction is a widespread phenomenon in our daily life, medicine, industry, etc. The friction processes occur when the surface layers in contact moving (Myshkin et al., 2006). Friction is a consequence of two main non-interacting components, adhesion, and deformation. This can be considered as an approach for all material including polymers. Polymers have a remarkable tribological behaviour some of that is indicated in (Briscoe, 1986; Singer and Pollock, 2012).

2.6.1. Friction of polymers

Many studies have dealt with the polymer tribology such as (Myshkin and Kovalev, 2009; Kragelskii, 1982). Hardness and elastic modulus are governed the penetration depth, maximum load, and strain rate (Kovalev et al., 2004). Microcuttings are a consequence of ploughing, and they may reinforce the friction force under specific conditions. Friction is resulting from elastic hysteresis known as deformation component (Bowden and Tabor, 1964; Moore, 1972). “The mechanical component results from the resistance of the softer material to "ploughing" by asperities of the harder one” (Yamaguchi, 1990). The adhesive bonds generated between the surfaces in the friction contact term as the adhesion component. The adhesion component is higher than the deformation (mechanical) one (Bely et al., 2013). From this, it can be understood the reason of polymer transferred layers forming on the metal counterface during friction contact. The transferred films are an essential factor which must be taken into consideration during estimate the tribological behaviour of polymers (Kragelskii, 1982).

Theory of sliding friction

The “adhesion-shearing theory” was presented primarily by Bowden and Tabor (1964) to calculate the sliding friction and Lee (1974) “more presently” has been presented a theory based on surface energy. “Adhesion-shearing theory” presents the frictional resistance mechanism is a force relative to the required shearing force to break the interface of the contacting parts, as shown in Fig. 2.24. Moreover, the real contact surface area RCA ($=\int_o^n a$) is far smaller than the apparent contact area A_o. Precise contact areas such as a_1, a_2 shown in Fig. 2.24 a), adhere to each other under a normal load P, and relative sliding motion between A and B. The influence of normal load P on frictional

force and coefficient illustrated in Fig. 2.25. The resistance to movement along the contact surface (friction force) is the sum of the destructive shearing force F_s and the resistance to deform the contact part F_d (Yamaguchi, 1990), i.e. friction force is equal to the sum of the adhesion and the deformation components. This can be mathematically interpreted in Eq. 2.4 (Kalácska, 2013):

$$F_f = F_s + F_d\,[N], \tag{2.4}$$

at low loads, $F_f \approx F_s$ since F_d is far smaller than F_s; thus, F_f can be defined as the shear strength of the interface at the real contact area as given in Eq. 2.5.

$$F_f = RCA * \tau\,[N], \tag{2.5}$$

where RCA is the real contact area, and τ is the shear strength at the interface. The real contact area RCA is presented in Eq.2.6:

$$RCA = kP^m\,[\mu m^2], \tag{2.6}$$

where P is the normal load, k and m are constants which depend on the material and surface properties.

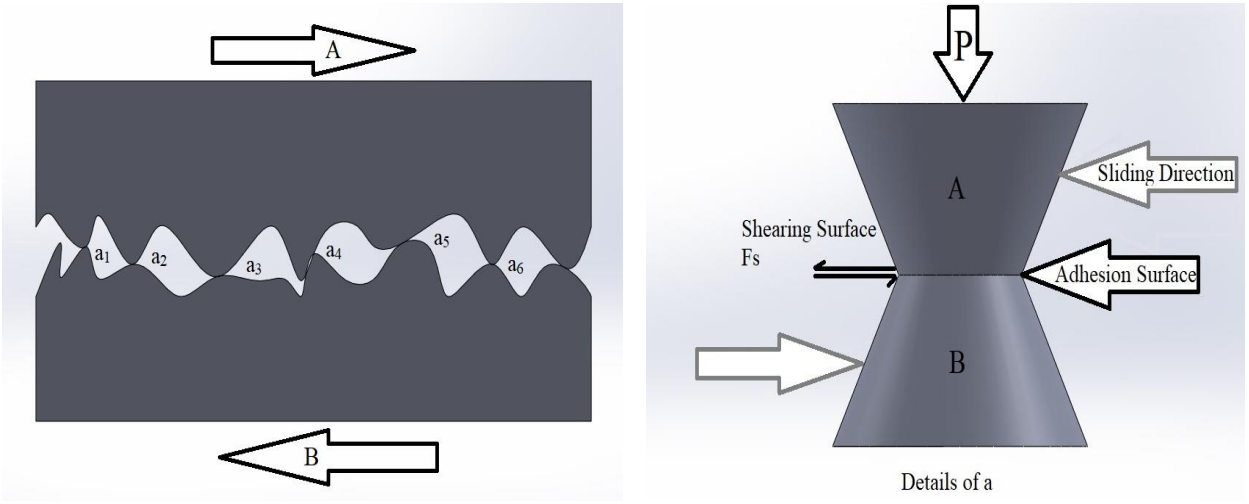

a) b)

Fig. 2.24. Macroscopic section of sliding contact surfaces extracted from (Yamaguchi, 1990)

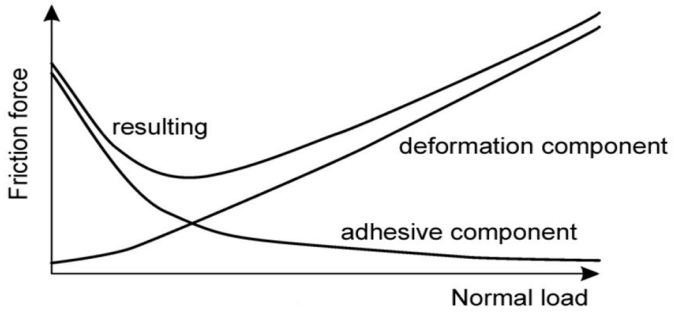

Fig. 2.25. Theory of friction components (Kalácska, 2013)

Real contact area

The highest opposing asperities during approach two surfaces are coming into contact. Increase the load leads the lesser height of new pair asperities to form individual spots of contact. The summation of these spot areas is called the real contact area (RCA). Many important factors should

be taken to consider such load, temperature, and sliding velocity while studying the real contact area of plastics (Bowden and Tabor, 1964; Myshkin and Petrokovets, 2004). There are several studies such as (Myshkin and Petrokovets, 2004; Petrokovets, 1999) have investigated the contact of two bodies the first is rigid and rough, while the second is smooth elastic half space. The latter has to be homogeneous and isotropic with Young's modulus *E*, Poisson's ratio *ν*, and thermal expansion coefficient α.

Effect of load on friction

According to the first law of friction, the friction force is proportional to the normal applied load. Many researchers have examined this law; the research outputs concluded that "first law of friction" is valid for some polymers under specific conditions as shown in Table 2.1. To name a few, (Shooter and Tabor, 1952) found that the friction coefficient of PTFE, PMMA, PVC, PE and PA6 illustrates constant behaviour during slide against steel ball of radius 6.35 mm and 10–100 N load range. Others have obtained similar results for instance (Bowers et al., 1953) examined PTFE, PTFCE, PVC, PVDC, PE with load range 2–15 N. Also, (Shooter and Thomas, 1949) examined PTFE, PMMA, PS and PE with load range load 10–40 N. The proportionality between friction force and applied load breaks down when the load exceeds this ranges. In contrast, turned out that the friction coefficient decreases with increasing the load in mild load range 0.02–1 N (Rees, 1957). This behaviour may be interpreted by elastic deformation of the surface asperities (Kragelskii, 1982). In parallel, rubbers show similar behaviour due to its typical elastic deformation (Schallamach, 1952). Whereas, the friction coefficient increases with increasing the load where this behaviour probably attributed to plastic deformation of asperities. The correlation between the friction of polymers and load varies in the manner, this was explained by (Kragelskii, 1982), i.e. the friction coefficient passes a minimum, which corresponds to transition from elastic to plastic contact. This means that the load can vary the temperature of viscoelastic transitions in polymers thus the mechanism of friction (Myshkin et al., 2006).

Effect of sliding velocity on friction

The hypothesis of independence the friction force on sliding velocity is valid to a reasonable extent only when the contact temperature slightly varies; thus, there is no change in the interface behaviour. However, it is very complicated to separate the effect of velocity and friction temperature. Some researchers had been studied the effect of sliding velocity on friction where the results were such diversity as shown in Table 2.2. The proposal of independent friction on the velocity was valid only within a small velocity range 0.01–1.0 cm/s for PTFE, PE, PMMA, and PS (Shooter and Thomas, 1949) and fibber-fibber contact as well (Gralén and Olofsson, 1947). On the other hand, more complicated behaviours of friction depended on the sliding velocity has been observed. One of these relationships related to polymer viscoelastic behaviours where the viscous resistance in the contact zone increases with increasing velocity in the low-velocity ranges. When the pressure in the contact zone comes high, this leads to abnormally viscous flow, which causes a sharp rise in viscosity due to velocity increasing (Flom and Porile, 1955; White, 1956). Almost Molecular-kinetic leads to the same dependence as well (Schallamach, 1953; Bartenev and Lavrent′ev, 1981). The elastic behaviour is often observed in the contact zone with high-velocity ranges, and the friction force shows just slightly depending on the velocity, or it may be decreased with increasing the velocity (Milz and Sargent, 1955; Tanaka, 1984). At high velocity, the contact duration is short, and this leads to more decreasing in the friction force. In the moderate velocity

ranges, a maximum friction force appears in the curve, and the position of maximum value depends on the relaxation of polymer (Fort Jr, 1962). Besides, it should be kept in mind that the relationship between friction force and sliding velocity mainly depends on the temperature (Vinogradov et al., 1970). If the contact temperature near the glass-transition, the sliding velocity has a noticeable effect on friction, but the lower contact temperature leads to slightly dependent friction on the sliding velocity (Myshkin et al., 2006).

Effect of temperature on friction

It is known the sensitivity of polymers to frictional heat due to the viscoelastic properties. The generated heat during friction process is a consequence of converting the mechanical energy to heat in the contact zone. The heat of friction is produced at contact spots as a consequence of the polymer plastic deformation, hysteresis, dispersion, and viscous flow. The forming and breakdown of adhesion bonds is an additional source of heat generation in the interface. In the same context, (Fort Jr, 1962; Ludema and Tabor, 1966) have observed a relationship of friction coefficient with hardness and shear strength of several polymers. Temperature cannot affect adhesion thereby friction (King and Tabor, 1953). Some possible friction correlations with temperature are presented in Table 2.3. Adhesion is the dominant mechanism of polymer friction when a polymer is sliding over smooth surfaces in the highly elastic state. However, other mechanisms can be noted when the polymer is becoming closer to the glassy state.

Table 2.1. The effect of load on friction coefficient extracted from (Myshkin et al., 2006)

Author(s)	**Materials and load**	**Graphical representation**
Bowers, Clinton, Zisman	2–15 N Steel–polymer (PTFE, PFCE, PVC, PVDC, PE)	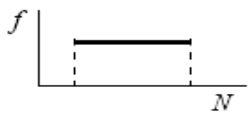
Shooter, Thomas	10–40 N Steel–polymer (PTFE, PE, PMMA, PC)	
Shooter, Tabor	10–100 N Steel–polymer (PTFE, PE, PMMA, PVC, Nylon)	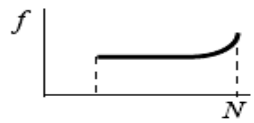
Rees	Steel–polymer (PTFE, PE, Nylon)	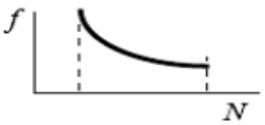
Bartenev, Schallamach	Theory Steel–rubber	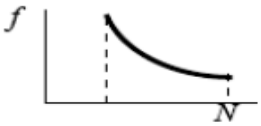
Kragelskii	Theory Steel–rubber	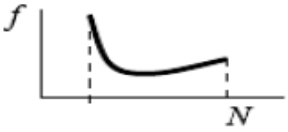

Table 2.2. The effect of sliding velocity on friction coefficient extracted from (Myshkin et al., 2006)

Author(s)	Materials and sliding velocity	Graphical representation
Shooter, Thomas	0.01–1.0 cm/s Steel–polymer (PTFE, PE, PMMA, PC)	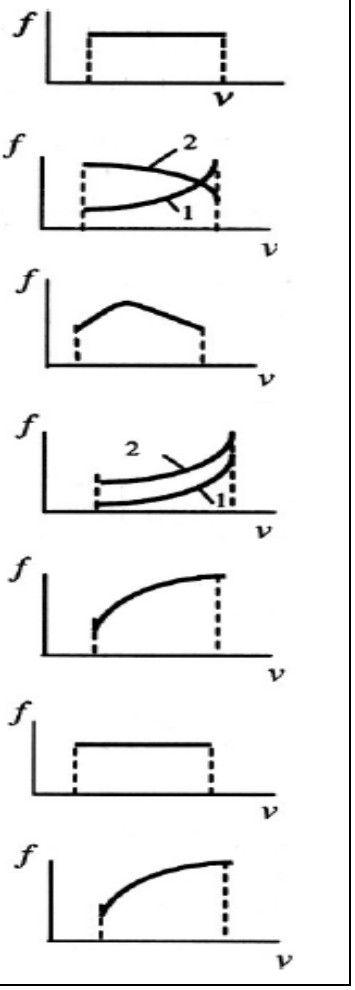
Milz, Sargent	4 – 183 cm/s Polymer–polymer 1 – Nylon, 2 – PC	
Fort	10–5–10 cm/s Steel–polymer (PTFE)	
White	0.1 – 10 cm/s Steel–polymer (1 – PTFE, 2 – Nylon)	
Flom, Porile	1.1– 180 cm/s Steel–polymer (PTFE)	
Oloffson, Gralben	1.5 cm/s Polymer–polymer (fibers)	
Bartenev and Lavrentiev, Schallamach	Theory Steel–rubber	

Table 2.3. The effect of temperature on friction coefficient extracted from (Myshkin et al., 2006)

Author(s)	Material	Temperature, test conditions	Graphical representation
Shooter, Thomas	1 – PS, 2 – PTFE	20–80°C Steel–polymer	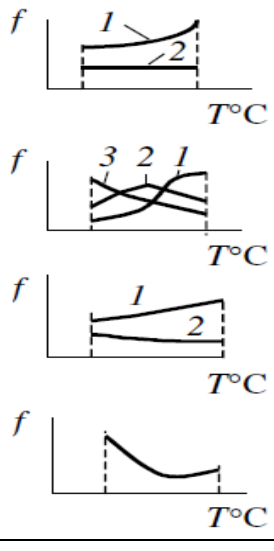
Ludema, Tabor	1, 2 – PCTFE, 3 – PP	–50–+150 °C Steel–polymer 1-v = 3.5×10-5 cm/s, 2- v = 3.5×10-2 cm/s	
King, Tabor	1 – PE, 2 – PTFE	–40–+20 °C Steel–polymer	
Schallamach	Rubber	20–200 °C Steel–polymer	

2.6.2. Wear of polymers

Wear is undesirably removed layers from the material surface. Wear occurs when two materials are coming into contact with the presence of movement. Mechanical stresses, temperature and chemical reactions directly influence the surface layer characterisation. Polymers are sensitive to these factors due to their specific structure and mechanical behaviour. The interface temperature could be significantly higher than the temperature of the environment. Some polymers had been examined by (Lancaster, 1968) during sliding against steel; he was found that the temperature influences the wear of polymer where polymers pass a minimum at the characteristic temperature. It is thorny to enumerate an exact classification polymer wear due to the high diversity of the mechanisms (Blau, 1989; Kragelskii, 1982; Myshkin et al., 1997). However, abrasion, adhesion, and fatigue are the three common types of polymer wear occur during the sliding process.

Abrasive wear

When the polymer surface is cut or ploughed by harder particles or asperities this process called abrasive wear. The cut parts are either be embedded in the counterface (two-body abrasion) or lost out to the contact area (three-body abrasion). The abrasion process produces fine cutting chips. The wear rates mainly depending on the abrasive asperities shape and apex angles of the countersurface besides polymer mechanical. Two different deformation modes can be observed while an abrasive particle moves over the plastic material. The first mode is called plastic grooving (ploughing). Ploughing is pushing ahead the particles and contents; it is continually drifted sideways to form ridges adjacent, and generate grooves; in this mode, there is no removed material from the plastic surface. The second mode is called cutting, due to its similarity to micromachining; in this mode, there are chips removed from the plastic surface as a consequence of erosion by particles (Myshkin and Kovalev, 2009).

Adhesion wear and friction transfer

The wear results from the shear of the friction junctions known as adhesion wear. This wear depended on the adhesion mechanism which is an essential component of friction. This type of wear arises from a growth and fracture of adhesion junction. The material transfer from one surface to another occurs due to the localised bonding between the contacting solid surfaces. The transfer of polymer layers observed as most important characteristic of polymer adhesive wear (Bely et al., 2013). It is also possible that other wear types (fatigue, abrasion etc.) accompany the adhesive wear. The consequences of material transfer are substantially pronounced on tribological behaviour of the friction pairs. When micrometre size particles transfer from one surface to the other, then the wear variety is slight. However, wear variety takes place if a thin film of soft material is transferred onto the harder mating surface, e.g. (polymer on metal). If the transferred polymer film is removed away from the metal surface and new film formed, in this case, the wear rate increases. Whereas, if the film sticks to the metal surface, thus the friction occurs between same materials (Myshkin and Kovalev, 2009). In contrast, the hard material also may transfer to the soft surface under certain conditions, e.g. bronze transfers to a polymer surface. Here, the transferred particles are held in soft material and work as abrasive particles which lead to scratch the host material. The transferred particles of polymer expose a wide diversity of forms this depending on polymer properties and friction conditions. Further, due to the polymer transfer the roughness of both surfaces in contact zone as well as being modified (Pratt, 1986).

Fatigue wear

Fatigue is defined as a change in the material state which occurs due to repeated (cyclic) stressing and marks a progressive fracture. Every asperity of friction surface is sequential loading from the asperities of countersurface. This resulting different stress fields in surface and sub-surface regions are with two different scales; the first is the apparent contact area and the second is the real contact spots. These stress fields cause the material fatigue in these regions which leads to the generation and diffusion of cracks and the formation of wear particles. This process is called friction fatigue, and it differs from the bulk fatigue where it occurs only in surface and sub-surface regions. The loss in material surfaces resulting from friction fatigue is named fatigue wear. The cracks of fatigue are occurring where the maximum tangential stress or the tensile strain takes place. The maximum tangential stress position is dependent on friction coefficient. At low friction coefficient ($\mu<0.3$) the point of maximum shear stress is located somewhere under the surface. If the friction coefficient increases ($\mu>0.3$), the point appears on the surface. When a solid is exposed to a combination of normal and tangential loading, the surface and sub-surface regions emerge if the tensile strain thus frictional heating occur. Therefore, the core of cracks is formed either in the surface or below it (Myshkin and Kovalev, 2009).

2.6.3. Tribological behaviour of polymer surface treated by plasma

The effects of plasma surface modification on tribological properties of polymers is not uniformly predictable, due to the multitude of governing mechanisms. It can be expected that functionalization, crosslinking, or chain scission will affect chemical and mechanical surface properties after plasma treatment, which in turn will alter shear strength, friction and wear. The effect of plasma treatments on tribology has mainly been studied for rubbers, indicating improvements in friction and wear resistance (Segu, 2016). The pin-on-disc test shows lower coefficient of friction of PC and PP, whereas LEPE and PS exhibit higher coefficient of friction after atmospheric plasma treatment than the pristine one. Bismarck et al., (2008) attributed the significant decrease in friction of PC either to the largest reduction in contact angle or the changes in the chemical and simultaneously the physical properties after treatment. On the other hand, the increase in crosslinking after atmospheric plasma treatment resulted in lower friction and wear of PEEK composites (Zhang et al., 1995), while an argon plasma treatment resulted in higher friction of PET (Leggett and Beake, 1998). The effects of nitrogen plasma immersion ion implantation (N PIII) on PET were indicating improvements in the scratch resistance (Kereszturi et al., 2008). Kalácska et al. (2009) demonstrated that the benefits of tribological properties strongly depend on the sliding conditions: the lower friction and better wear performance of PET treated by PIII only occurred at low *pv* regime under dry and water lubrication sliding conditions. Kalácska et al. (2012) studied the tribological behaviour of PA6 treated by (N PIII) under different conditions (dry, water and oil lubrication) and various *pv* regimes. The results show that the friction coefficient and specific wear of treated PA6 are lower than the untreated one under dry sliding conditions and low *pv* factor, while friction, wear and the interface temperature of treated PA6 are going higher than the pristine one at high *pv*. On the other hand, the water lubricant decreases the adhesive component of friction after treatment, this reflected as fluctuation in the friction behaviour of treated surface. However, the run-out oil lubrication conditions show lower friction coefficient for treated PA6 than the pristine one under low *pv* regime as a consequence to increase of the dispersive component. Under continuous oil lubrication, no difference could be detected

between the treated and untreated parameters therefor the run-out type was preferred to detect the difference.

Five minutes of air-plasma treatment are sufficient to reduce the coefficient of friction and enhance the wear life of UHMW-PE film at constant *pv* regime (Samad et al., 2010). In contrast, UHMW-PE treated by atmospheric pressure gas plasma does not show a significant change in wear after two minutes treatment time, while the wear reduced to the half after longer time of treatment. This indicates that plasma exposure time plays a major role in the tribological properties of treated surface in particular for UHMW-PE (Perni et al., 2012). Evidence of the above, UHMW-PE treated by cold argon plasma using dielectric barrier discharge (DBD) shows (under dry conditions) an increase in the friction coefficient with the treatment time whereas wear volume was reduced over the treatment time due to surface structure change after modification. Under N-saline lubricant conditions, wear volume and friction were reduced over the treatment time, this indicates to increase the surface wettability implying enhance surface lubrication capability (Naresh et al.,2016). Sagbas (2016) reported an increase in friction and improving in wear of conventional UHMW-PE after plasma treatment, whereas the fiction was not affected for vitamin E blended UHMW-PE under the same test conditions. However, the wear factor was slightly decreasing compared of the significant wear improvement of conventional UHMW-PE as a consequence of high cross-linked of conventional UHMW-PE.

2.7. Summary of litreture review evaluation

According to the previous reviewed research, it has apparently seen the plasmas have the capability of polymer surface modification implying surface adhesive ability and tribological properties, where the effect of plasma depended on several factors such as plasma sources, exposure time, vacuum, temperature, pressure, etc. Although the diversity of plasmas and surface modification methods, the literature brings to light the cold atmospheric plasma in particular with DBD source as one of the unique and efficient variants that can be used to enhance polymer adhesive and tribological properties because it does not need vacuum, versatility, small contact times, continuous in-line technology and cheap equipment compared to its peers. Further, there is a scarcity in addressing of its effect in literature from the point of adhesive and tribology behaviour of polymers. Based on the preceding, this field was attractive enough to go into it. The developments of polymer adhesive bonding, tribology and surface treatment according to the reviewed literature are summarised in following points:

- Polymer surface treatment concerning adhesive and tribological behaviour studies has started since the beginning of the sixth decade of the last century. Since that time, many studies have been progressively conducted on the characterisation of friction and wear of natural polymers,
- Due to quick progress in engineering materials science, especially in the treatment surfaces of polymers, the tribological testing for these surfaces has represented the starting point of the competition in polymers tribology science,
- The conventional polymers surface modification has an extensive attraction in both academia and industry. However, surfaces modification which includes a change in the surface energy (adhesion) has prompted the researchers to delve into inspecting the impact of surface treatments on the surface energy,

- The emergence of the polymer composites and the important study of adhesive and tribological behaviour in terms of surface modification were essential steps which had given us the fundamental ideas and data about the modified surfaces which based on our study,
- Various applications for polymer composites and scope effect of surface modification (adhesion) on its functional properties have inspired me to investigate the present topic,
- In spite of progressing in surface treatment technologies, the ion surface treatments, for example, hydrogen, nitrogen and oxygen ions is still limited. This limitation inspires researchers toward the study the tribological and adhesive properties of treated surfaces. Presently, the literature can give us a good perception of the ions effect on the properties of polymer surfaces,
- Atmospheric plasma treatment is one of advanced surface modification techniques which emerged during last few years. Many studies have investigated the effect parameters of this technology on the treated surfaces. However, these studies were limited to a discussion and dealing with limited points of the atmospheric plasma treated surface such as surface characterization,
- There are a few articles which have addressed the effect of atmospheric plasma treatment on the polymer surfaces in terms of friction or wear only for single or couple of polymers. Also, there is no integrated database can be observed regarding the influence of cold atmospheric plasma treatment on the tribological behaviour of a wide range of polymers such as thermoplastics,
- Because of the effective role of DBD atmospheric plasma in the surfaces treatment, many researchers have extensively studied this method. However, these studies didn't take into consideration the investigation of its effect on adhesive bonding and tribological behaviour of polymer treated surfaces where this effective parameter will be considered in the present study.

The comparative investigations between the previous studies and the present findings have been reviewed in Table 2.4. I could conclude that the polymer surface treatments have been developed with the time, and there are limited spots of knowledge about the DBD atmospheric plasma-treated polymer surfaces concerning adhesive bonding and tribological behaviour which in turn opened the debate to achieve the desired objectives of the present research. In brief, I am trying in this study to highlight the missed data and introduce a new contribution to the literature by my findings and results concerning this topic.

Table 2.4. The scientific developments of adhesive bonding and tribological investigations concerning plastic surface treatments

Topic \ Date	1960	1970	1980	1990	2000	2010	Current decade
Examination of Friction and wear of natural fibres (natural polymers)	X	X	X	X	X	X	X
surface energy (adhesion) of modified surfaces of polymers		X	X	X	X	X	X
tribological testing of composite polymers			X	X	X	X	X
Adhesive of composite polymers and surface modification				X	X	X	X
Effect of ions such as H, N and O ions on the surface tribological properties					X	X	X
Atmospheric plasma surface modification of polymers						X	X
Atmospheric plasma treatment of polymer surfaces from the point of friction or wear							X
Atmospheric plasma treated polymer surfaces from the point of adhesive bonding and tribological behaviour							

3. MATERIALS AND METHODS

The present chapter is introducing the materials and their preparations which used in my research in addition to the engineering and scientific methods involved experimental measurements, characteristics, methodological knowledge and description of the test systems to achieve the research goals.

3.1. Materials and preparations

3.1.1. Experimental materials

Eight types of commercially available thermoplastic (semi-crystalline) polymers (distributed by Quattroplast Ltd., Hungary and produced by Ensinger GmbH, Germany) were used in bulk conditions (unfilled). The polymers are distinguished to two groups to facilitate comparison process: 1) Engineering polymers, and 2) Polyolefin polymers and PTFE. The polymer properties according to the catalogue data from the supplier for each polymer are in below:

Engineering polymers:

1) Polyether etherketone

Polyether etherketone (Fig. 3.1) or PEEK (DocaPEEK), the mechanical properties as follows: elastic modulus E= 4200 MPa, tensile strength σ= 116 MPa, glass transition temperature T_g= 150°C.

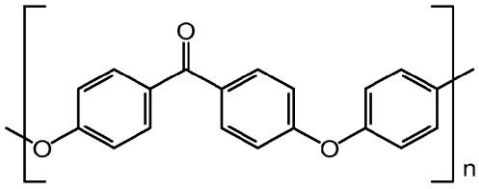

Fig. 3.1. PEEK chemical formula

2) Polyethylene terephthalate

Polyethylene terephthalate (Fig. 3.2) or PET (DocaPET), the mechanical properties as follows: elastic modulus E= 3100 MPa, tensile strength σ= 79 MPa, glass transition temperature T_g= 8 °C.

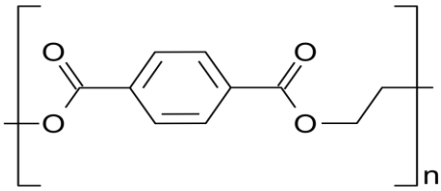

Fig. 3.2. PET chemical structure

3) Polyamide 6 Extruded

Polyamide 6 Extruded (Fig. 3.3) or PA6-E (Docamid-6-Extruded), the mechanical properties as follows: elastic modulus E= 3300 MPa, tensile strength σ= 79 MPa, glass transition temperature T_g= 45°C.

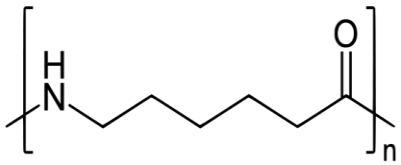

Fig. 3.3. PA6 chemical structure

4) Polyoxymethylene

Polyoxymethylene Copolymer (Fig. 3.4) or POM-C is known as Acetal Copolymer as well (Docacetal copolymer), the mechanical properties as follows: elastic modulus E= 2800 MPa, tensile strength σ= 67 MPa, glass transition temperature T_g= -60°C.

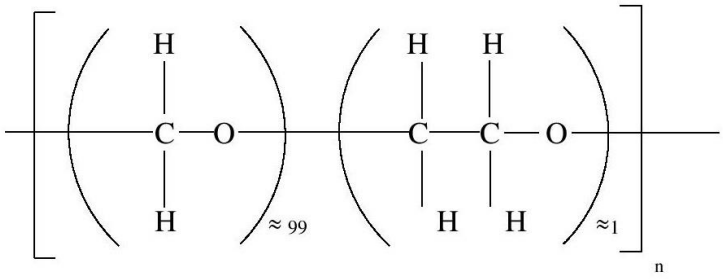

Fig. 3.4. POM-C chemical structure

Polyolefin and PTFE

1) Polypropylene

Polypropylene (Fig. 3.5) or PP (Docapren), the mechanical properties as follows: elastic modulus E = 1200 MPa, tensile strength σ = 32 MPa, melting temperature T_m= 165 °C.

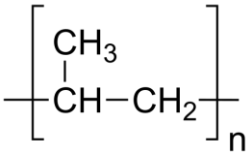

Fig. 3.5. PP chemical structure

2) Polyethylene

Two types of commercial Polyethylene (Fig. 3.6) or PE have applied: (1st) Ultra High Molecular Weight Polyethylene High Density 1000 (UHMW-PE HD500) or (Docalene-HD500), the mechanical properties as follows: elastic modulus E = 1200 MPa, tensile strength σ = 24,5 MPa, glass transition temperature T_m = 135°C. And (2nd) Ultra High Molecular Weight Polyethylene High Density 1000 (UHMW-PE HD1000) or (Docalene-HD1000), the mechanical properties as follows: elastic modulus E = 680 MPa, tensile strength σ = 22 MPa, glass transition temperature T_m = 135°C.

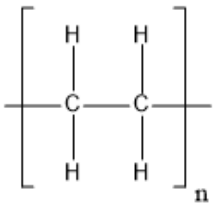

Fig. 3.6. PE chemical structure

3) Polyetrafluoroethylene

Polytetrafluoroethylene (Fig. 3.7) or PTFE (Docaflon- PTFE-N), the mechanical properties as follows: tensile strength σ = 22 MPa, glass transition temperature T_g = -20 °C.

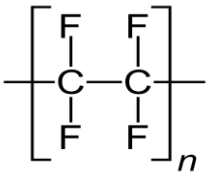

Fig. 3.7. PTFE chemical structure

Adhesives

The commercial adhesives with a controlled bond line thickness of 0.1 mm were applied following the manufacturer procedures (Henkel AG & Co., Germany), including: (i) Loctite 406 (Ethyl cyanoacrylate) with Loctite 770 (Primer-Cyanoacrylate-Aliphatic amine) as activator, (ii) Loctite 9466 (two-component epoxy), (iii) Loctite 330 (Acrylic-Urethane metacrylate ester), (iv) Loctite 3035 (Acrylic-Methacrylate) as shown in Fig. 3.8. Technical details of Loctite 406 and Loctite 9466 are adjusted in Table 3.1, Loctite 330 Loctite 3035 are adjusted in Table 3.2, and Loctite 770 are adjusted in Table 3.3 from Technical Data Sheet (TDS) of Loctite (Henkel, 2017).

Fig. 3.8. the adhesive types which used in adhesive bonding tests

Table 3.1. Technical details of Loctite 406 and Loctite 9466 extracted from TDS (Henkel, 2017)

	Loctite 406	**Loctite 9466**
Technology	Cyanoacrylate	Epoxy
Chemical Type	Ethyl cyanoacrylate	Epoxy
Components	One part – requires no mixing	Two component - requires mixing
Cure	Humidity	Room temperature cure after mixing
Working Time, 25 °C, (maximum time before assembly):	3min	7 min
Fixture Time	5-10 sec	1 h
Full strength	24 h	24 h
Shear Strength	8-15 N/mm^2	5-32 N/mm^2

Table 3.2. Technical details of Loctite 330 and Loctite 3035 extracted from TDS (Henkel, 2017)

	Loctite 330	**Loctite 3035**
Technology	Acrylic	Acrylic
Chemical Type	Urethane methacrylate ester	Methacrylate
Components	One part – requires no mixing	Two component - requires mixing
Cure	With activator	Room temperature cure
Working Time, 25 °C, (maximum time before assembly):	3min	7 min
Fixture Time	30 min	10 h
Full strength	6 h	72 h
Shear Strength	15-30 N/mm^2	2.5-14 N/mm^2

Table 3.3. Technical details of Loctite 770 primer extracted from TDS (Henkel, 2017)

Chemical type	Solution of aliphatic amine in solvent
Appearanc	Colourless
Viscosity, 20°C, mPa.s	1.25
Flash point (COC), °C	-1
Drying time, 20°C, second	30
On part life, hour	8
Typical Range, product	406, 496, 460,

3.1.2. Specimens preparation

For tribological tests, polymer specimens were machined into pins with a diameter of 10 mm and thickness of 4 mm. The surfaces were subsequently polished with wet SiC paper (grid numbers P1200 and P400) and felt sheet toward required surface roughness (see below). The same surface preparation was applied for samples used in tribological tests, surface chemical composition,

topography, and energy measurements except morphology scan and AFM measurements where extruded polymer surface was applied. However, adhesive test specimens were cut from extruded plates in a rectangular shape with dimensions: 25.4 mm x 100.0 mm x 2.0 mm as shown in Fig. 3.9 and applied to the test with the virgin extruded surface. Before testing, all samples were cleaned in an ultrasonic bath with distilled water and 96% ethanol (Reanal, Hungary).

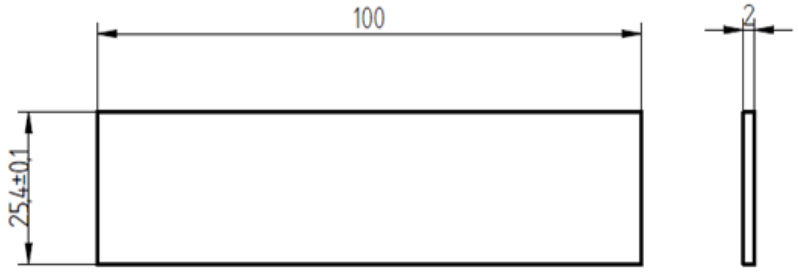

Fig. 3.9. Sample dimensions of adhesive tests

Steel surfaces (counterfaces) were first ground and polished with SiC abrasive paper (grid numbers 400 and 600) with grooves oriented parallel in a single direction. For tribological and adhesive tests, the average roughness of the steel plates was R_a=0.72±0.02 μm perpendicular to the grinding direction and R_a=0.46 ±0.02 μm parallel to the grinding direction (measured with SurfTest SJ-201, Mitutoyo, Japan). The steel specimens of adhesive tests have the same dimensions of polymer specimens as mentioned above. The surfaces were subsequently cleaned with Loctite SF 7063 (Henkel AG & Co., Germany) according to the supplier's technology.

3.2. Plasma treatment

The polymer surfaces were modified by cold atmospheric plasma treatment using a dielectric barrier discharge (DBD) equipment (manufactured by Roplass s.r.o., Brno, Czech Republic, the equipment is available at AKI, MTA) operating under controlled air atmosphere (temperature 23°C, relative humidity 50%) (Černák et al., 2009; Šimor et al., 2002), as shown in Fig. 3.10. The plasma panel consists of two systems of parallel strip-like electrodes (with typical dimensions of: 1.5 mm wide, 0.5 mm thick, 1 mm strip to strip) embedded in aluminum oxide matrix. The ceramic layer between the plasma and electrodes has a thickness of typically 0.4 mm. The plasma is ignited with a high frequency (10–20 kHz), high voltage with peak-to-peak values of 20 kV. The elementary discharge involves a diffuse surface discharge developed over the metal electrodes and a filamentary streamer discharge created between the electrodes giving its H shape. Visually homogenous plasma can be reached with increasing voltage and absorbed power as more and more elementary discharges are generated (Fig. 3.11). The applied high voltage may give rise to the heating of the dielectric surface and the surrounding gas, too. In order to keep the system at the lowest possible temperature, oil is circulated over the system, which allows to keep the gas temperature around 320 K. The power of the DBD plasma system is set to 320 W, which provided a quasi-homogeneous diffuse plasma with air as process gas. The plasma treatment time is one minute for each polymer sample. The treatment time was decided to obtain the maximum surface modification according to early stege of surface energy investigations as shown in Table 8.1 in A3.

The samples were stored in aluminum foil until further use. The following surface characterisation, adhesive and tribological testing were all done within 24 hours after the surface plasma treatment to fully include the effects of surface modification and under ambient air conditions (T= 23°C, H= 50%). Preliminary results revealed that the plasma-treated surfaces start to recover toward their original state after longer time (i.e., after two days).

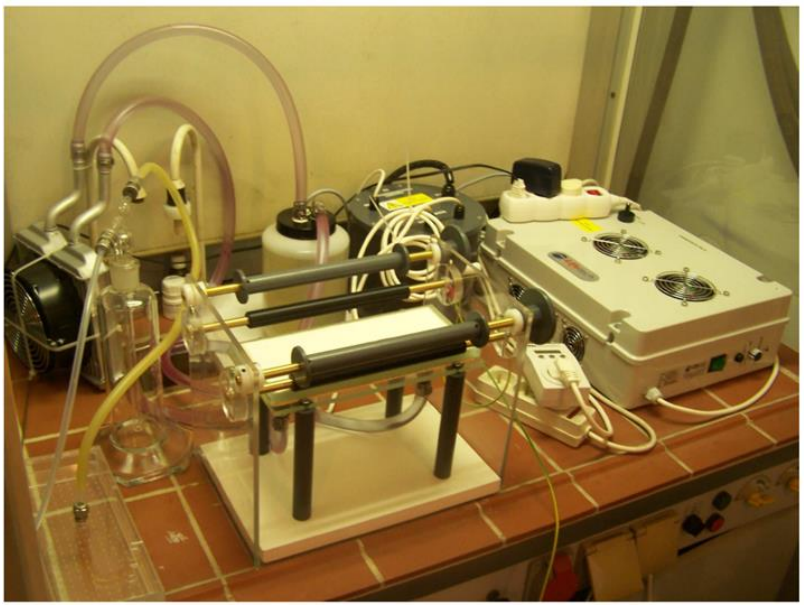

Fig. 3.10. DBD laboratory equipment which used for polymer surfaces treatment

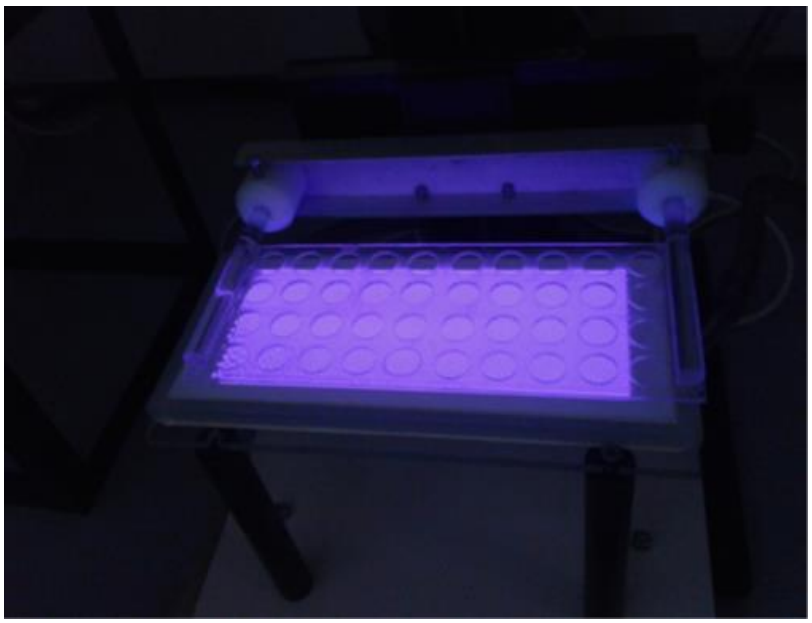

Fig. 3.11. Visual homogenous atmospheric cold plasma in DBD plasma reactor with specimen holder above it

3.3. Surface characterisation

3.3.1. Chemical composition

The X-ray photoelectron spectroscopy (XPS) was carried out on a XSAM 800 spectrometer (Kratos, Manchester, UK, the equipment is available at AKI, MTA) equipped with a non-monochromatic Mg $Ka_{1,2}$ radiation source (1253.6 eV) operating under a fixed analyser transmission mode (chamber pressure<10^{-7} Pa) to investigate the chemical composition of polymer surface (Fig. 3.12). The pass energy was set at 80 eV for survey spectra (wide scan) and at 40 eV for high resolution (detailed) spectra. The wide scan spectra were recorded at 0.5 eV steps in the 50 to 1300 eV energy range while the detailed spectra were recorded at 0.1 eV steps for the respective main elements. As a reference, the C1s line for the hydrocarbon C-H_x component was set to a binding energy of 285 eV. The accuracy of binding energy determination was $\pm$0.2 eV. The data acquisition and processing was performed with the Kratos Vision 2 software, applying a Shirley type background subtraction and decomposition of the peaks using a mixed Gaussian-Lorentzian shape of equal full-width-at-half-maximum. The quantitative analysis of the surface composition was based on integrated peak areas calculated by the XPS MultiQuant program and is expressed in at.-% (Mohai, 2004), using experimentally determined photo-ionisation cross-section data of Evans et al. (1978) and asymmetry parameters of Reilman et al. (1976).

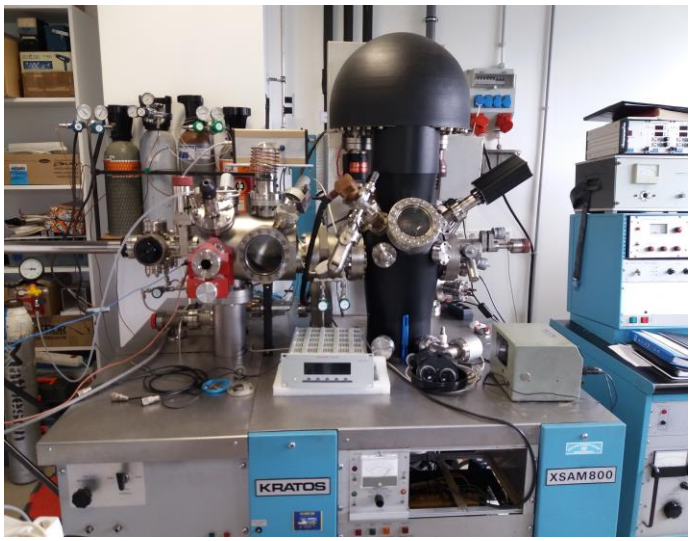

Fig. 3.12. X-ray photoelectron spectrometer (XPS) which used to analyse chemical composition of polymer surfaces

3.3.2. Wettability

For surface energy values (wettability), contact angles were measured by static sessile drops, using the Surface Energy Evaluation (SEE) System apparatus (Advex Instruments, Czech Republic, the equipment is available at AKI, MTA) as shown in Fig. 3.13. Double distilled water and diiodomethane (CH_2I_2) (Sigma-Aldrich, Reagent Plus 99% grade) were used as testing liquids deposited as 2 ml droplets by a Hamilton syringe. The contact angles were measured after stabilisation of the drop shape (typically after 5 sec) and are reported as an average of five measurements with standard deviation. From these measurements, the total surface energy together with polar and dispersive components are calculated following the Owens-Wendt method (Owens, and Wendt, , 1969). The calculations are based on Eqs. 3.1 and 3.2:

$$\sigma_S = \sigma_S^P + \sigma_S^D, \tag{3.1}$$

$$\sigma_L = \sigma_L^P + \sigma_L^D, \tag{3.2}$$

where σ_S is the surface energy of the solid surface, σ_S^P is the polar component of the surface energy of the solid surface, σ_S^D is the dispersive component of the surface energy of the solid surface. The "L" index refers to applying similar and known reference liquid. Two reference droplets of known energy components are using to determine unknown surface energy components of solid where at least the polar component of one one droplet have to be > 0. σ_S^P and σ_S^D are determining by using the known energy relations of two reference droplets, by applying the Eq. 3.3:

$$\frac{\sigma_L(\cos\Theta+1)}{2\sqrt{\sigma_L^D}} = \frac{\sqrt{\sigma_S^P}\cdot\sqrt{\sigma_L^P}}{\sqrt{\sigma_L^D}} + \sqrt{\sigma_S^D}\,. \tag{3.3}$$

Occasionally the literature is using γ symbol instead of σ for the expression of surface energy and its components.

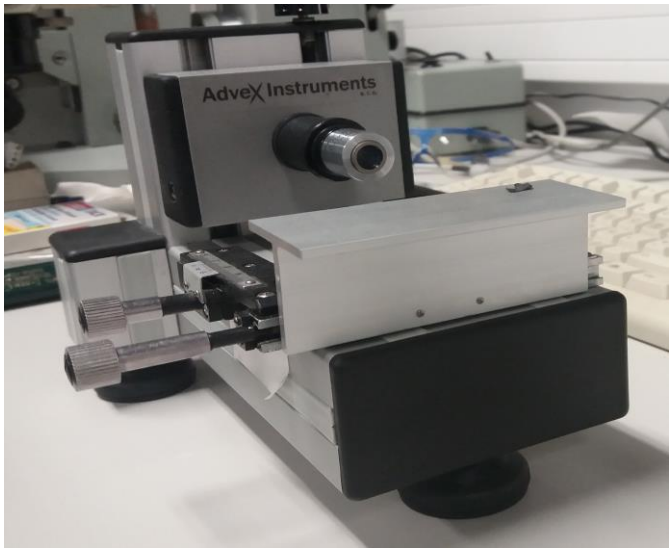

Fig. 3.13. SEE System apparatus which used to evaluate the contact angle of polymer surfaces

3.3.3. Morphology

The surface morphology of extruded polymer surfaces was analysed by scanning electron microscopy SEM (Carl Zeiss EVO, 40 XVP microscope, Germany, the equipment is available at AKI, MTA) as shown in Fig. 3.14 with heated tungsten source. Before the shots, samples were plated by gold to compensate the insulation properties of the plastics and avoid interference with the measurements. SEM resolution is 3 nm at 30 kV(SE and W), and 4.5 nm at 30 kV (BSD - XVP® mode) with 0.2 to 30 kV Acceleration Voltage. The magnification capability is 7 to 1000 000×, the field of view is 6 mm at the Analytical Working Distance (AWD); the X-ray Analysis is 8.5 mm AWD and 35° take-off angle. More details about the used SEM are available in (ZEISS, 2017).

In addition to SEM investigations, the average surface roughness of extruded surface was measured by atomic force microscopy (AFM) (Fig. 3.15). The measurements were performed in ambient condition, at room temperature, in contact mode using multimode AFM (Dimenson 3100 with NanoScope IIIa controller) (Digital Instruments/Veeco, USA) The following parameters were applied: several different scan areas on each sample, scan size 10 μm, scan rate 2 Hz, 512 × 512 pixel images. Silicon nitride cantilevers were used with force constant of 0.12 N m^{-1}. The analysis was performed with Nanoscope 7.30 software.

Fig. 3.14. Scanning electron microscope SEM which used to scan polymer surfaces morphology

Fig. 3.15. Atomic force microscope (AFM) device

3.3.4. Topography

The surface topography was evaluated from non-contact profilometry, using a 3D optical profilometer Coherence Correlation Interferometry (CCI) HD type (Taylor Hobson, Leicester, England, the equipment is available at Soete Laboratory, Ghent University), Fig. 3.16, with an ultra-high precision closed loop piezoless z-scanner having a resolution in z-direction of 0.1 Å. The white light illumination was produced from a Fibre lite DC-950 source and measurements were made at 50% light intensity. A surface area of 330 × 330 μm^2 was imaged by vertical

scanning interferometry, with an objective lens at magnification 50X and numerical aperture= 0.55. The scanning arrays contained 2048 × 2048 pixels with a field-of-view= 330 μm, corresponding to a pixel size of 0.165 μm. The images were processed by Talymap software (Digiserve) to calculate the 3D surface roughness parameters according to ISO 25178, including Sa (average roughness), Sz (maximum height), Sku (kurtosis), and Ssk (skewness) (Deltombe et al., 2014). The roughness values were determined as average from three measurements at independent surface locations, with repeatability Sa<0.2 Å. More details about (CCI) theory and measurements in (Kaplonek and Lukianowicz, 2012).

Fig. 3.16. 3D optical profilometer Coherence Correlation Interferometry (CCI) HD type

3.4. Adhesive testing

Lap-shear tests were done according to DIN EN 1465 on single lap joints of polymer/polymer or polymer/steel pairs (bonded area 25.4 × 12.5 mm= 317.5 mm^2). The pairs were bonded by using the apparatus was specifically designed for this purpose to ensure the accurate overlapping and bonding as shown in Fig. 3.17. The apparatus was made of PTFE to reduce the possibility of specimens sticking to the apparatus (knowing, the low sticking ability of PTFE). The commercial adhesives with a controlled bond line thickness of 0.1 mm were applied in the jig following the manufacturer procedures (Henkel AG & Co., Germany), as Table 3.4 shows. The bonding area was maintained under a constant normal load of 5 N during curing. The prescribed amounts of glue are approximately 0.035 ml of Loctite 406 and 0.1 ml for the other structural adhesives, respectively. The test samples were glued immediately after plasma treatment and stored in aluminum foil until adhesive testing was done. For adhesive testing, the coupons were mounted in a universal mechanical tensile bench (Zwick Roell Z100, max. 100 kN, at Szent István University) and the heads were pulled at 1.3 mm/min following ISO 527-1 standard as shown in Fig. 3.18. The adhesive bonding force was determined as the maximum load on failure of the bond, and the adhesive shear strength was calculated as the average of five repeated measurements of force at failure per bonded surface area.

Table 3.4. Materials and adhesives plan for the adhesive bonding test (according to manufacturer's Technical Data Sheet (TDS) recommendations)

Engineering polymers		
Pair	**Adhesive**	**Primer / Activator**
PEEK-PEEK	Superglue: Loctite 406	-
	Structural adhesive: Loctite 9466 (Epoxy)	-
	Structural adhesive: Multibond 330	-
PEEK-S235 steel	Superglue: Loctite 406	-
	Structural adhesive: Loctite 9466 (Epoxy)	-
	Structural adhesive: Multibond 330	-
PET-PET	Superglue: Loctite 406	-
	Superglue: Loctite 406	-
	Structural adhesive: Loctite 9466 (Epoxy)	-
	Structural adhesive: Multibond 330	-
PET-S235 steel	Superglue: Loctite 406	-
	Structural adhesive: Loctite 9466 (Epoxy)	-
	Structural adhesive: Multibond 330	-
PA6-E–PA6-E	Superglue: Loctite 406	-
	Structural adhesive: Loctite 9466 (Epoxy)	-
	Structural adhesive: Multibond 330	-
PA6-E–S235 steel	Superglue: Loctite 406	-
	Structural adhesive: Loctite 9466 (Epoxy)	-
	Structural adhesive: Multibond 330	-
POM-C–POM-C	Superglue: Loctite 406	Primer: Loctite 770
	Structural adhesive: Loctite 9466 (Epoxy)	-
	Structural adhesive: Multibond 330	-
POM-C–S235 steel	Superglue: Loctite 406	Loctite 770 only on POM-C
	Structural adhesive: Loctite 9466 (Epoxy)	-
	Structural adhesive: Multibond 330	-
Polyolefin polymers and PTFE		
Pair	**Adhesive**	**Primer / Activator**
PP-PP	Superglue: Loctite 406	Primer: Loctite 770
	Structural adhesive: Loctite 3035	-
PP-S235 steel	Superglue: Loctite 406	Loctite 770 only on PP
	Structural adhesive: Loctite 3035	-
PE HD1000-PE HD 1000	Superglue: Loctite 406	Primer: Loctite 770
	Structural adhesive: Loctite 3035	-
PE HD1000-S235 steel	Superglue: Loctite 406	Loctite 770 only on PE HD 1000
	Structural adhesive: Loctite 3035	-
PE HD500-PE HD500	Superglue: Loctite 406	Primer: Loctite 770
	Structural adhesive: Loctite 3035	-
PE HD500-S235 steel	Superglue: Loctite 406	Loctite 770 only on PE HD 500
	Structural adhesive: Loctite 3035	-
PTFE-PTFE	Superglue: Loctite 406	Primer: Loctite 770
	Structural adhesive: Loctite 3035	-
PTFE-S235 steel	Superglue: Loctite 406	Loctite 770 only on PTFE
	Structural adhesive: Loctite 3035	-

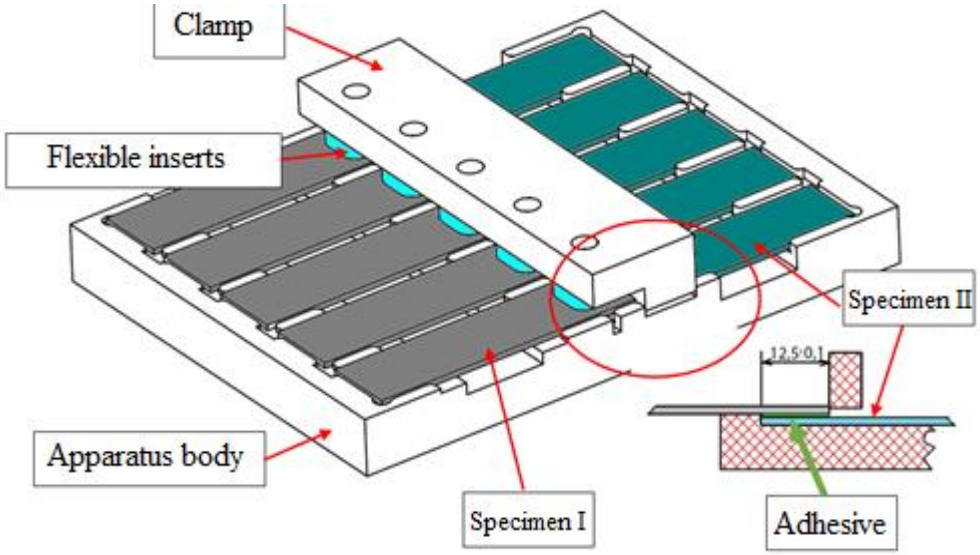

Fig. 3.17. Scheme of apparatus which used to bond the specimens during curing

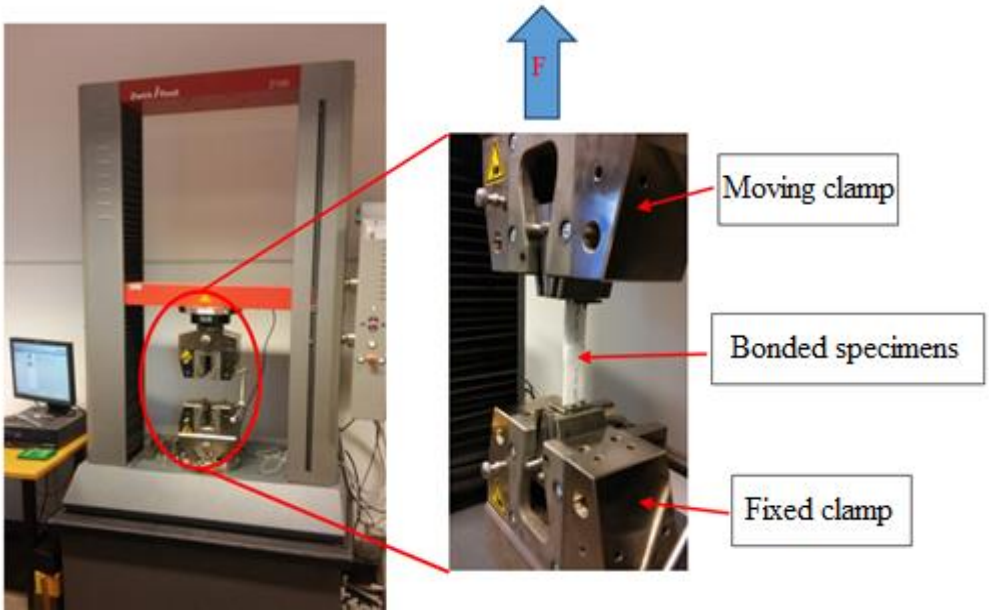

Fig. 3.18. Zwick Roell Z100 tensile machine with polymer pair

The Marking System of Pairs for Adhesive Bonding Tests

The different combinations of specimens have to be distinguished; therefore, the following identification has been introduced, for instance, PA6-E/PA6-E pair is marking as below:

$$0^{(1)}\_PA6\text{-}E^{(2)}\_PA6\text{-}E^{(3)}\_406^{(4)}\_11^{(5)}\_1^{(6)}$$

- Marking (1): It indicates the condition of the surface (0- pristine surface without plasma treatment, 1- treated surface),
- Marking (2 and 3): refer to the conjugated materials (polymer type or steel),
- Marking (4): refers to the type of adhesive,
- Marking (5): refers to the utilising of the activator (If 11means activator was utilised for both surfaces, 00 not one of them, 10, 01–only one surface),
- Marking (6): refers to the serial numbers of the specimen in the bonding test (from 1 to 5).

3.5. Tribological testing

The tribological tests were done on a pin-on-disc configuration according to the VI. wear test category of the German standard DIN 50322 using a dynamic tribotester constructed at Szent István University shown in Fig. 3.19, with polymer pin (diameter 10 mm, thickness 4 mm) mounted in a stationary holder and loaded against a rotating steel counterface (disc diameter 100 mm, thickness 12 mm). The counterfaces of standard and non-alloy steel with low carbon content (0.17 %) and tensile strength= 400-500 N/mm2, grade S235 (Ferroglobus Ltd., Hungary) were applied for both adhesive and tribological testing. A homogeneous and parallel contact area is assured by aligning the polymer pin with a small bearing ball at the top and fixing it with a needle to avoid rotation during sliding as shown in Fig. 3.20. The polymer pin is mechanically loaded against the steel counterface through a dead-weight loading system. The radius of the frictional track can be selected by the position of the cross guiding rail and is fixed at 40 mm for each experiment. The friction force is measured from the bending moment induced to the pin under sliding and recorded by strain gauges. The wear is characterised by the drop-in height of the polymer specimen and is measured as the vertical displacement of the pin holder with a contactless proximitor. The temperature rise is measured by a thermocouple introduced in the polymer pin at 1 mm above the contact zone (i.e., the polymer bulk temperature). During testing, the friction coefficient μ, the vertical displacement (Δh= wear + deformation) and the temperature *T* are continuously monitored. The tribological results are calculated as an average of three repeated measurements. Two testing protocols were followed to study the sliding under mild conditions:

- sliding tests under "dry" conditions were performed by applying a sliding velocity v= 0.05 m/s and stepwise increasing contact pressures p= 0.5, 1, and 2 MPa (i.e., *pv*-conditions 0.025, 0.05 and 0.1 MPa.m/s) over a sliding distance of 60 m (i.e., sliding time 20 min) for each load. The applied time per load level was experienced as sufficient to establish steady state sliding conditions. The total sliding distance was 180 m (i.e., total sliding time of 60 min),
- sliding tests under "run-out" lubrication conditions were performed, using commercial gearbox oil (SAE 80W90): a drop of oil (10 ml) was added onto the steel disc through a pipette in front of the polymer contact zone during a first sliding period (0.5 m distance), followed by the automatic cleaning of the lubricant layer by wiping the sliding track on the steel surface with a sponge during a second sliding period (9.5 m distance) (Fig. 3.21). As such, (i) the first period of sliding corresponds to an oil-lubricating regime, while (ii) the second period of sliding is representative for a mixed or boundary lubrication regime, although the exact thickness of the lubricating oil film has not been further assessed due to its permanent change in thickness over time. The tests were run under a sliding velocity v= 0.05 m/s, contact pressure p= 0.5 MPa (i.e, *pv*-condition 0.025) and total sliding distance 10 m.

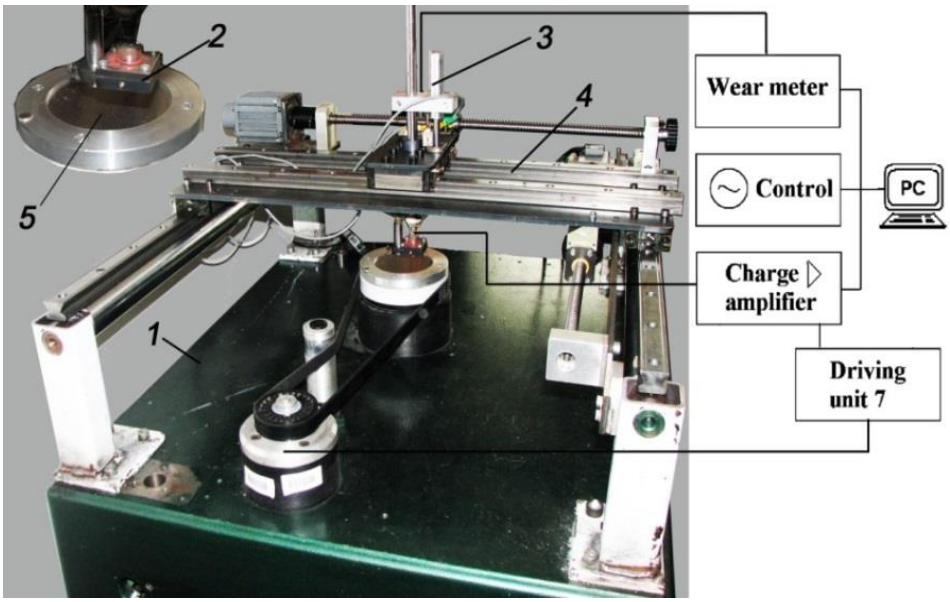

Fig. 3.19. Experimental set-up of the Pin on Disc tribotester: 1) base frame, 2) Pin holder, 3) loading head, 4) positioning rail, 5) rotating steel disc

Fig. 3.20. The specimen holder and polymer pin configurations

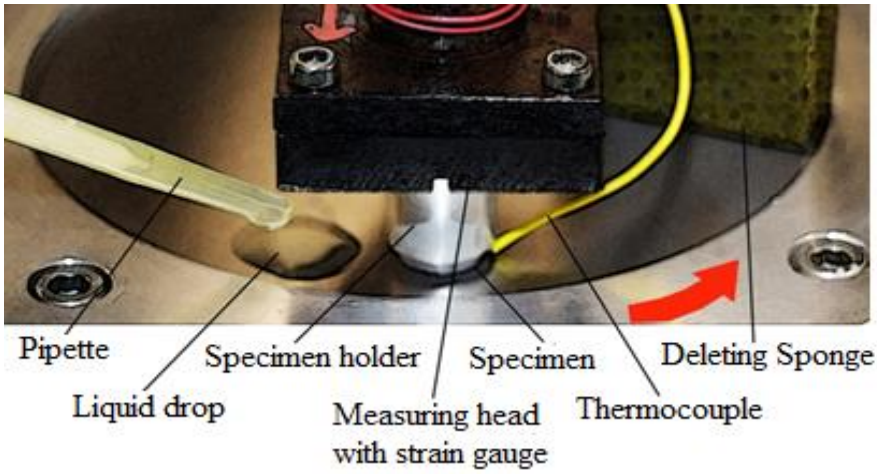

Fig. 3.21. “Run-out” oil lubrication testing.

4. RESULTS

The present chapter displays the achieved results and their discussion implying a highlight of the new scientific findings. The results include polymers surface characterisation, adhesive bonding and tribological tests for pristine and plasma-treated surfaces.

4.1. Surface characterisation

Surface characterisation is done according to the surface chemical composition, wettability, morphology, and topography which control the latter polymer's behaviour in adhesive and tribological measurements.

4.1.1. Chemical composition

Engineering polymers:

The changes in chemical surface composition after plasma treatment were monitored by XPS analysis of engineering polymer surfaces. The wide-scan spectra indicated three characteristic peaks at 285.0 eV (C1s), 533.2 eV (O1s), and 400.4 eV (N1s). The elemental composition (at.-%) before and after plasma treatment was calculated from high-resolution XPS spectra (Table 4.1). The presence of nitrogen on the pristine samples of some polymers presumably results during the preparation of the materials where the nitrogen atoms are covalently bonded to the carbon chain. After plasma treatment, the oxygen content has increased and carbon content has decreased (see ratio *n*O/*n*C), while some more atmospheric nitrogen may have further reacted with the activated surface of PEEK, PET and PA6-E whereas there is no presence of nitrogen can be observed on POM-C surfaces before and after treatment. The slight increase in nitrogen has been observed previously for some polymers due to atmospheric plasma jet such as PA6 and PET (Noeske et al., 2004) also in case of laser surface modification and is typically ascribed to the combination with oxygen at the surface (Wilson et al., 2015).

The elemental composition (at.-%) corresponding to the different components (C1, C2, C3, C4) for the C1s carbon peak and components for the O1s oxygen peak and N1s nitrogen peak were further analysed from high-resolution XPS spectra, comparing theoretical calculations with values for pristine and plasma-treated (Fig. 4.1). The XPS spectra agree with literature data for PET (Doren et al., 1994), PEEK (Louette et al., 2005), PA6 (Wei et al., 2005), and POM (Grimblot et al., 2000) and clearly show a different state of chemical surface composition after plasma treatment. The surface of pristine polymers is contaminated with a hydrocarbon layer that is typical for each polymer stored in ambient conditions and efficiently removed after plasma treatment. In addition, the variations in chemical states of carbon and oxygen are detected after plasma treatment, which might relate to surface destruction. For PEEK and PET, the C1 (285.0 eV) state of carbon [C-C, C-H] has decreased in parallel with the decrease in C2 (286.0 eV) state of carbon [C-O] and C3 (288.7 eV) state of carbon [C=O, O-C-O], while the C4 (289.5 eV) state of carbon [O-C=O] only appeared after plasma treatment of PEEK: the latter can typically be attributed to the formation of carboxylic acid and ester bonds by oxidation in parallel with the scission of bonds in the backbone polymer due to the energy input by plasma treatment. The increase in O-C=O groups and the decrease in C-O groups suggest a replacement of the original C=O groups of the PEEK structure with new carboxylic acid groups at the chain ends. For PA6-E, the C1 (285.0 eV) state of carbon has decreased, while C2 (286.0 eV) state of carbon and C3 (288.7 eV) state of

carbon, and the C4 (289.5 eV) state of carbon have increased in parallel after plasma treatment. In the same context, POM-C's state of carbon [C-H] decreases in parallel with the increase of [C-CO]. The components in high-resolution O1s spectra confirm the previous trends with a reduction in intensity for peaks at 531.2 eV [C=O] and higher intensity for peaks at 533.2 eV [C-O] due to surface degradation and creation of carboxylic acids. Ketone groups for PEEK and PET are oxidised and eliminated and after or parallel new OH groups are developed; both in oxidative reactions. The same increase was detected for oxygen content of PA6-E and POM-C with an appearance of O2 for PA6-E after DBD treatment. As a result, the relative carbon content decreased with a parallel increase in overall oxygen content. This is in agreement with reports where a surface layer of water-soluble low molecular weight oxidized polymer material had formed after DBD treatment (Kostov et al., 2013). In parallel, the nitrogen-containing functionalities such as N-COO or OC-N-CO can be detected in minor amount for PEEK, PET and PA6-E. In conclusion, the formation of polar groups containing oxygen on the surface can contribute to a hydrophilic improvement after plasma treatment.

Table 4.1. Elemental composition of pristine and plasma-treated engineering polymer surfaces determined from high-resolution XPS spectra

Sample		O (at.-%)	C (at.-%)	N (at.-%)	*n*O/*n*C
PEEK	Theoretical	13.63	86.35	0	0.158
	Untreated	25.3	73.4	1.4	0.345
	Plasma-treated	27.2	70.6	2.2	0.385
PET	Theoretical	28.58	71.44	0	0.4
	Untreated	31.6	68.4	0	0.462
	Plasma-treated	36.2	62	1.9	0.584
PA6-E	Theoretical	12.5	75	12.5	0.167
	Untreated	12.8	74.5	12.5	0.172
	Plasma-treated	20.3	66.6	13.1	0.305
POM-C	Theoretical	50	50	0	1
	Untreated	39	60.9	0	0.64
	Plasma-treated	46.5	53.5	0	0.869

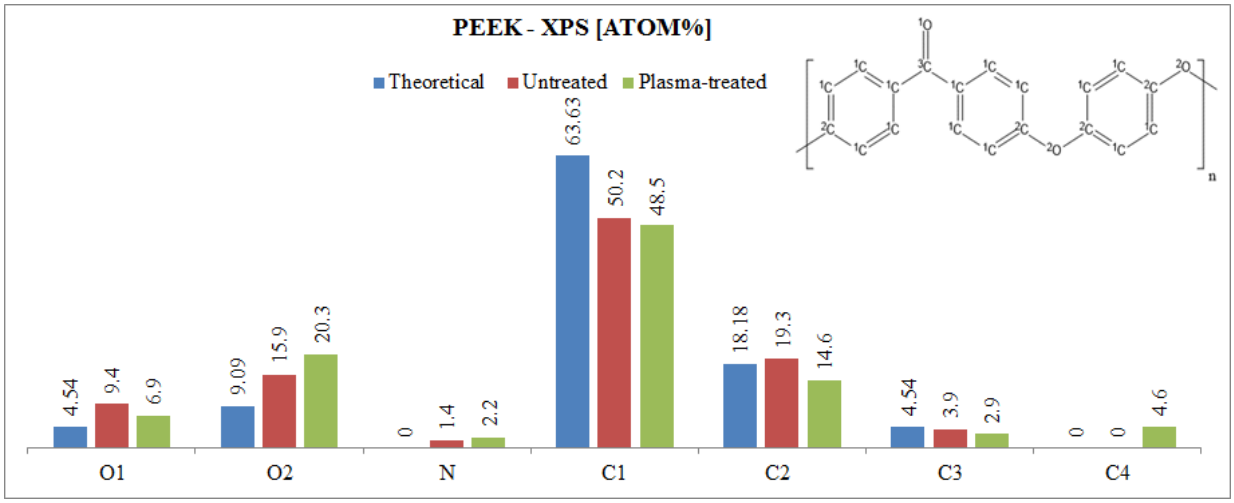

a) Continued

(Continued)

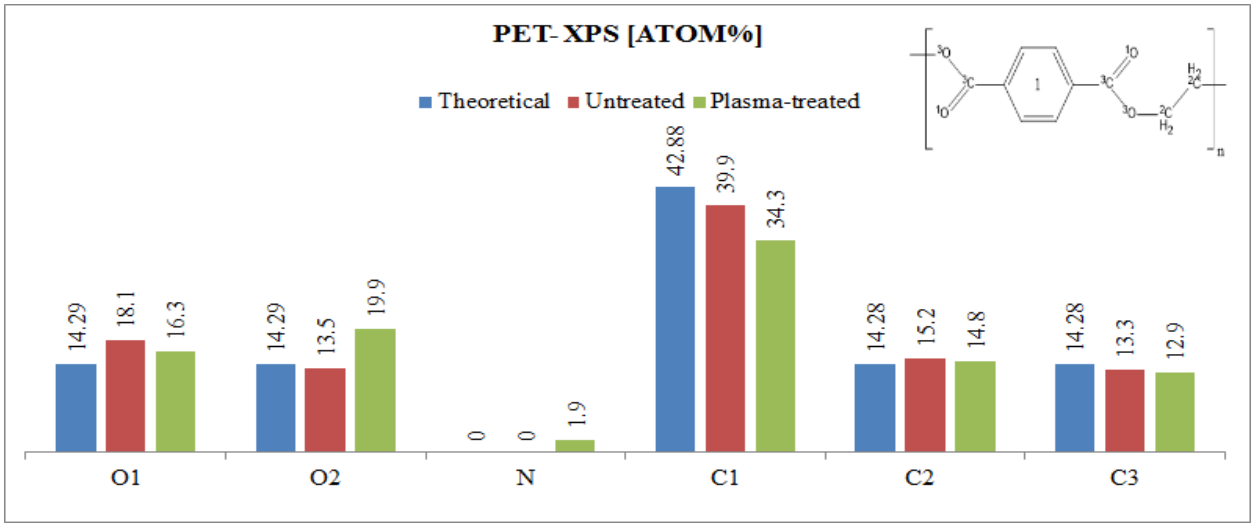

b)

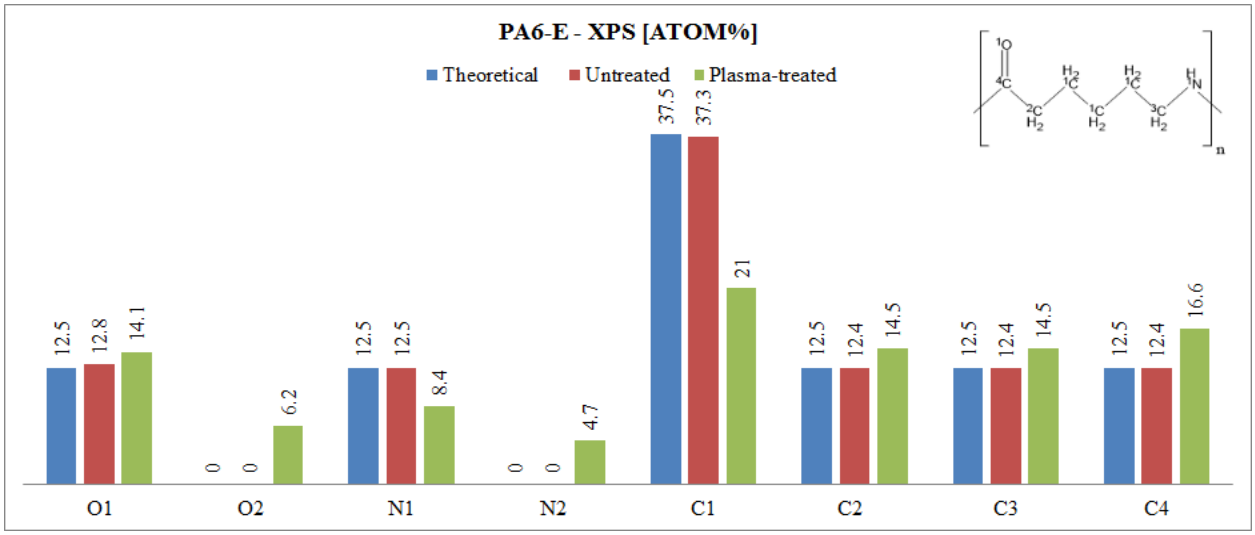

c)

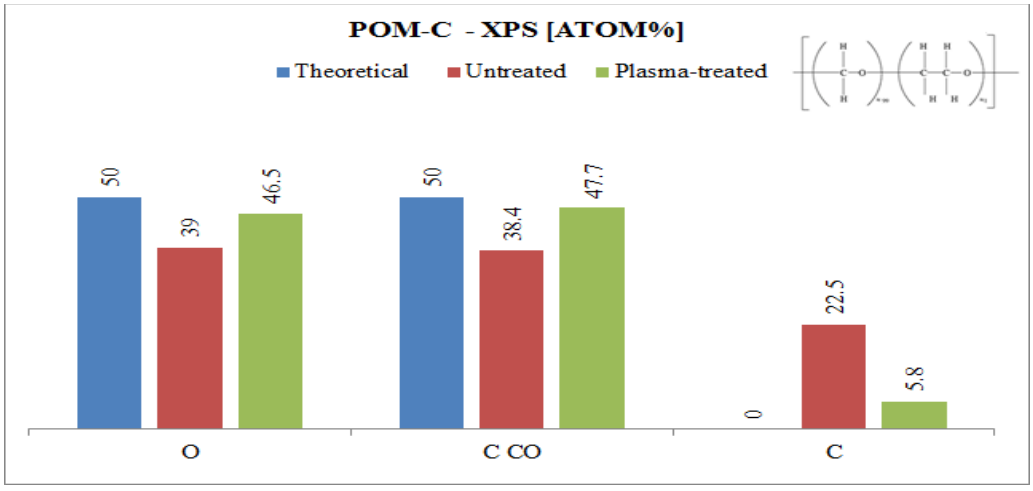

d)

Fig. 4.1. Analysis of elemental composition from high-resolution XPS spectra: a) PEEK, b) PET, c) PA6-E, and d) POM-C

Polyolefin polymers and PTFE:

The elemental composition (at.-%) before and after plasma treatment was calculated from high-resolution XPS spectra (Table 4.2 for polyolefin polymers). The high resolution XPS analysis of C1s, O1s and N1s spectra were analysed to determine the ratio of the various polar groups developed on the surface, comparing theoretical calculations with values for pristine and plasma-treated as shown in Fig. 4.2. As unavoidable surface contamination, a small amount of oxygen and nitrogen could be detected on the pristine polyolefin polymer surfaces. Upon plasma treatment, the oxygen content increased with the parallel decrease of the carbon content indicated by the changes of *n*O/*n*C atomic ratios. This suggesting incorporation of oxygen-containing polar groups into the surface that provides reason to the better wettability. In the C1s spectra of untreated polyolefin polymers, the peak at 285.0 eV suggests that the majority of carbon is in C-C and C–H bonding state. A tiny peak at 287.5 (labelled as C3) can be attributed to C-N and O-C-O bonds. The plasma treatment could effectively break up primarily the C-H, and C-C bonds, decreasing the corresponding C1 peak down to 17 at.-%, 46 at.-% and 48 at.- % for PP, UHMW-PE HD500, and UHMW-PE HD1000 respectively. While component peaks at 286.4, 288.2 and 289.3 eV indicating formation of new functional groups such as hydroxyl (OH), carbonyl (C=O), and carboxylic acid (O=C-O). These results are agreed with many earlier findings such as (Bertóti et al., 2015; Kostov et al., 2014a; Noeske et al., 2004), even though different cold plasma methods performed surface modification. In parallel, new nitrogen containing groups, such as OC-N, OC-N-CO, could also be detected in minor quantity by XPS due to the activated surface after treatment.

The elemental composition of pristine PTFE surface is pretty close to the theoretical one (Table 4.3), while the *n*F/*n*C atomic ratio significantly decreases after plasma treatment which proves the significant defluoronization ability of DBD plasma, same results was mentioned in a previous work for PTFE treated by DBD plasma (Williams et al. 2013). Although the oxygen content also changed, the moderate increase suggests a limited build-up of oxygen containing groups, comparing to other polymers. The C1s spectrum of pristine PTFE consists of practically a single peak at 292.5 eV that is attributed to -CF2- bonds. The lower binding energy region of the spectrum can be decomposed into several peaks with rather low intensity, indicating a negligible amount of other components. Upon plasma treatment, the intensity of the peak at 292.5, corresponding to -CF2- bonds significantly decreased. In parallel, peaks in the 286-290 eV range are increased due to the formation of various CF species with reduced F content. The peak at 289.8 eV can be attributed to -CF- bonds, while peaks at 287.9 eV and 286.4 eV correspond to C-CF and C-CF2 groups, indicating that DBD plasma treatment could break the CF2 bonds. The peak at 286.4 eV could also refer to C-O bonds, although their contributions cannot be distinguished due to the low oxygen content. Finally, we can say that atmospheric DBD plasma can produce oxidizing carbon atoms and forming polar groups containing oxygen on all studied polymer surfaces. However, engineering polymers were recorded higher percentage compared to polyolefin polymers, while PFTE has the lowest content of polar groups after plasma treatment.

Table 4.2. Elemental composition of pristine and plasma-treated polyolefin polymer surfaces determined from high-resolution XPS spectra

Sample		O (at.-%)	C (at.-%)	N (at.-%)	*n*O/*n*C
PP	Theoretical	0	99.93	0	0
	Untreated	5.3	94.7	0	0.056
	Plasma-treated	23.6	74.6	1.7	0.316
PE HD500	Theoretical	0	100	0	0
	Untreated	7.8	90.7	1.5	0.086
	Plasma-treated	24.9	71.4	3.7	0.349
PE HD 1000	Theoretical	0	100	0	0
	Untreated	7.2	91.2	1.6	0.079
	Plasma-treated	23.8	73.2	3	0.325

Table 4.3. Elemental composition of pristine and plasma-treated PTFE surfaces determined from high-resolution XPS spectra

	O (at.-%)	C (at.-%)	F (at.-%)	*n*F/*n*C	*n*O/*n*C
Theoretical	0	33.3	66.6	2	0
Untreated	0.5	31.5	68	2.159	0.016
Plasma-treated	0.8	37.2	62.3	1.675	0.022

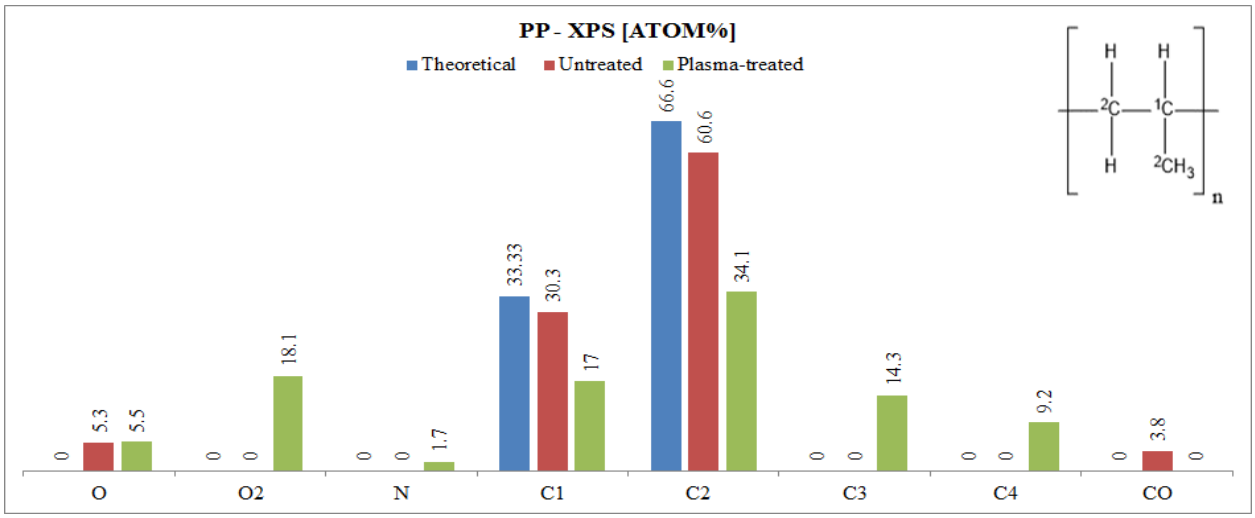

a) Continued

(Continued)

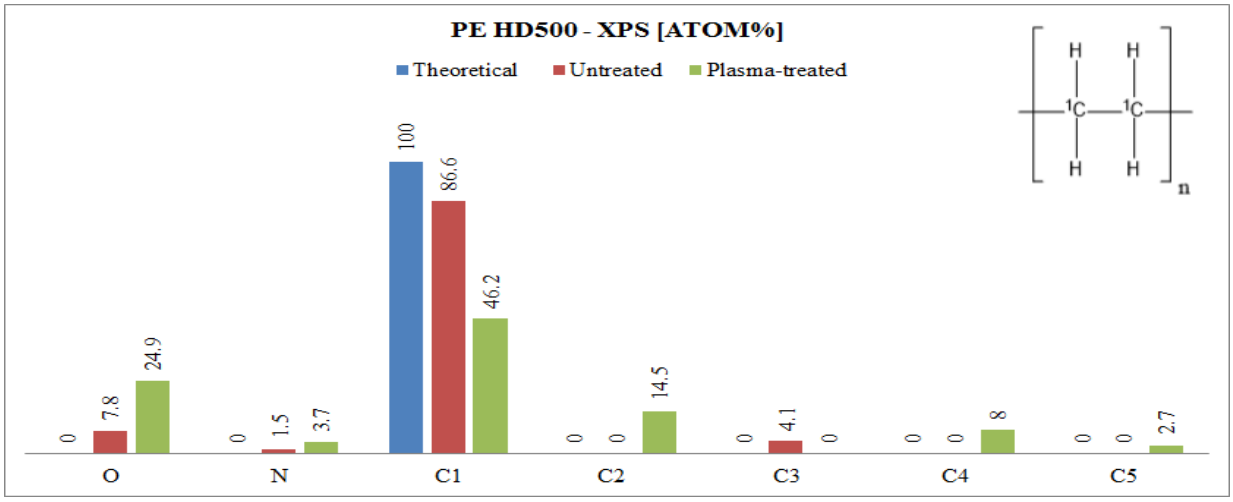

b)

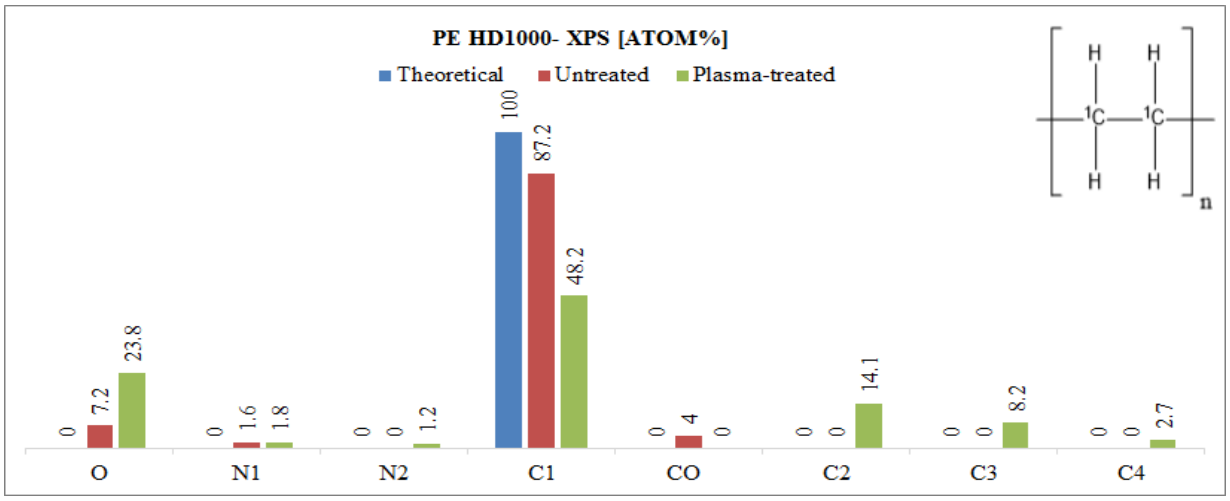

c)

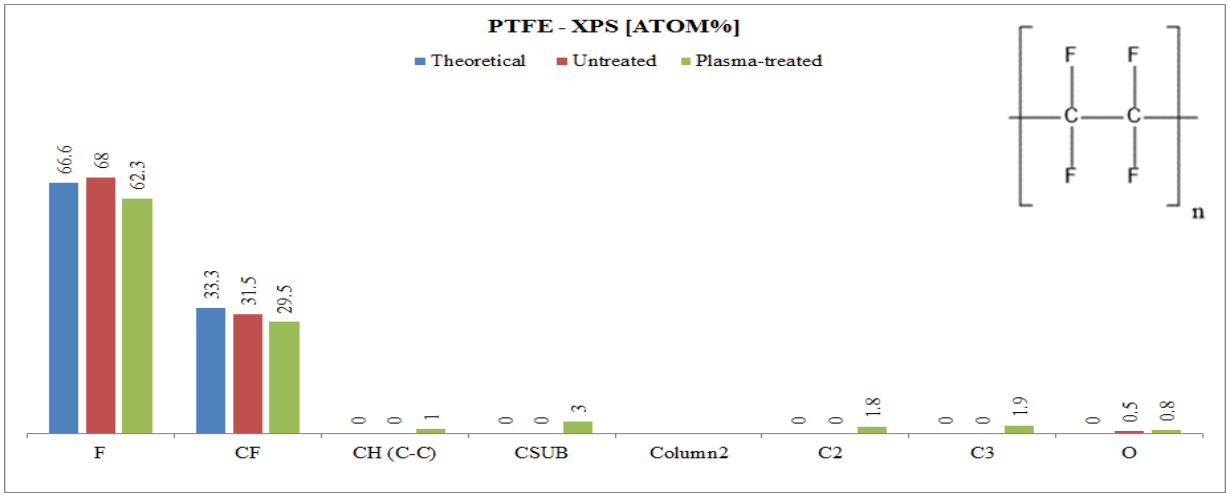

d)

Fig. 4.2. Analysis of elemental composition from high-resolution XPS spectra: a) PP, b) UHMW-PE HD500, c) UHMW-PE HD1000, and d) PTFE

4.1.2. Wettability

The contact angle values of water (γ_w) and diiodomethane (γ_{CH2I2}) together with calculated surface energies of pristine and plasma-treated samples (after 24 h and 80 days) are summarised in Table 4.4, including total surface free energy (γ_{tot}) with its polar component (γ_{polar}) and dispersive component (γ_{disp}). The contact angles and surface energies for pristine engineering polymers also UHMW-PE HD500, and UHMW-PE HD1000 are very similar due to their comparable chemical composition. After plasma treatment, the contact angle of all polymers decreases (Fig. 4.3) and the surface energy increases mainly due to an increase in polar component engineering polymers: PEEK 332%, PET 315%, PA6-E 360%, and POM-C 250%; polyolefin polymers and PTFE: PP 17700%, UHMW-PE HD500 854%, UHMW-PE HD1000 1200%, and PTFE 3650%). Polyolefin polymers and PTFE were observed a higher increase in surface polarity after treatment rather due to their hydrophobicity (although UHMW-PE polymers have lower contact angle than 90°, they are considered as hydrophobic) thereby low surface energy in the initial state. However, engineering polymers have higher surface energy after treatment due to their high surface energy in the initial state. The dispersive component slightly increases or remains almost constant for engineering polymer while moderately increases for polyolefin polymers. However, PTFE was observed the highest increase in dispersive component (46%).

The higher surface wettability after plasma treatment is in line with the presence of polar functional groups at the surface, as confirmed by the previous XPS data. The higher hydrophilicity of polymer surfaces after DBD plasma treatment is a common feature (Kostov et al., 2014b) in particular for polyolefin polymers and PTFE (Dixon and Meenan, 2012). The plasma treatment effect is abating in long terms as it is indicated by the slight increase of the WCA toward values corresponding to the original surface state concerning the days passed after treatment. This phenomenon was commonly found for plasma treated polymers and was attributed to the chemical instability of the surface modification and the reorientation of polymer chains. The rate of aging can greatly vary and is affected by various factors such as the type of polymer, the applied plasma process, treatment time, etc. (Novák et al., 2014). Restoration of the structure starts quite rapidly, and the most significant change in the contact angle occurs within 24 h, the increased WCA remained well below that of the pristine polymer even after 80 days. From an application point of view, the obtained results suggest that any planned follow up processing step (e.g., functionalizing, dyeing, employing adhesives) on these polymers shall be carried preferably within 24 h.

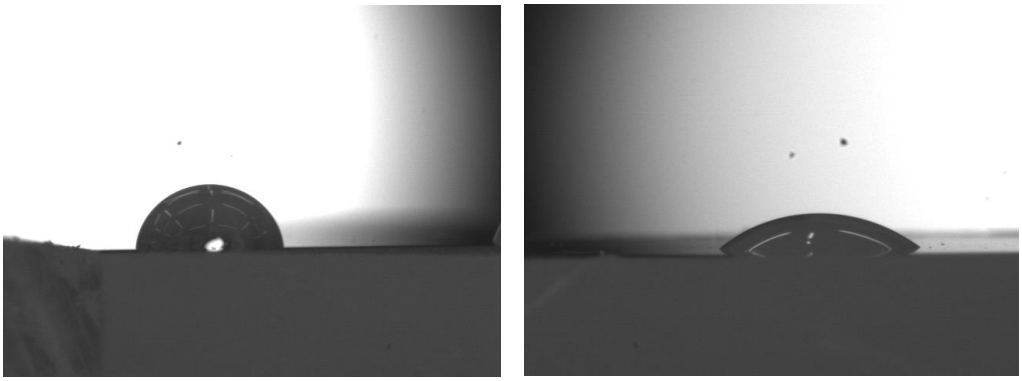

Untreated Treated

Fig. 4.3. Water contact angle of PA6-E before and after plasma treatment

Table 4.4. Surface energy of pristine and plasma-treated polymer surfaces (after 24 h and 80 days) determined from contact angle measurements (Owens-Wendt method)

Engineering polymers						
Sample		θ_w **(deg)**	θ_{CH2I2} **(deg)**	γ_{pol} **(mJ/m^2)**	γ_{disp} **(mJ/m^2)**	γ_{tot} **(mJ/m^2)**
PEEK	Untreated	70±1.5	30±6.4	6.1	44.3	50.4
	Treated (24 h)	29±2.2	29±3	26.4	44.9	71.3
	Treated (80 day)	48±3	35±2	17.4	40.1	57.5
	Δ 24h/80 day %			332/-34	1.4/-10	41/-19
PET	Untreated	71±3.3	32±3.1	6.1	43.4	49.5
	Treated (24 h)	30±2.7	24±0	25.3	46.6	71.9
	Treated (80 day)	45±2.7	34±1.7	19.7	42.4	62.1
	Δ 24h/80 day %			315/-22	7.5/-9	23/-14
PA6-E	Untreated	70±7.2	32±2.1	6.3	43.6	50.0
	Treated (24 h)	21±0.5	26±1.5	29.1	45.8	74.9
	Treated (80 day)	45±5.6	27±0.6	18	45.4	63.4
	Δ 24h/80 day %			360/-38	5/-1	50/-15
POM-C	Untreated	73±4.2	32±2.1	5.2	43.6	48.8
	Treated (24 h)	43±4.2	20±3.2	18.2	48.0	66.1
	Treated (80 day)	56±5.1	23±1.3	11.8	46.8	58.6
	Δ 24h/80 day %			250/-35	10/-2.5	35/-11
Polyolefin polymers and PTFE						
Sample		θ_w **(deg)**	θ_{CH2I2} **(deg)**	γ_{pol} **(mJ/m^2)**	γ_{disp} **(mJ/m^2)**	γ_{tot} **(mJ/m^2)**
PP	Untreated	101±6.9	52±2.6	0.1	33.4	33.5
	Treated (24 h)	51±9.9	41±1.6	17.8	39.1	56.9
	Treated (80 day)	62±2.2	55±2.3	14.4	31.6	46
	Δ 24h/80 day %			17700/-19	17/-19	67/-19
PE HD500	Untreated	83±1.8	38±3.3	2.4	40.7	43.1
	Treated (24 h)	36±2.4	29±2.7	22.9	44.9	67.7
	Treated (80 day)	50±3.6	47±2	19.6	35.7	55.4
	Δ 24h/80 day %			854/-14	10/-20	57/-18
PE HD1000	Untreated	87±0.4	47±1.9	1.9	36.2	38.1
	Treated (24 h)	35±2.3	35±5.8	24.7	42.2	67
	Treated (80 day)	53±4.6	43±6.1	16.8	38.2	55
	Δ 24h/80 day %			1200/-32	17/-9.5	76/-18
PTFE	Untreated	108±1.5	73±3.2	0.2	21.2	21.5
	Treated (24 h)	75±1	56±1	7.5	30.9	38.4
	Treated (80 day)	98±16	75±7.1	2.1	20.2	22.3
	Δ 24h/80 day %			3650/-72	46/-35	79/-42

4.1.3. Morphology

The morphology of polymer surfaces was studied by scanning electron microscopy SEM from several positions for each polymer surface. Surface morphology has been examined for extruded polymer surfaces later have used for adhesive bonding tests. The magnitude of magnification was assigned depending on which level the surface morphology change can be detected. In spite of small parallel scars, and spherical surface impurities can be visible, the pristine surface of PEEK runs mostly smooth. However, there is some tiny unevenness on the right-hand side of the surface which gives a rough pattern (Fig. 4.4 left). On plasma treated sample, there are small areas formed on the molten surface, while the small parallel scars disappeared (sample orientation and measuring site were almost identical). The tiny small spheres and the brighter area in the upper right corner are made of more significant amounts of oxidised materials (Fig. 4.4 right).

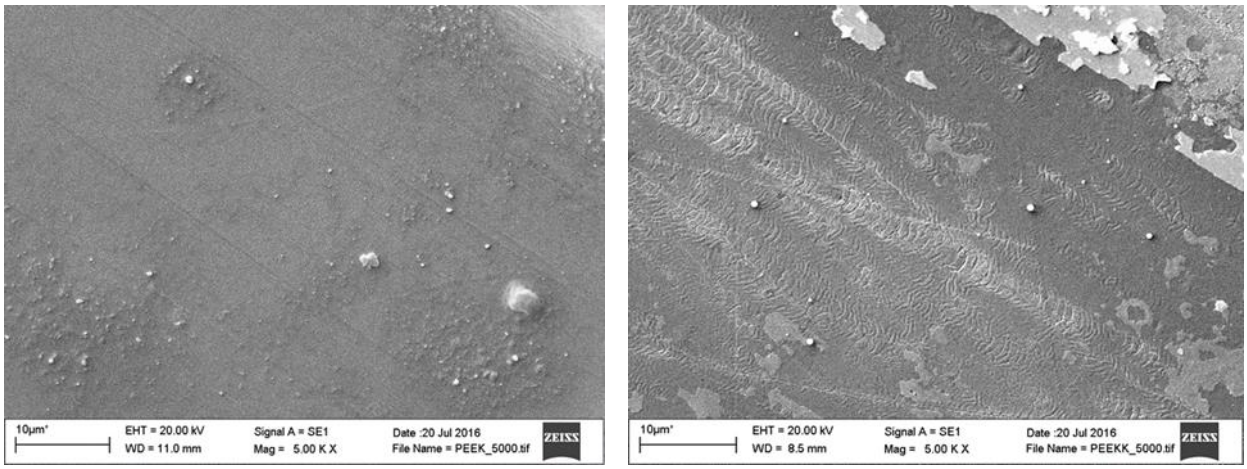

Fig. 4.4. Surface morphology of PEEK from scanning electron microscopy SEM, left: untreated, right: treated (5000X magnification)

Compared to the flat untreated PET sample, PET has many small grooves after the plasma treatment. Their width is small, and the low contrast indicates that their depth is not significant (Fig. 4.5).

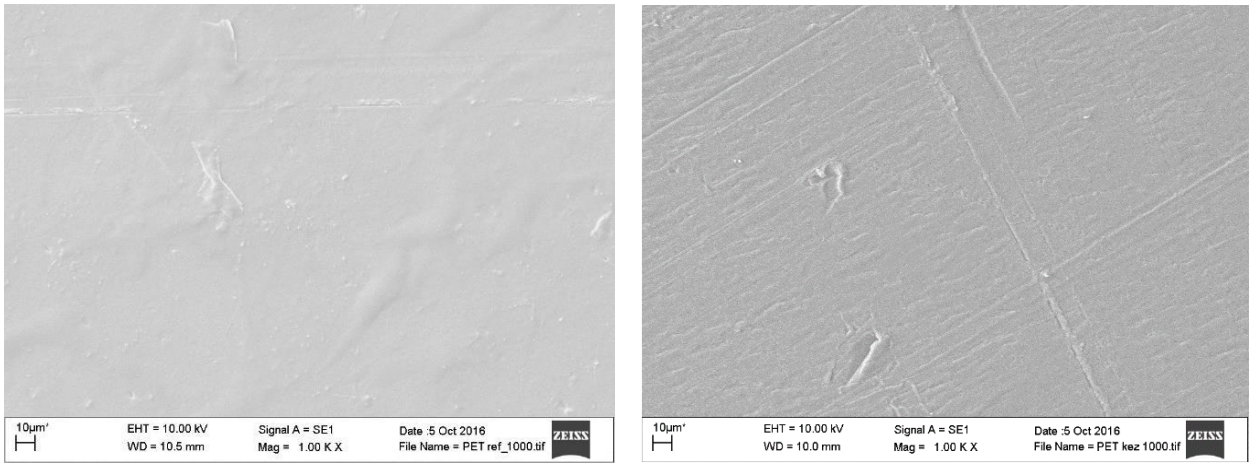

Fig. 4.5. Surface morphology of PET from scanning electron microscopy SEM, left: untreated, right: treated (1000X magnification)

In spite of smaller and larger scars, PA6-E untreated sample shows a more coherent surface at 1000X magnification, while many small trenches appear on the surface as a result of plasma treatment (Fig. 4.6) In addition, it is noted that the edges of scars running on the surface have become irregular and randomly widened, their edges being more exposed to the effect of the treatment. The trenches are divided into two groups of magnitudes ≈ 1 micron, and 5-10 microns are also visible.

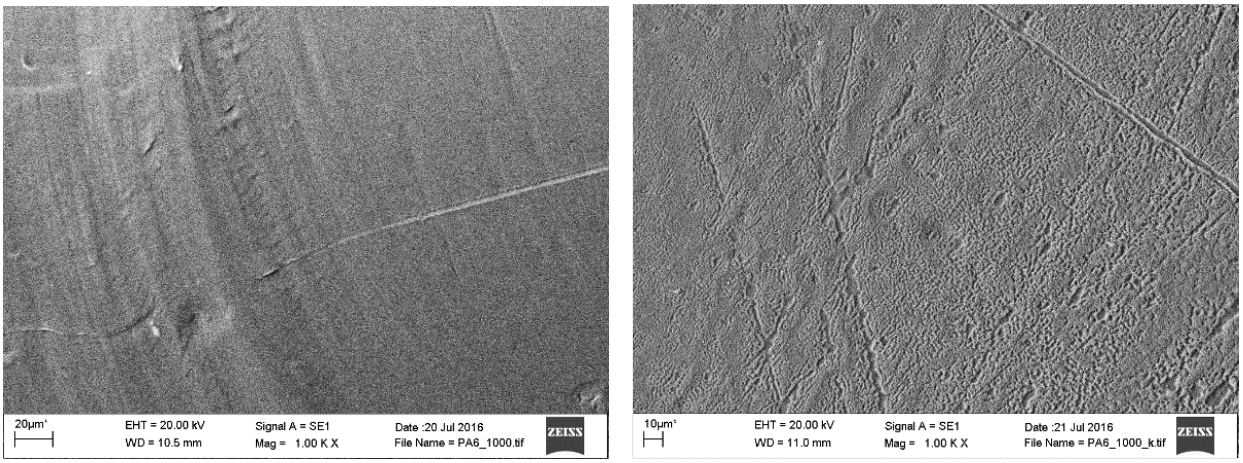

Fig. 4.6. Surface morphology of PA6-E from scanning electron microscopy SEM, left: untreated, right: treated (1000X magnification)

As seen on the 5000X magnification of PA6-E sample (Fig. 4.7), the surface formed trenches contain further smaller pores (5000X magnification) which provide rougher surface. From this, it can be concluded that plasma treatment concentrates on certain points although it has a degrading effect on the entire surface. This structure is not similar to the initial sample, so some other effect can control this process, such as the ratio of amorphous crystalline phases. Oxidised materials were formed as well which are seen as bright areas on the right side of the image.

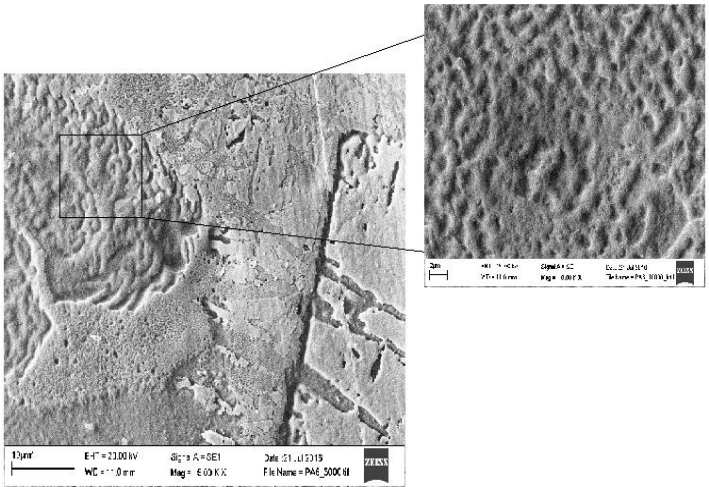

Fig. 4.7. Surface morphology of plasma treated PA6-E from scanning electron microscopy SEM (5000X and 15000 magnification)

It is clear that the DBD plasma treatment caused substantial changes on POM-C surface morpholgy, with a few small scratches and deep grooves (Fig. 4.8), which are almost parallel. For pristine sample, there are tiny dense trenches. (black square, Fig. 4.8 left). The trenches themselves

and their edges could provide a better attack surface for plasma, but their location cannot be related to the random orientation of the grooves after treatment. The plasma-treated sample grooves are noticeably irregular, deep, and slightly hollow.

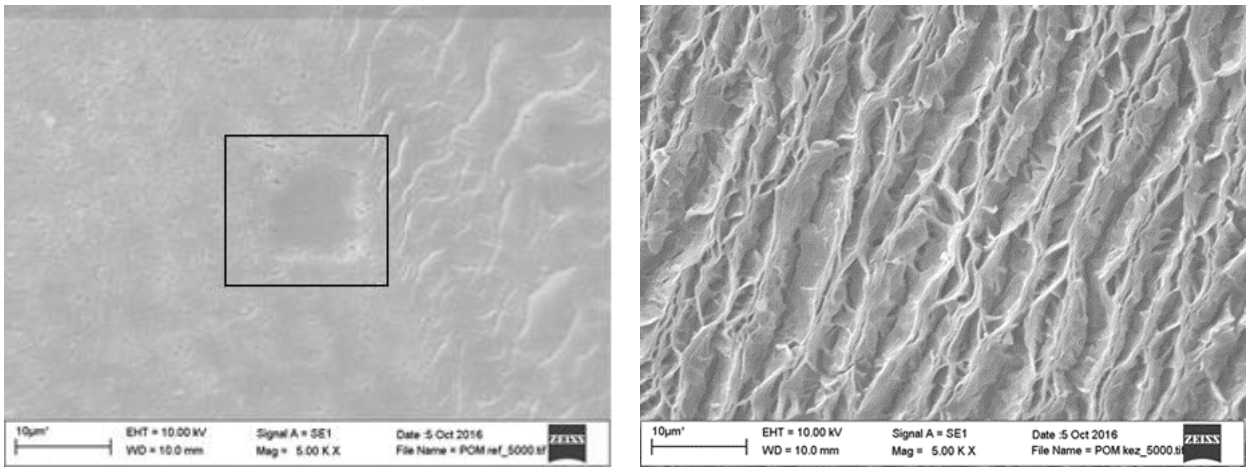

Fig. 4.8. Surface morphology of POM-C from scanning electron microscopy SEM, left: untreated, right: treated (5000X magnification)

The pristine sample of PP is smooth, slightly granular and there are some shallow scratches. However, a deep scratch with sharp edge has appeared on the treated surface (Fig. 4.9), which may have been presented before treatment, and it enlarged due to DBD plasma effect. In general, DBD plasma treatment has made the entire surface of PP slightly rougher.

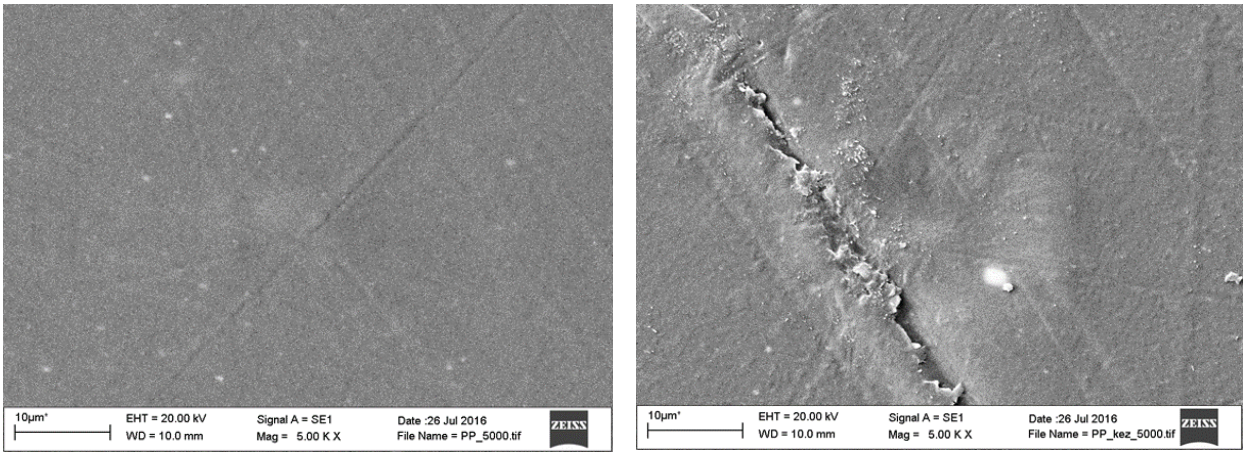

Fig. 4.9. Surface morphology of PP from scanning electron microscopy SEM, left: untreated, right: treated (5000X magnification)

1000X magnification shows that pristine surface of UHMW-PE (HD500 and HD1000, both due to the same surface composision) is uneven and has larger recesses and protuberances. As a result of plasma treatment, such a resolution can confirm that the surface is smoother than pristine one, and there are some scratches presented in the middle with rounded edges (Fig. 4.10). The 10000X magnification (Fig. 4.11), on the other hand, points out that the unevenness of UHMW-PE pristine sample at this resolution is less, and apart from surface mechanical damage, the pristine sample surface is rougher than plasma-treated sample. During the treatment, very small micro-grooves were formed. This pattern appears to be repeated throughout the examined surface, suggesting that

plasma-treated surface interaction occurs everywhere, the groove shape itself may depending plastic properties and/or the degradation rates.

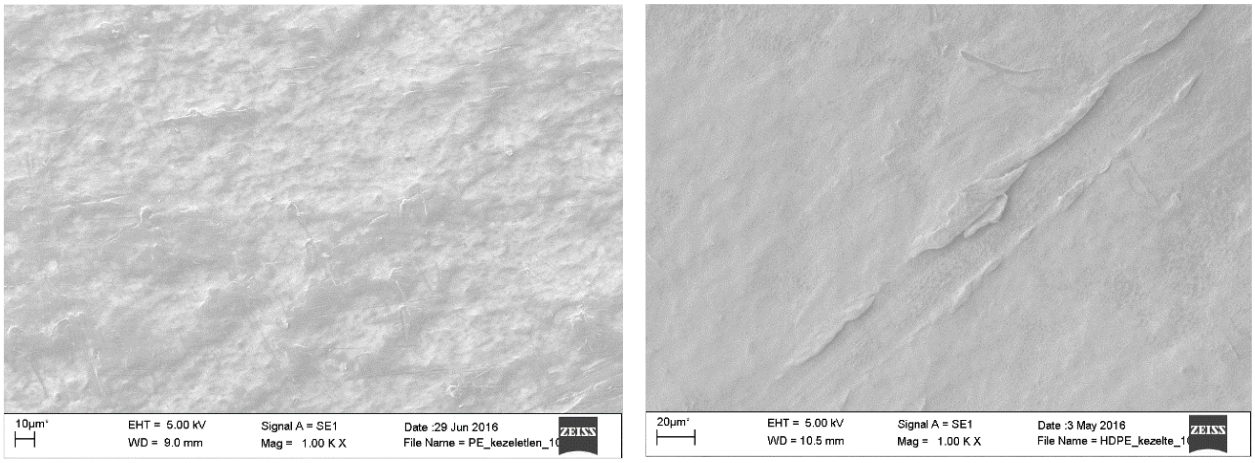

Fig. 4.10. Surface morphology of UHMW-PE from scanning electron microscopy SEM, left: untreated, right: treated (1000X magnification)

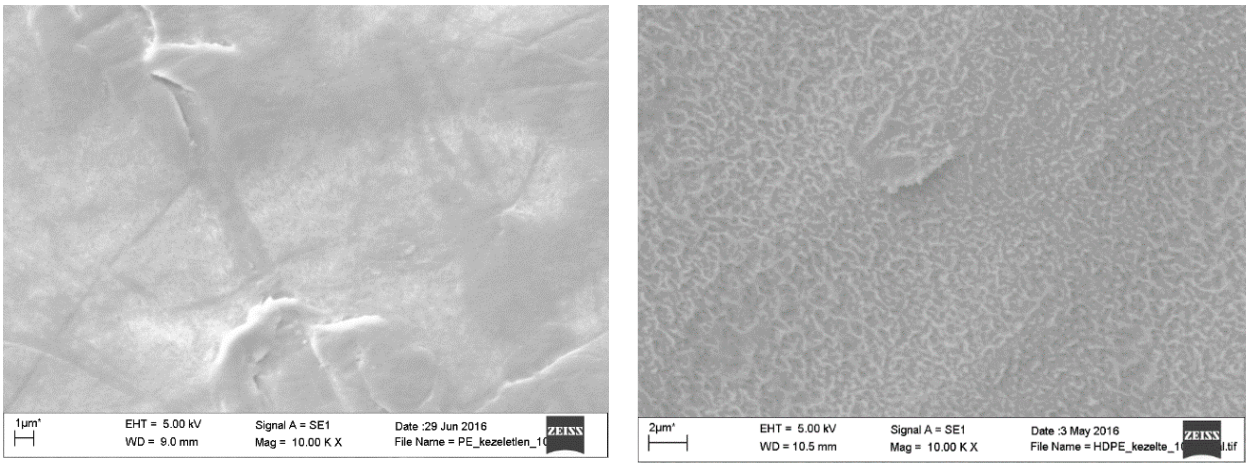

Fig. 4.11. Surface morphology of UHMW-PE from scanning electron microscopy SEM, left: untreated, right: treated (10000X magnification)

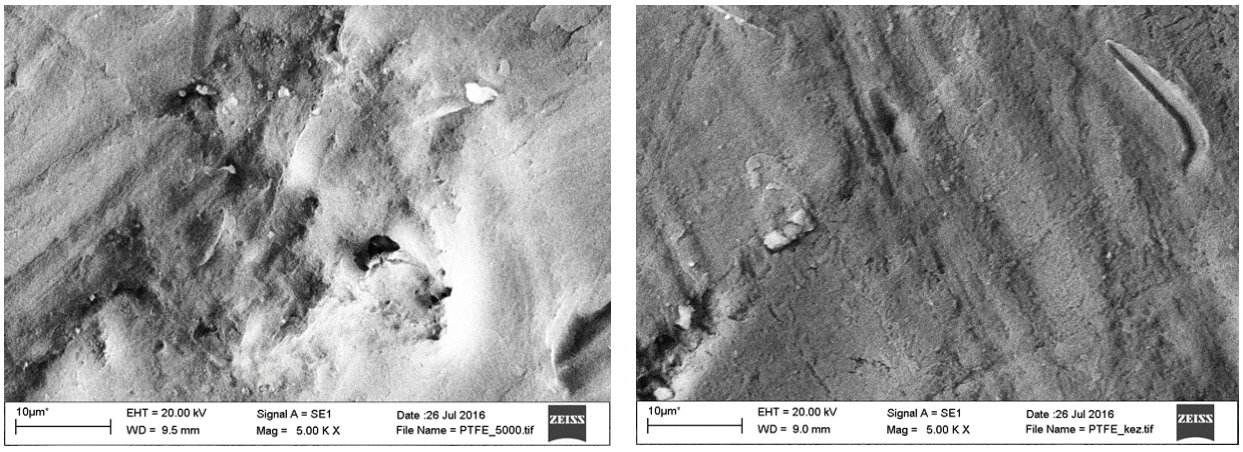

Fig. 4.12. Surface morphology of PTFE from scanning electron microscopy SEM, left: untreated, right: treated (5000X magnification)

It is not easy to detect surface morphology of PTFE by SEM compared to other polymers. If the measurement of pristine surface is omitted from the error spot in the centre and the smoother surface in the upper and right corners of the image is compared to the treated sample, then a very moderate increase in roughness can be observed (Fig. 4.12). The surface morphology of PTFE is slightly changing upon DBD plasma treatment.

In parallel, the mean (average) roughness of extruded surface was measured by atomic force microscopy AFM (Table 4.5). The measurements were carried out in nanoscale to detect the effect of plasma where it is impossible to detect the effect of plasma at microscale due to the fineness of extruded surface morphology. The results are typically agreed with SEM findings where the surface roughness of polymer surfaces is increasing due to DBD plasma treatment except UHMW-PE which is shown a reduction in the surface roughness. Further, the POM-C surface roughness slightly reduces or almost remain at the same roughness, in spite of, the remarkable surface morphology changes as SEM shown.

Table 4.5. Average roughness of extruded polymer surfaces from atomic force microscopy (AFM)

Sample	Treatment	Ra nm
PEEK	Untreated	4.07
	Treated	7.19
PET	Untreated	6.67
	Treated	12
PA6-E	Untreated	13.9
	Treated	15.1
POM-C	Untreated	31.1
	Treated	28.5
PP	Untreated	46.6
	Treated	86.2
UHMW-PE	Untreated	376
	Treated	185
PTFE	Untreated	53.2
	Treated	85

In summary, atmospheric DBD plasma treatment can increase the surface roughness of studied (extruded) polymer surfaces (except UHMW-PE where the roughness is increase and POM-C remains the same) by surface degradation due to plasma etching effect and/or composing of nodule-link features (highly oxidized short polymer fragments), which called in the literature low molecular-weight oxidized materials (LMWOMs) (Kostov et al., 2013).

4.1.4. Topography

Engineering polymers:

The changes in surface topography of polished pristine and plasma-treated samples are illustrated by 3D non-contact profilometry surface scans of engineering polymers in Fig. 4.13. The polymer surfaces after plasma treatment are flattened due to removal of the top layer and “melting” of the surface asperities, while the original machining (polishing) grooves remain visible. The surface

scans were repeated at 24 h and 800 h after plasma treatment, showing good stability in surface topography. The 3D roughness parameters before and after surface treatment are summarised in Table 4.6 (after 24 h and 800 h). The initial Sa (average roughness) values of PEEK and PET are mostly close, while PA6-E and POM-C have pretty far values despite their similar preparation method before plasma treatment. For engineering polymers, the surface roughness values Sa (average roughness) and Sz (maximum height) reduced, where Sa (average roughness) decreased -44%, -52%, -67%, and -26% for PEEK, PET, PA6-E, and POM-C respectively, PA6-E exposes the higher reduction in the surface roughness parameters due to plasma treatment. Sku (kurtosis) greater than 3 for all the surfaces shows the sharp roughness peaks which appear to be reduced after the plasma treatment. Ssk (skewness) of PEEK and PET is negative and became more negative after plasma treatment, Ssk (skewness) of PA6-E is positive and reduced toward the negative value after treatment but did not reach it which observed remain the sharp roughness peaks although they decreased after treatment from 2.11 to 0.27. On the other hand, Ssk (skewness) of POM-C shows a reduction in the negativity value, corresponding to the melting effect of plasma source causing general decrease of the original roughness. The values remain mostly stable for 24 and 800 h after treatment. The surface smoothening is characteristic for the used plasma processing conditions and measurements at microlevel scale.

Table 4.6. Three-dimensional surface roughness parameters of pristine and plasma-treated of engineering polymer surfaces determined from non-contact profilometry

Sample		**Sa µm**	**Sz µm**	**Sku**	**Ssk**
PEEK	Untreated (24 h)	0.5	5.94	3.81	-0.33
	Untreated (800 h)	0.5	5.8	3.55	-0.42
	Treated (24 h)	0.28	2.65	3.44	-0.38
	Treated (800 h)	0.25	2.84	3.86	-0.18
	Δ 24h/800 h %	-44/-10	-55/7	-10/12	15/-53
PET	Untreated (24 h)	0.67	7.33	3.8	-0.065
	Untreated (800 h)	0.58	7.56	4.89	0.21
	Treated (24 h)	0.32	3.36	3.49	-0.27
	Treated (800 h)	0.31	3.17	3.43	-0.19
	Δ 24h/800 h %	-52/-3	-54/-6	-8/-2	315/-30
PA6-E	Untreated (24 h)	1.35	20.43	10.57	2.11
	Untreated (800 h)	1.14	19.51	8.9	1.84
	Treated (24 h)	0.45	6.16	4.94	0.27
	Treated (800 h)	0.46	6.1	4.74	0.11
	Δ 24h/800 h %	-67/2	-70/-1	-53/-4	-87/-59
POM-C	Untreated (24 h)	0.2249	3.4	6.739	-0.95
	Untreated (800 h)	0.1945	2.618	4.396	-0.2146
	Treated (24 h)	0.1664	1.743	4.018	-0.35
	Treated (800 h)	0.1938	1.985	3.341	-0.32
	Δ 24h/800 h %	-26/16	-49/14	-40/-17	-63/-10

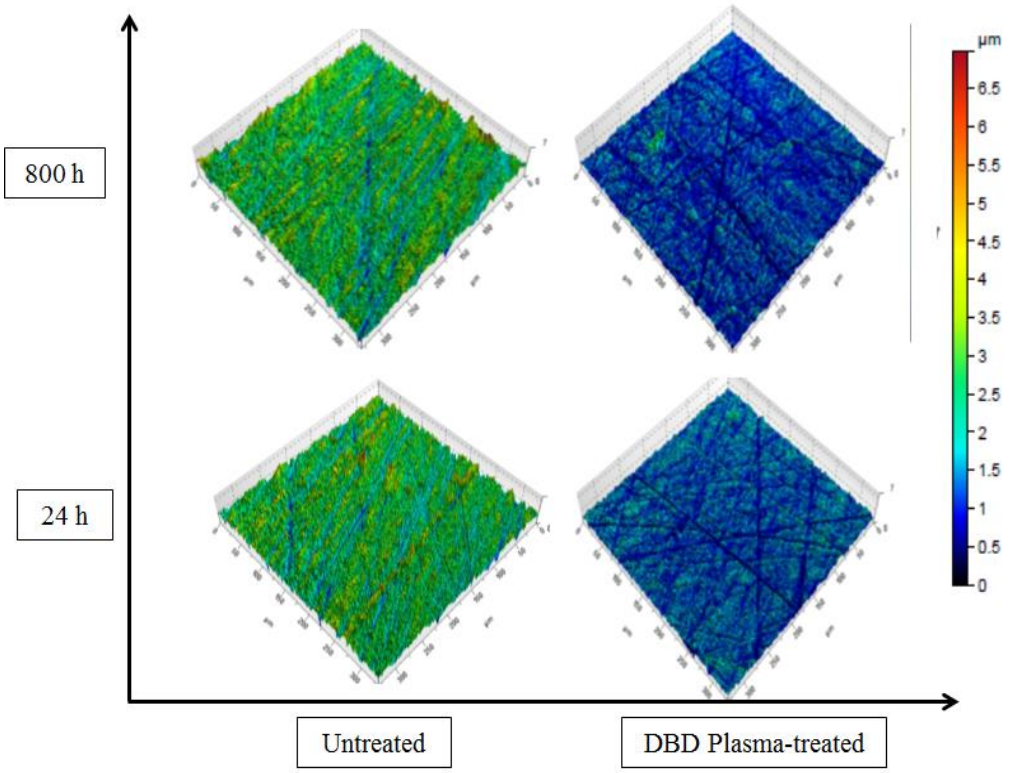

a)

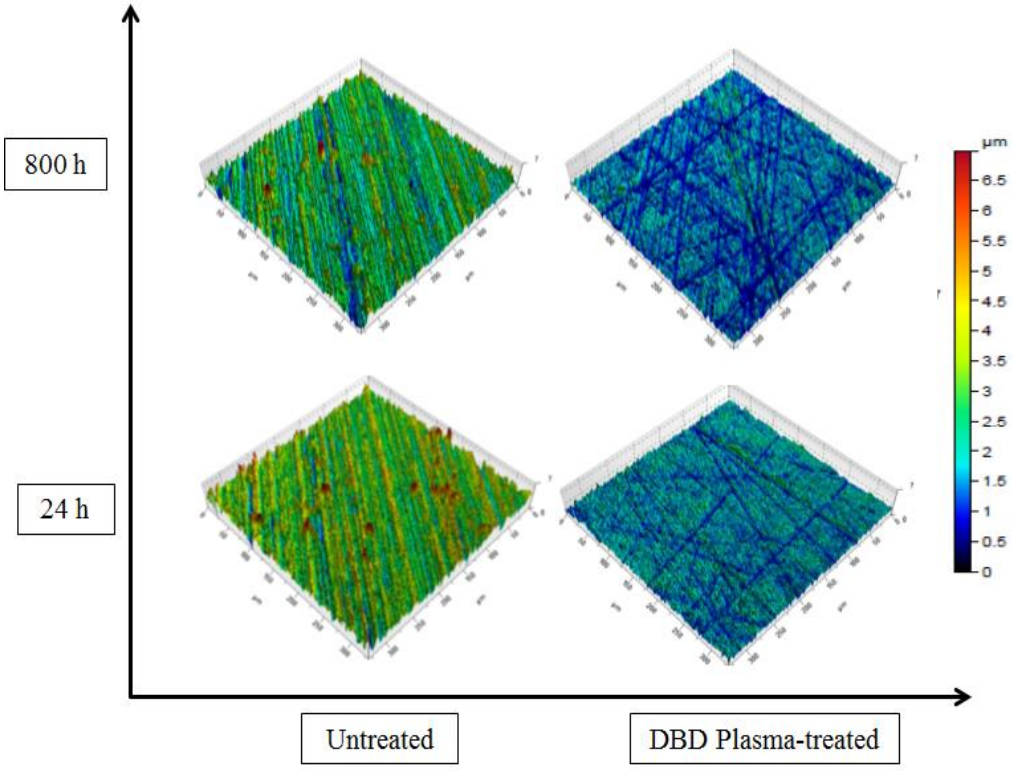

b) Continued

(Continued)

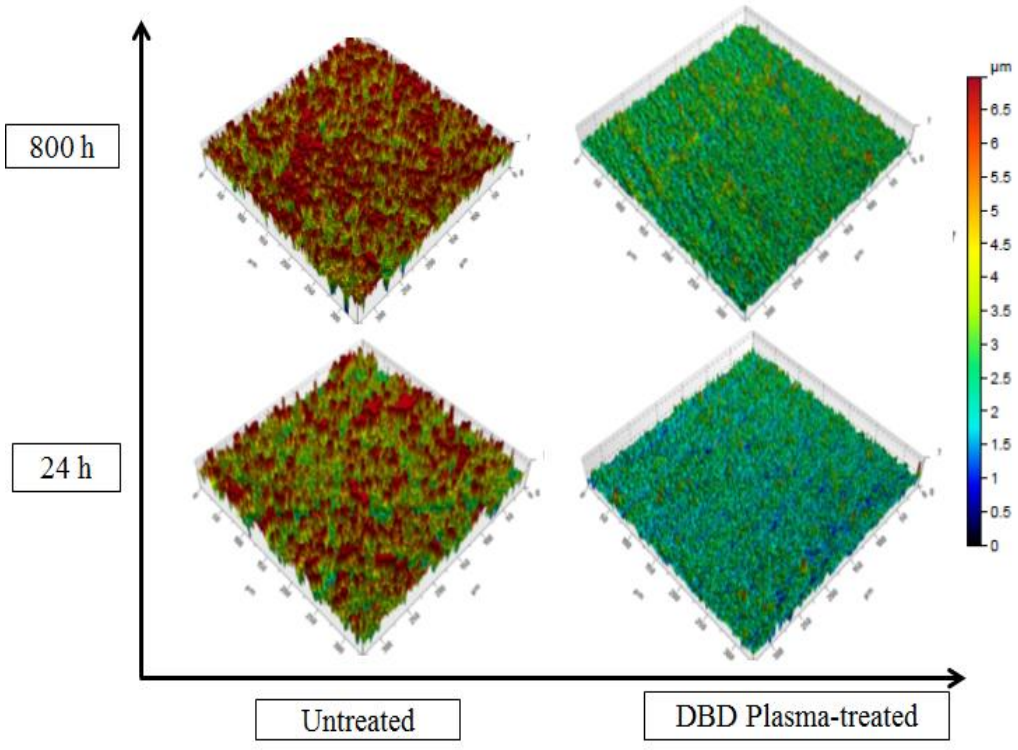

c)

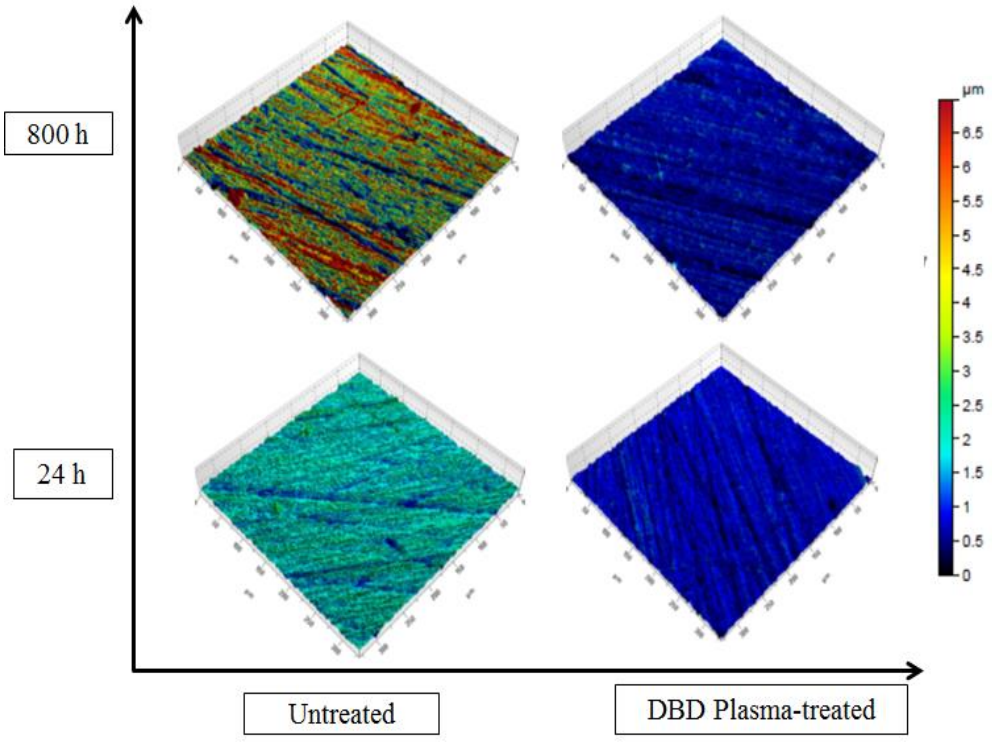

d)

Fig. 4.13. Non-contact profilometry of pristine and plasma-treated samples (330 × 330 mm^2 surface area) for a) PEEK, b) PET, c) PA6-E, and d) POM-C (same scale applies to all images)

Polyolefin polymers and PTFE:

Surface topography of pristine and plasma-treated samples monitored by non-contact profilometry is illustrated by 3D surface scans for polyolefin polymers and PTFE in Fig. 4.14. The 3D surface roughness parameters before plasma surface treatment and afterward are compared in Table 4.7. The initial Sa values of PP, UHMW-PE HD1000, and PTFE are almost identical being around 0.5 μm, while UHMW-PE HD1000 has 1.2 μm Sa value, despite their similar preparation method before plasma treatment. Such difference in the roughness could be expected considering the dissimilar surface hardness and strain capability of the particular polymers. Due to the plasma surface treatment, an opposing trend can be observed in the topography of the particular polymers. The roughness somewhat increased for PP (Sa 67%) and UHMW-PE HD1000 (Sa 25%) whereas considerable decrease occurred for UHMW-PE HD500 (Sa -68%) and slightly for PTFE (Sa -11%).

DBD plasma commonly increases the surface roughness of polymers due to etching effects (Yeh et al., 2011; Tosun et al., 2012; Pandiyaraj et al., 2016) that is more pronounced for the amorphous regions (Lopez et al., 2009; Blackman and Guild, 2013). For PP and UHMW-PE-HD1000 the plasma etching may be affected the base plane and led to creating depressions increasing this way both the mean and maximum height of the peaks. Treatment in oxygen-rich plasma can also create oxidized short polymer fragments, so-called low-molecular-weight oxidized materials (LMWOMs) (Kostov et al., 2013) which can increase the roughness. In contrast, UHMW-PE HD500 having higher initial roughness acted the opposite way upon treatment. Also, PTFE having slightly higher initial roughness than PP and UHMW-PE HD1000 reacted in an opposite way for treatment. For PTFE the surface roughness plays a crucial role in wettability. Although plasma treatment commonly introduces new oxygen-containing functionalities into the surface, an increasing roughness can counterbalance the hydrophilic effect of the oxygen-containing moieties presenting on the surface only in moderate amount and thus may result in a superhydrophobic feature. The ultimate roughness after plasma treatment is affected both by the applied power and the type of the plasma (Liu et al., 2004). While low power plasma treatments decrease the surface roughness of PTFE (Salapare et al., 2013). The decrease of the maximum height (Sz) values suggests a greatly flattened surface probably owing to the removal of the top layer and melting of the surface asperities, while the original polishing grooves remain visible. Between the time interval of 24 h and 800 h surface roughness parameters for PP and UHMW-PE HD500 showing good stability, while for UHMW-PE HD1000 and PTFE increase with the time function after plasma treatment. Sku greater than 3 of all the surfaces shows the sharp roughness peaks which appear to be reduced toward value of 3 except PP which shows an increase after the treatment process. Except for UHMW-PE HD1000, the Ssk value remained the same for the pristine and the treated surface. The difference between the pristine and the treated is the positive and negative value of Ssk respectively. It is evident that the sharp peaks are damaged in the plasma treatment; however, the surface has become rougher for the treated surface.

Overall topographical results of both groups it can be observed that engineering polymers show a higher reduction in surface roughness and better stability with time function than polyolefin polymers and PTFE.

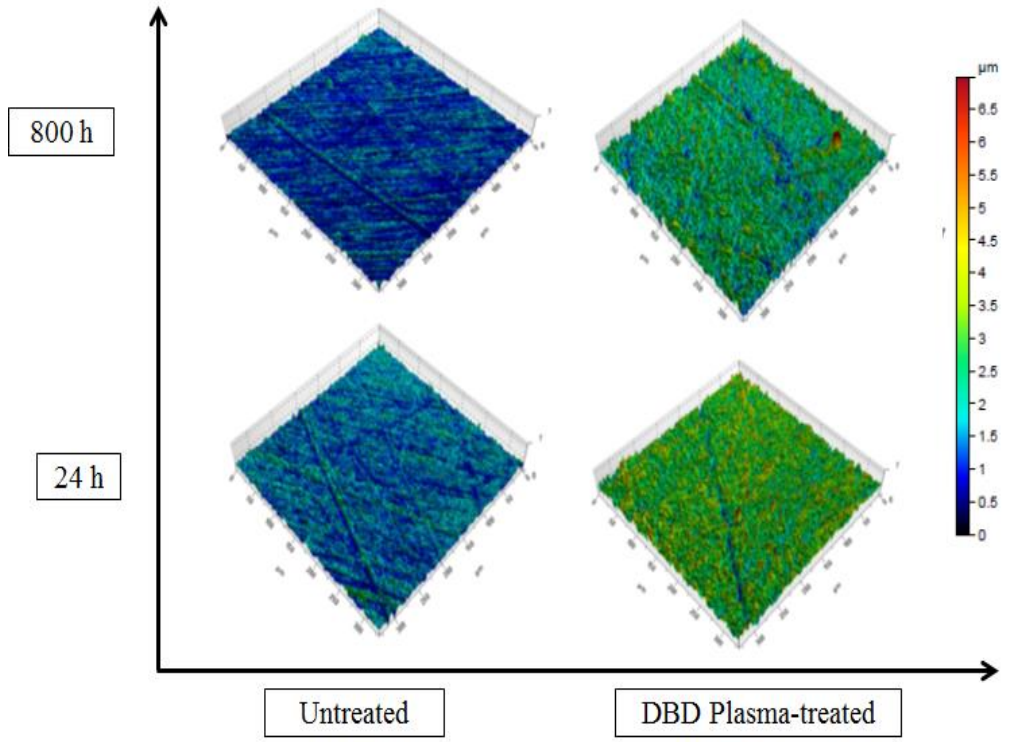

a)

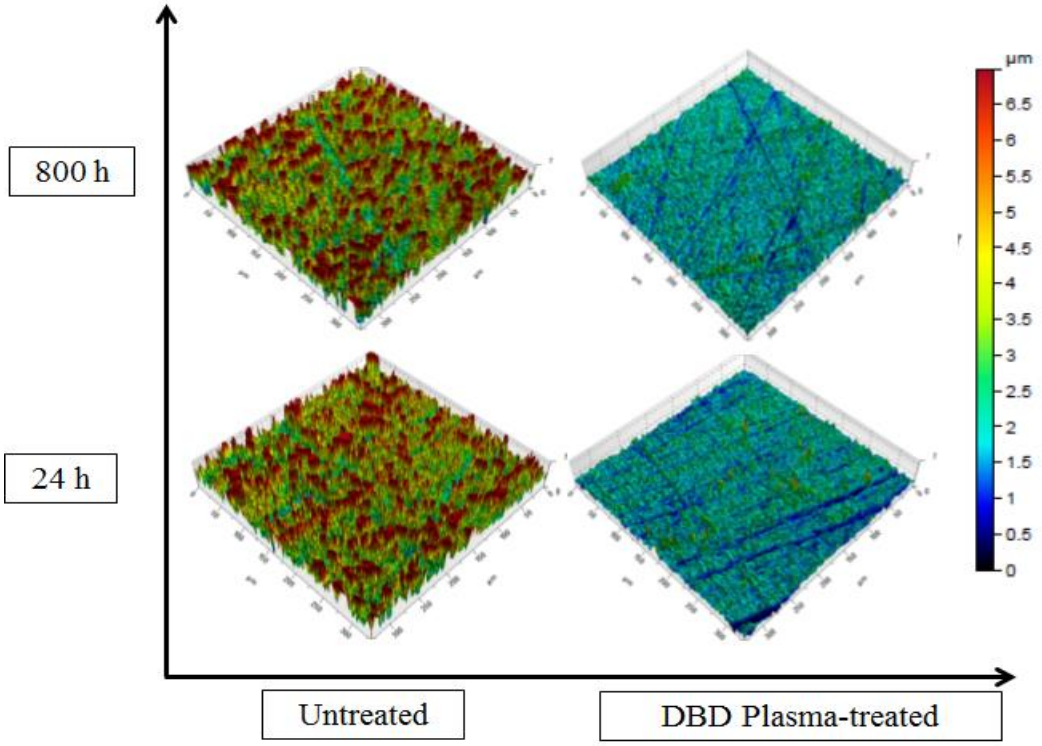

b) Continued

(Continued)

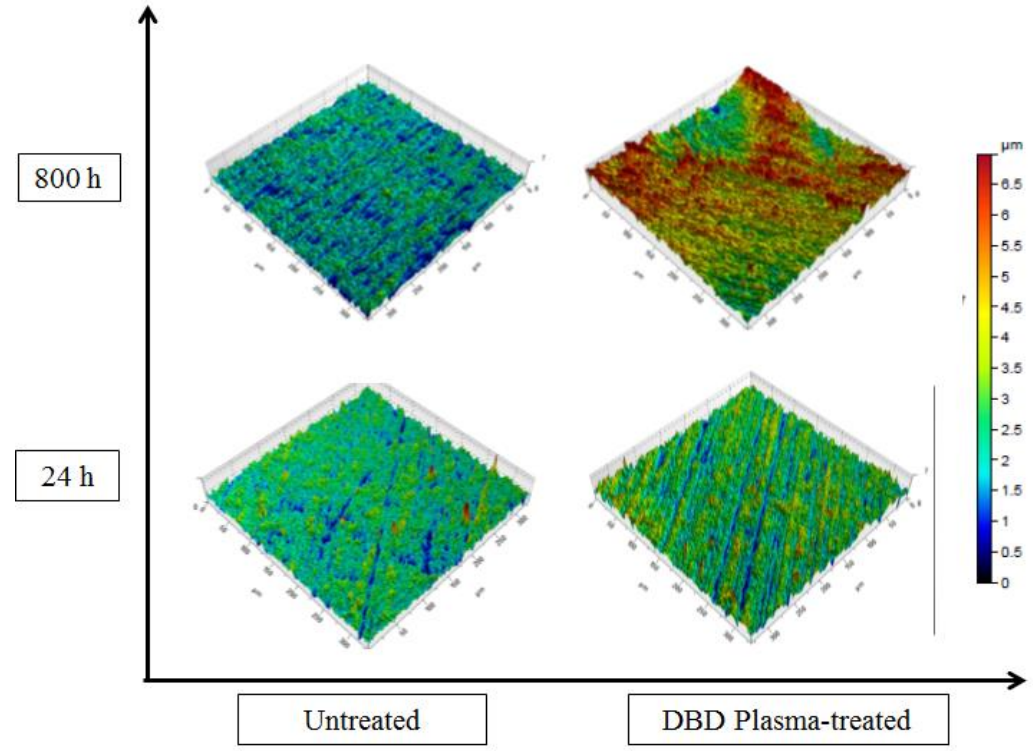

c)

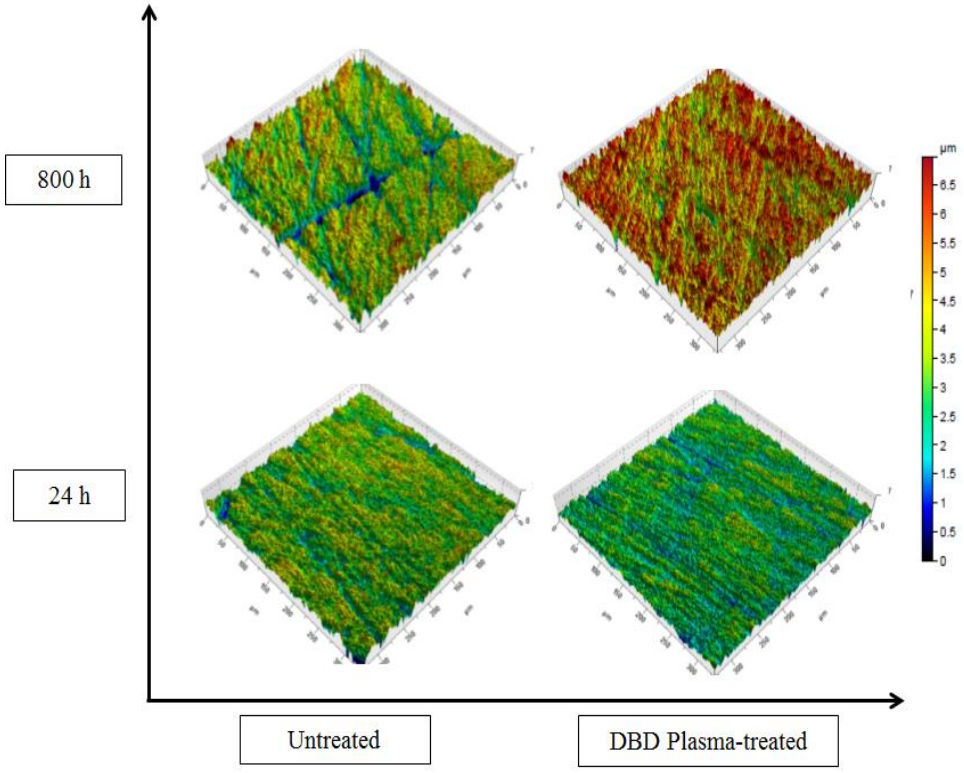

d)

Fig. 4.14. Non-contact profilometry of pristine and plasma-treated samples (330 × 330 mm^2 surface area) for a) PP, b) UHMW-PE HD500, c) UHMW-PE HD1000, and d) PTFE (same scale applies to all images)

Table 4.7. Three-dimensional surface roughness parameters of pristine and plasma-treated of polyolefin polymers and PTFE surfaces determined from non-contact profilometry

Sample		Sa µm	Sz µm	Sku	Ssk
PP	Untreated (24 h)	0.3	3.4	3.7	-0.02
	Untreated (800 h)	0.28	2.93	3.36	-0.05
	Treated (24 h)	0.5	6.53	4.52	-0.23
	Treated (800 h)	0.49	7.5	5.28	0.31
	Δ 24h/800 h %	67/-2	92/15	22/17	1050/-235
PE HD500	Untreated (24 h)	1.2	12.84	6.29	1.31
	Untreated (800 h)	1.17	14.67	7.05	1.59
	Treated (24 h)	0.38	5.91	5.611	0.33
	Treated (800 h)	0.31	3.89	4.3	0.009
	Δ 24h/800 h %	-68/-18	-54/-34	-11/-23	-75/-97
PE HD 1000	Untreated (24 h)	0.49	7.6	5.47	0.15
	Untreated (800 h)	0.44	4.52	3.09	-0.15
	Treated (24 h)	0.61	6.79	3.31	-0.16
	Treated (800 h)	1	10.38	3.2	-0.12
	Δ 24h/800 h %	25/64	-11/53	-40/-3	-207/-25
PTFE	Untreated (24 h)	0.56	5.4	3.99	-0.78
	Untreated (800 h)	0.77	6.8	3.44	-0.61
	Treated (24 h)	0.5	4.29	3.56	-0.6
	Treated (800 h)	0.76	9.12	4.47	-0.7
	Δ 24h/800 h %	-11/52	-21/113	-11/26	-23/17

4.2. Effect of atmospheric DBD plasma on adhesive bonding

4.2.1. Effect of atmospheric DBD plasma on adhesive bonding of engineering polymers

The shear strength (lap-shear tests) of pristine and plasma-treated polymer/polymer and polymer/steel joints is presented for engineering polymers (Fig. 4.15). In average, the statistical deviation (spread σ%) on the shear strength (5 repetitions) significantly reduces after plasma treatment for all polymers, that is, about 15% for pristine PEEK to 1% for plasma-treated PEEK; about 8% for pristine PET to 1% for plasma-treated PET; about 9% for pristine PA6-E to 3% for plasma-treated PA6-E; about 9% for pristine POM-C to 1% for plasma-treated POM-C (Tables 8.2, 8.3, 8.4, and 8.5 in A4). The observations of failure type for the adhesive bonds are documented in Table 4.8, either presenting adhesive failure on one or two surfaces (1), cohesive failure in the adhesive layer (2), or cracking in the bulk polymer (3). Overall, the tendency for adhesive-type of failure reduces after plasma treatment and changes into cohesive failure or adhesive-type failure with higher shear strength (Fig. 4.16). The pure cracking of the bulk polymer corresponds to highest shear strength in case of epoxy-type and cyanoacrylate adhesives on plasma-treated surfaces for PEEK and PET, irrespective of the counterface. In case of adhesive failure on dissimilar surface pairs (polymer/steel), it was observed that the glue most easily releases from the polymer surface and remains sticking on the steel surfaces. Regardless of the adhesive type and counterface, the plasma treatment improves the adhesive bonding compared to the pristine samples. The higher surface polarity after plasma treatment highly contributes to better

adhesive bonding. The adhesive strength of plasma-treated PEEK is somewhat higher than plasma-treated PET where the adhesive strength of PET is higher plasma-treated PA6-E and PA6-E higher than POM-C, in parallel with the surface polarity results (see Table 4.4, engineering polymers) and surface morphology after treatment. There is a trend that the surface activation was most efficient for the epoxy-type of adhesive for PEEK, PET, and POM-C. While the epoxy provides lowest shear strength for the pristine samples, it provides highest shear strength for the plasma-treated PEEK, PET, and POM-C, whereas somewhat urethane methacrylate ester provides the highest shear strength for PA6-E. The urethane methacrylate ester adhesive shows lower shear strength than the cyanoacrylate one for PEEK, PET, and POM-C plasma-treated samples, although the two acrylate-type adhesives show comparable shear strength for pristine PEEK samples. Considering the surface tension of the adhesives, the epoxy-type is higher (41 mN/m) than the cyanoacrylate (33 mN/m) and urethane methacrylate ester (29 mN/m). Based on this, not only the spreading of the adhesive on the polymer surfaces (which would theoretically be expected to be best for the lowest surface tension) is important, but the approximation between the higher surface tension of the epoxy-type adhesive with the surface energy of the polymer surfaces may be advantageous in adhesive bonding. Indeed, the initial adhesive spreading has a minor role as the normal load applied during drying increases the real wetted surface area. Moreover, it seems that the reactivity of the epoxy adhesive toward the carboxylic groups at the polymer surface after plasma treatment plays a dominating role: the polarity of the polymer surface and presence of more oxygen-rich fractions after plasma treatment may cause good interactions with the pendant hydroxyl groups of the epoxy resin to form a strong adhesive bond. On the other hand, the reason behind the highest shear strength of urethane methacrylate ester for treated PA6-E (irrespective of the counterface) that beside the improvement of the surface polarity is attributed to the low surface tension of the adhesive and the highest surface degradation of plasma-treated PA6-E (see Fig. 4.7) which provide a good penetration of the adhesive into the generated trenches in the polymer surface which in turn contain further smaller pores thereby generating strong mechanical bonds after curing. Moreover, the strong mechanical besides the chemical bonding of treated PA6-E are often allowed a cohesive failure in the adhesive layer only thus the failure strength of PA6-E joints should be exceeding the high shear strength of the adhesive itself (15-30 N/mm^2).

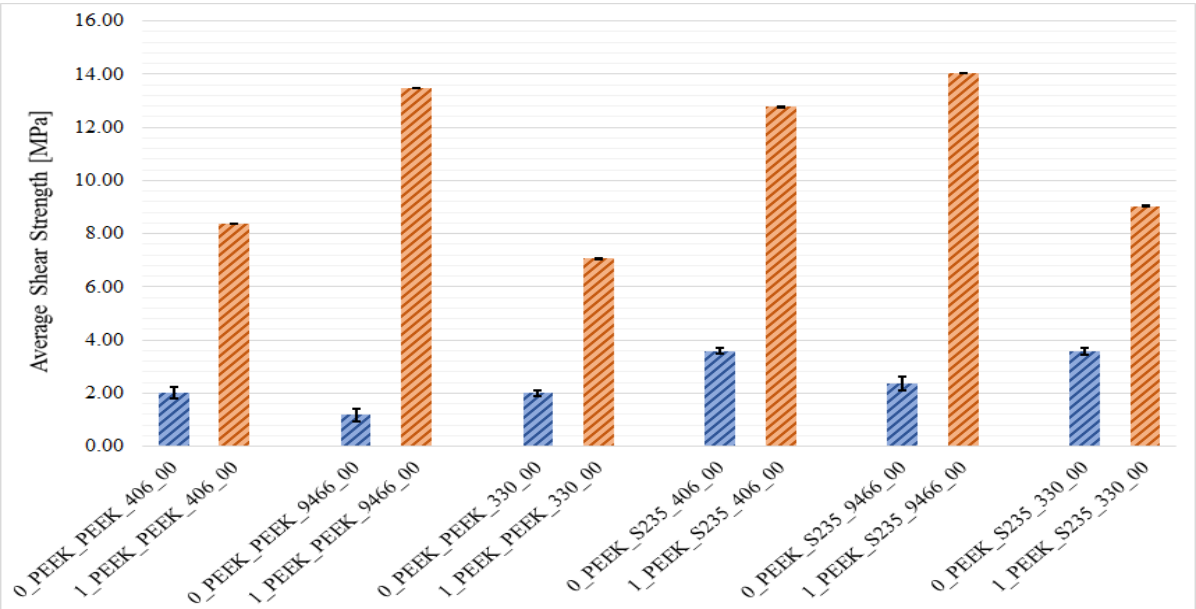

a) Continued

(Continued)

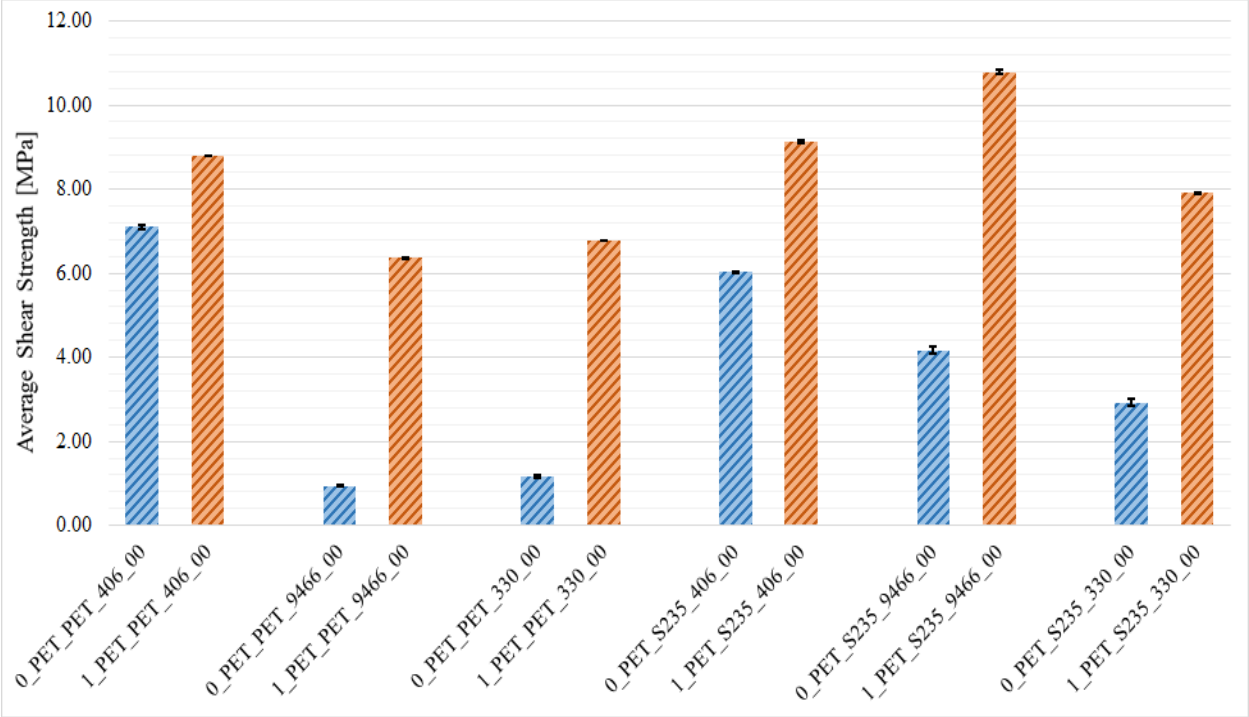

b)

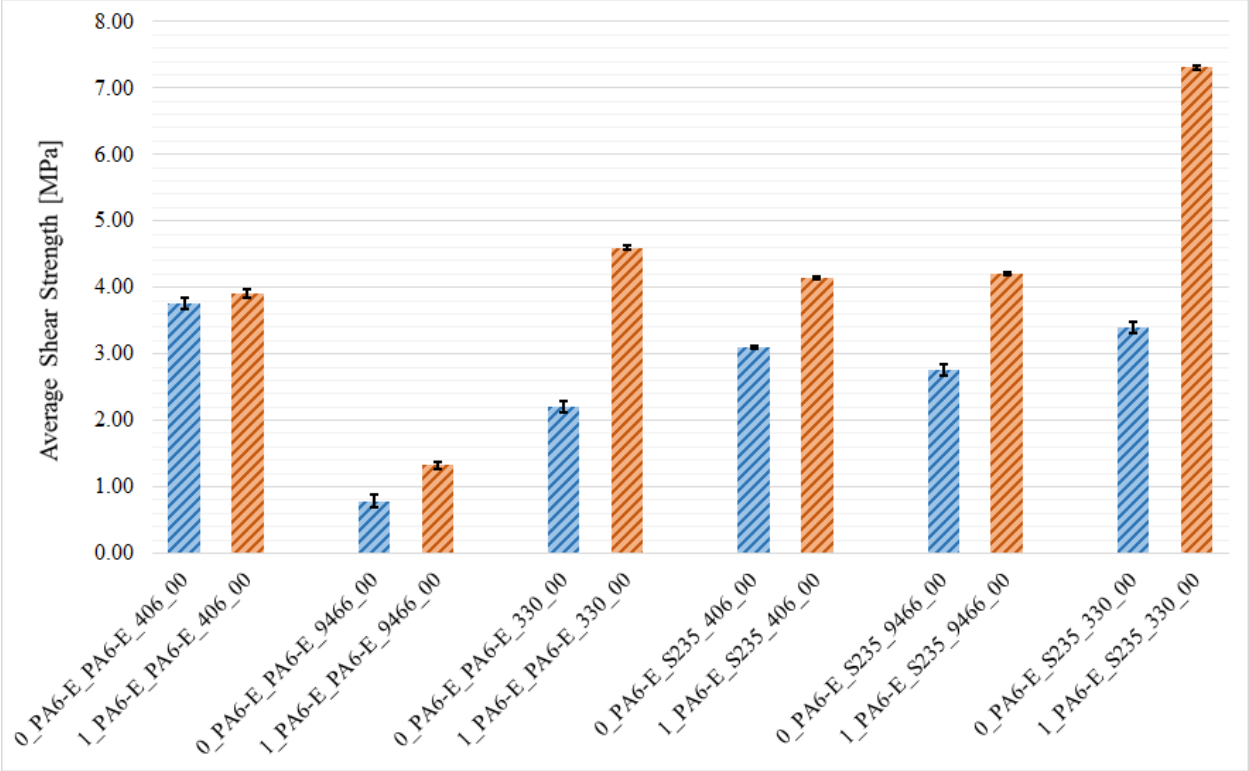

c) Continued

(Continued)

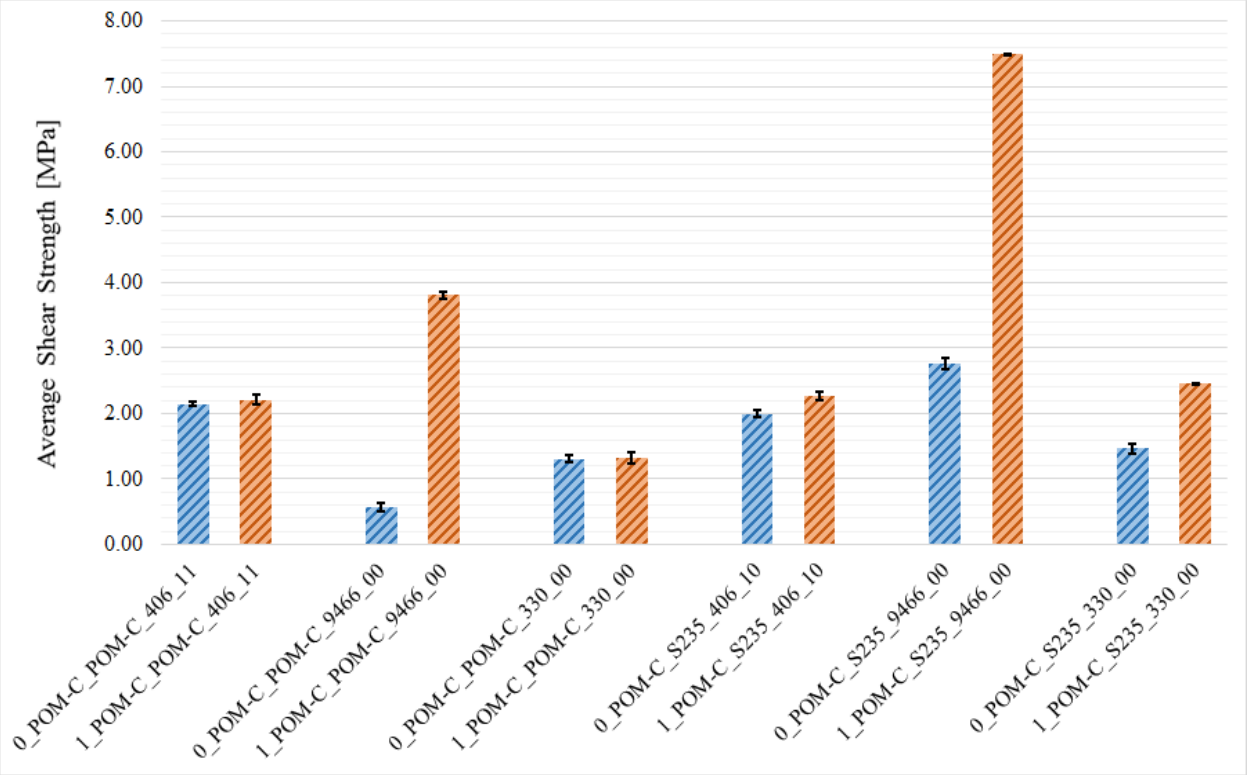

d)

Fig. 4.15. Adhesive testing of polymer/polymer and polymer/steel couples after application of different adhesive types for pristine samples and plasma-treated samples for a) PEEK, b) PET, c) PA6-E, and d) POM-C

Table 4.8. Failure type of adhesive bonds in lap-shear testing of engineering polymer before and after plasma treatment

	Pristine		**Plasma-treated**	
PEEK	PEEK/PEEK	PAEEK/Steel	PEEK/PEEK	PEEK/Steel
Ethyl cyanoacrylate	1	1,2	1,2	1,2,3
Epoxy	1	1	3	3
Urethane methacrylate ester	1	1	1,2	1,2
PET	PET/PET	PET/Steel	PET/PET	PET/Steel
Ethyl cyanoacrylate	1,2,3	1,2	3	2,3
Epoxy	1	1	2,3	3
Urethane methacrylate ester	1	1	2	2
PA6-E	PA6-E/PA6-E	PA6-E/Steel	PA6-E/PA6-E	PA6-E/Steel
Ethyl cyanoacrylate	1	1,2	1,2	1,2
Epoxy	1	1	1,2	1,2
Urethane methacrylate ester	1	1	2	2
POM-C	POM-C/POM-C	POM-C/Steel	POM-C/POM-C	POM-C/Steel
Ethyl cyanoacrylate	1	1	1,2	1,2
Epoxy	1,2	1	1,2	1,2
Urethane methacrylate ester	1	1	1,2	1,2
1. adhesive failure on one or two surfaces 2. cohesive failure in the glue layer 3. cracking in the bulk polymer				

a)

b) Continued

(Continued)

c)

d)

Fig. 4.16. Different failure types of different joints after lap-shear testing: a) PEEK, b) PET, c) PA6-E, and d) POM-C, (untreated to the left, treated to the right)

4.2.2. Effect of atmospheric DBD plasma on adhesive bonding of polyolefin polymers and PTFE

The shear strength (lap-shear tests) of pristine and plasma-treated polymer/polymer and polymer/steel joints of polyolefin polymers and PTFE is shown in Fig. 4.17. In average, the statistical deviation (spread σ%) on the shear strength (5 repetitions) significantly reduces after plasma treatment for all polymers, that is, about 8% for pristine PP, UHMW-PE HD500, and PTFE to 1.5%, 1%, and 2%, respectively, for plasma-treated samples; about 5% for Pristine UHMW-PE HD1000 to 1.5% for plasma-treated sample (Tables 8.6, 8.7, 8.8, and 8.9 in A4). Observations of failure type for the adhesive bonds are documented in Table 4.9, either presenting adhesive failure on one or two surfaces (1), cohesive failure in the adhesive layer (2), or cracking in the bulk polymer (3) as shown in Fig. 4.18. Concerning the pristine PP, the typical failure was adhesive type (1) and cohesive type (2) for both adhesives however one case of pure crack in the bulk polymer (3) was recorded for polymer/polymer joint with cyanoacrylate adhesive. After plasma treatment, the locus failure of bonded joints was altered into cohesive (2) and pure cracking (3) regardless countersurface and the adhesive. The pure cracking of the bulk polymer corresponds to highest shear strength of plasma-treated surfaces. Similar to engineering polymer, PP was observed that the glues released easier from the polymer surface and remained sticking on the steel surfaces in case of using dissimilar surface pairs (polymer/steel). For UHMW-PE HD500 and PFTE the primary cause of the failure was adhesive-type that did not transform after treatment; however, the failure occurred at higher shear strength. Analysing the main causes of UHMW-PE HD1000 failure, we found that mostly cohesive type failure occurred for polymer/polymer pairs, while in polymer/steel pairs the bond layer detached from the steel surface. The adhesive strength of plasma-treated PP is somewhat higher than other plasma-treated polymers in spite of higher surface energy of UHMW-PE HD polymers after plasma treatment this may be attributed to the high surface roughness of PP after plasma treatment which led to form a deep scratch with sharp edge (see Fig. 4.9), which provides a strong mechanical bonding between the polymer surface and adhesives thus high shear strength.

In average, the cyanoacrylate adhesive exhibits slightly higher shear strength compared with the methacrylate one for the pristine samples, while shear strength became more comparable for the plasma-treated samples. Irrespective of the surface pairs and the type of adhesive material, the plasma treatment significantly improved the adhesive bonding as compared to the pristine PP, UHMW-PE HD500 samples. UHMW-PE HD1000 shows a moderate improvement in the adhesion strength for Polymer/polymer joints (regardless the adhesive type) this can be attributed to the polymer structure and its high deformability. Due to the activation of both surfaces Polymer/polymer joints almost reached the adhesion values of polymer/steel bonding pairs. In contrast, polymer/steel joints exhibited a slightly shear strength enhancement after plasma treatment. For polymer/steel joints of UHMW-PE HD1000, the shear strength of cyanoacrylate is higher compared to methacrylate because the solidified cyanoacrylate is a rigid material which is unable to contraction when exposed to tension. When the polymer is bonded to steel the steel prevents the contraction of the adhesive layer. Methacrylate adhesive seems to be better for joining polymer/steel of UHMW-PE HD1000 as this glue is softer and capable of following the changes in the dimension of the polymer occurring during the tension. Although the adhesion strength of PTFE was significantly lower than other polymers, which is expected due to the low surface energy of PTFE, it can be considered that the adhesion strength of polymer/polymer pairs higher regarding polymer/steel bonding pairs since the steel does not let the contraction of the bonds at the cross-section. Plasma treatment did not improve adhesion strength irrespective of the type of adhesive material or surface pairs for UHMW-PE HD1000 and PTFE. The better adhesive bonding can be attributed to the increase in surface polarity of the plasma-treated specimens (see Table 4.4).

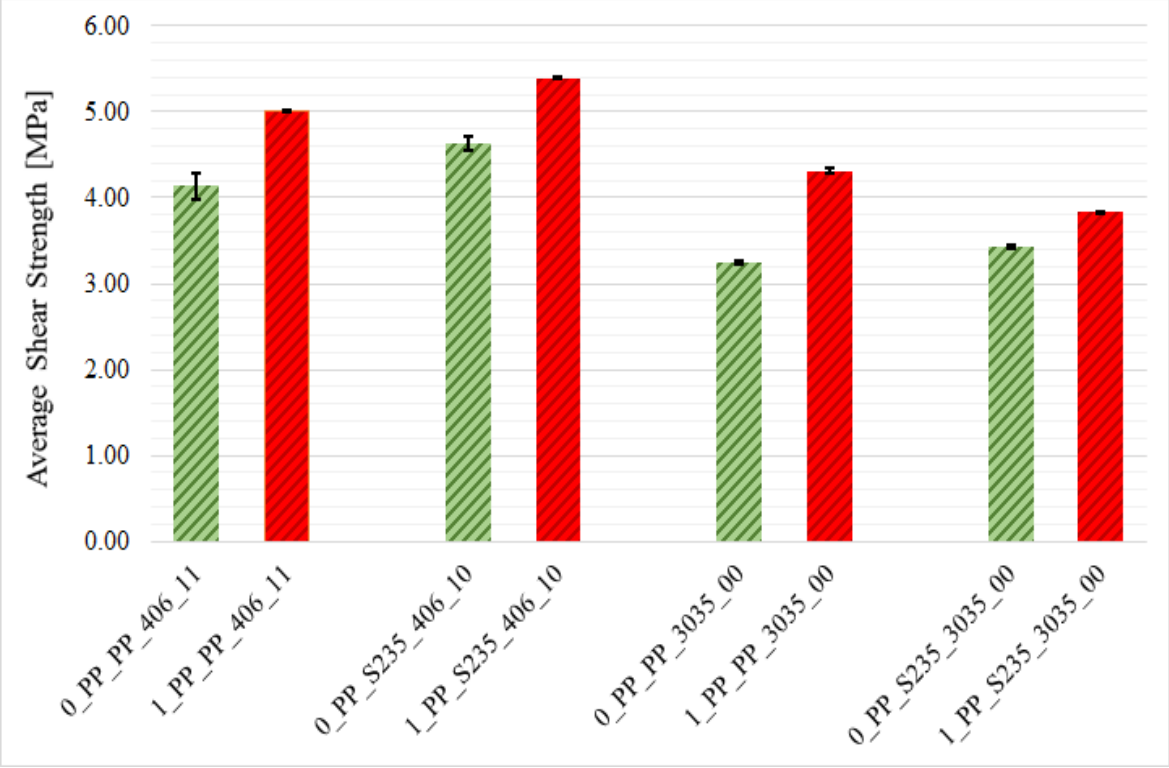

a) Continued

(Continued)

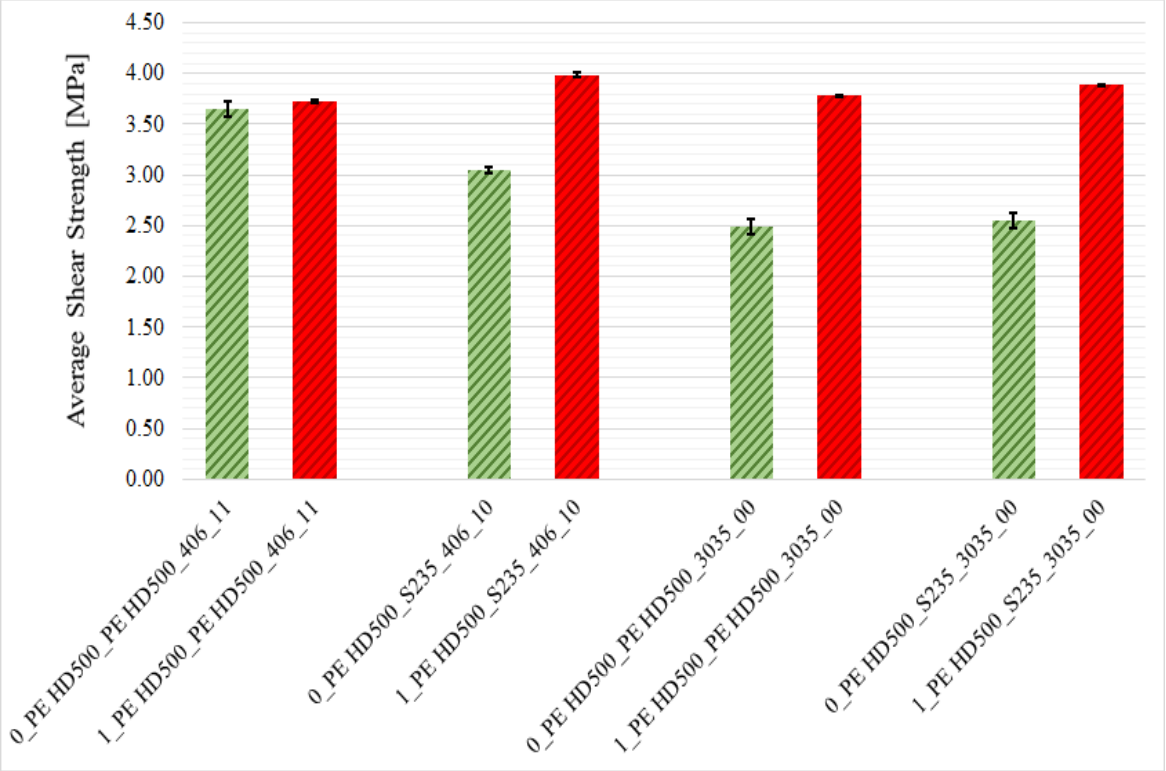

b)

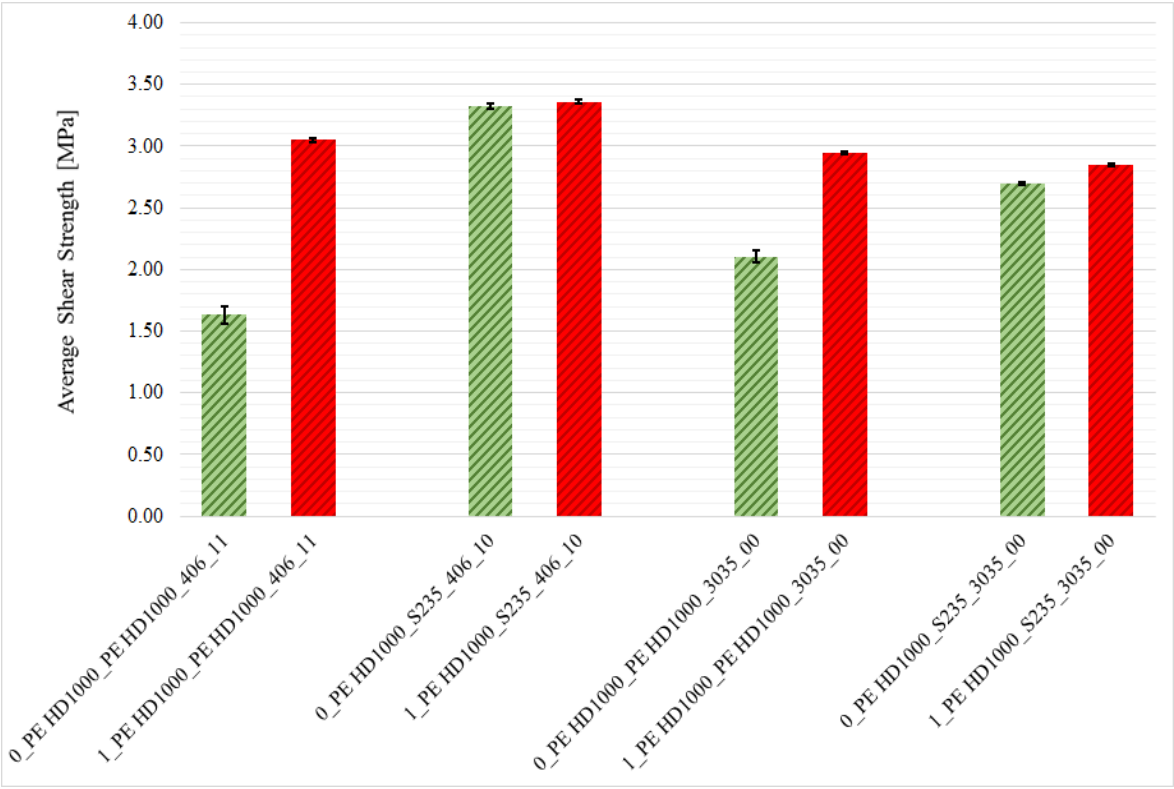

c) Continued

(Continued)

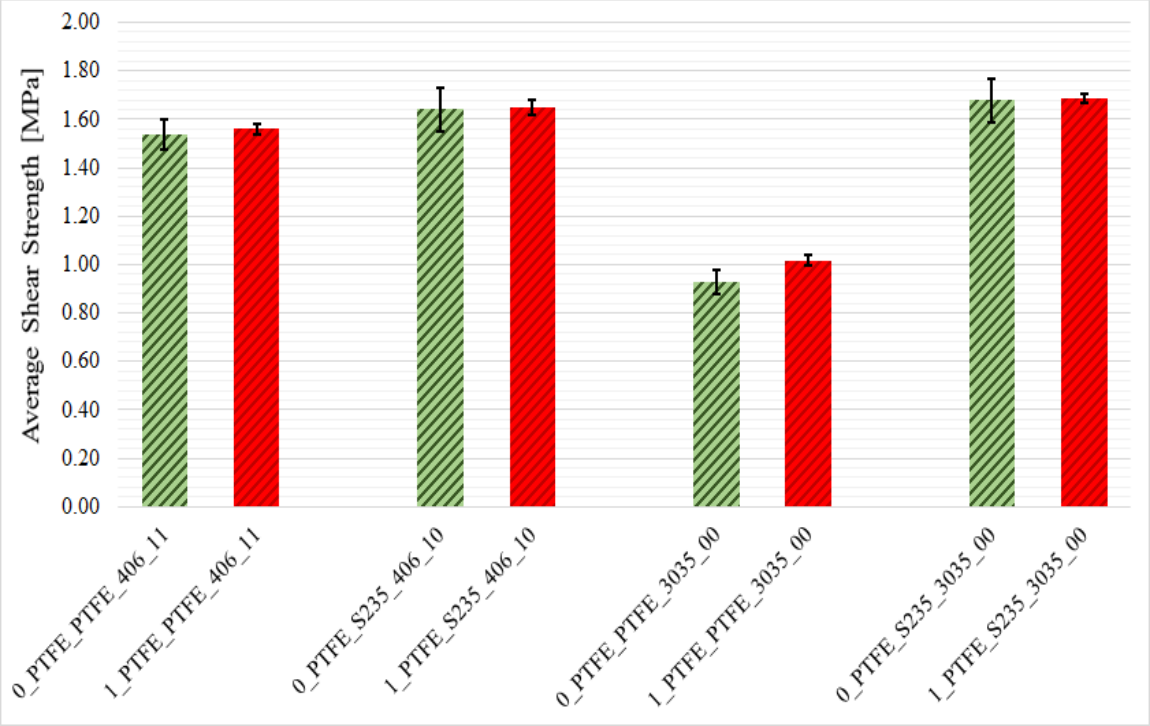

d)

Fig. 4.17. Adhesive testing of polymer/polymer and polymer/steel couples after application of different adhesive types for pristine samples and plasma-treated samples for a) PP, b) UHMW-PE HD500, c) UHMW-PE HD1000, and d) PTFE

Table 4.9. Failure type of adhesive bonds in lap-shear testing of polyolefin polymers and PTFE before and after plasma treatment

PP	**Pristine**		**Plasma-treated**	
	PP/PP	PP/Steel	PP/PP	PP/Steel
Ethyl cyanoacrylate	1,2,3	1,2	2,3	2,3
Methacrylate	1,2	1,2	2,3	2
PE HD500	PE500/PE500	PE500/Steel	PE500/PE500	PE500/Steel
Ethyl cyanoacrylate	1	1	1	1
Methacrylate	1	1	1	1
PE HD1000	PE1000/PE1000	PE1000/Steel	PE1000/PE1000	PE1000/Steel
Ethyl cyanoacrylate	1	1	1,2	1
Methacrylate	1	1	1,2	1
PTFE	PTFE/PTFE	PTFE/Steel	PTFE/PTFE	PTFE/Steel
Ethyl cyanoacrylate	1	1	1	1
Methacrylate	1	1	1	1
1. adhesive failure on one or two surfaces 2. cohesive failure in the glue layer 3. cracking in the bulk polymer				

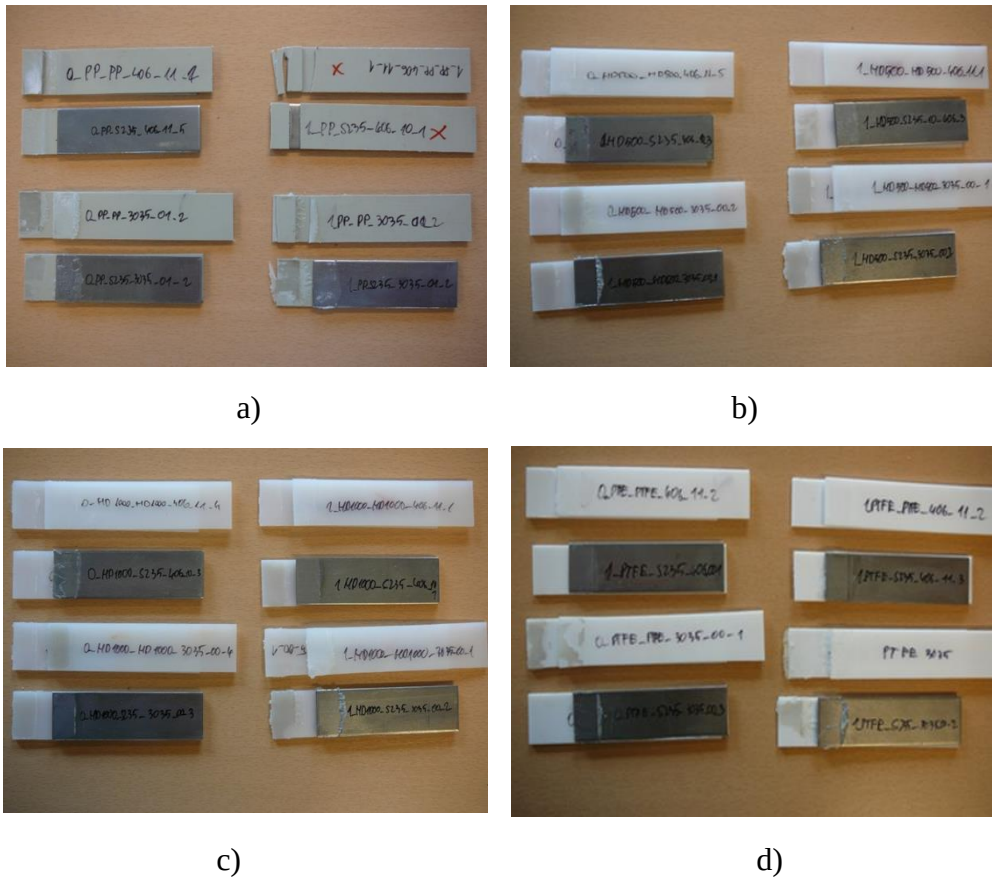

a) b)

c) d)

Fig. 4.18. Different failure types of different joints after lap-shear: a) PP, b) UHMW-PE HD500, c) UHMW-PE HD1000, and d) PTFE, (untreated to the left, treated to the right)

4.3. Effect of atmospheric DBD plasma on tribological behaviour

4.3.1. Effect of atmospheric DBD plasma on tribological behaviour of engineering polymers

Dry sliding tests

The on-line measurements for coefficients of friction, wear, and bulk temperature during dry sliding tests on pristine and plasma-treated samples under different normal loads are shown for engineering polymers in Fig. 4.19. The average values for coefficients of friction μ and vertical displacement Δh per load are summarised in Fig. 4.20. The coefficients of friction and wear were determined from three repetitions with a statistical variation of ± 2.5% on pristine and ± 1% on plasma-treated samples. The coefficients of friction for all pristine surfaces show significant running-in phenomena with a peak value during the first couple of meters, which can be explained by the presence of a contaminating hydrocarbon layer on the untreated polymers. Overall, the friction for pristine PEEK and POM-C are slightly higher compared to pristine PET and PA6-E for the same normal loads, which can be attributed to the higher mechanical strength and stiffness of PEEK, providing higher sliding resistance (the surface properties of PEEK and PET can be considered as similar based on surface energy values, but the more complex aromatic structure of PEEK compared to PET may induce higher rigidity at molecular level). Whereas, the lowest mechanical properties of POM-C may play a similar role to increase the real contact area (RCA) with load increasing implies higher friction. The coefficients of friction do not (significantly) decrease with increasing the normal loads, which is an indication that softening mechanisms and

temperature rise do not influence the sliding processes (the latter would traditionally cause decreasing friction for thermoplastics under thermally controlled sliding conditions). Therefore, it can be assumed that mechanical interactions and surface interactions are dominating effects. The plasma-treated polymer surfaces present lower friction than pristine polymers, except for the PEEK at highest normal load. It can be observed, however, that the differences in coefficients of friction between untreated and plasma-treated polymers become smaller at high loads. The observations for lower friction after plasma-treatment are in contrast from what would be expected from the higher surface energy and adhesive strength of plasma-treated surfaces, which would both imply a higher coefficient of friction. In parallel, it has also to be considered that the lower roughness of plasma-treated polymer surfaces can either increase or decrease the coefficients of friction. According to Archard's theory of friction (Archard, 1953), F_f the friction force equals the sum of an adhesion force component F_a and a deformation force component F_d: under low loads, the deformation component is generally smaller than the adhesion component ($F_d<F_a$).

From present results, however, it can theoretically be assumed that the lower friction for plasma-treated polymers under low loads should be attributed to the smaller contributions of a deformation component. The reduction in surface roughness for plasma-treated polymers can confirm that the deformation component near the surface asperities of the polymer should likely be reduced. At low loads, a smaller real contact area of the plasma-treated polymer surfaces can exist through the effects of plasma treatment. At higher load levels of 1 MPa, the real contact area enlarges and the higher surface energy of plasma-treated polymers could elevate the adhesive component of friction and reduce the gap between pristine and treated coefficient of friction. Further increase of load level to 2 MPa showed that the increased real contact area resulted in higher friction than it was found for pristine PEEK, and the higher surface energy started dominating the friction more importantly than other polymers. In parallel with the increase in surface energy (polarity) after plasma-treatment, a partial surface degradation and creation of a fraction oxidized material (carboxylic acid) with lower molecular weight can provide a kind of lubricating mechanism at the polymer surface, which additionally contributes to the lower friction for plasma-treated surfaces under dry sliding conditions at low loads and is worn away under high loads. The wear and deformation Δh of the pristine samples gradually increases at higher loads and wear of PEEK is lower than wear of PET, PA6-E, and POM-C respectively at all load levels, regardless the vertical displacement (in opposite to the higher friction for PEEK and POM-C than PET and PA6-E) confirming the mechanical strength and stiffness in combination with smaller contributions of deformation for PEEK. An estimation of wear and deformation under each normal load was made from the slope of the graph. After the plasma treatment and sliding under highest load level, the Δh values for PET, PA6-E, and POM-C increase (in opposite to the lower friction after plasma treatment) while they remain almost similar for PEEK (in opposite to the higher friction after plasma treatment). It can be also remarked that the static deformation of all polymers was decreased during increase of the load. However, the measurements of Δh are only an indicative measurement for a couple of events over short sliding distances, including (i) heat expansion that counteracts the "real" wear, and (ii) creep that cooperates with the "real" wear. As a consequence of higher friction of plasma-treated PEEK under highest load, the thermal expansion should there be at highest and suppresses the wear at most. Thus, higher "real" wear than indicated by measurements under highest load can also be expected for the plasma-treated PEEK, which would than relate with the measurements for other polymers. The higher "real" wear for plasma-treated

samples after short sliding distances could be logically explained by the formation of a degraded surface layer as mentioned before. The bulk temperatures of the polymer samples closely follow the trends for coefficients of friction for PEEK, PET, and POM-C, while opposite trends have been noticed with higher temperatures corresponding to the lower friction after plasma treatment for PA6-E. The latter can be understood by the reduction in heat conductivity of the plasma-modified surface layer in case of PA6-E, as quantified before (Kalácska et al., 2016).

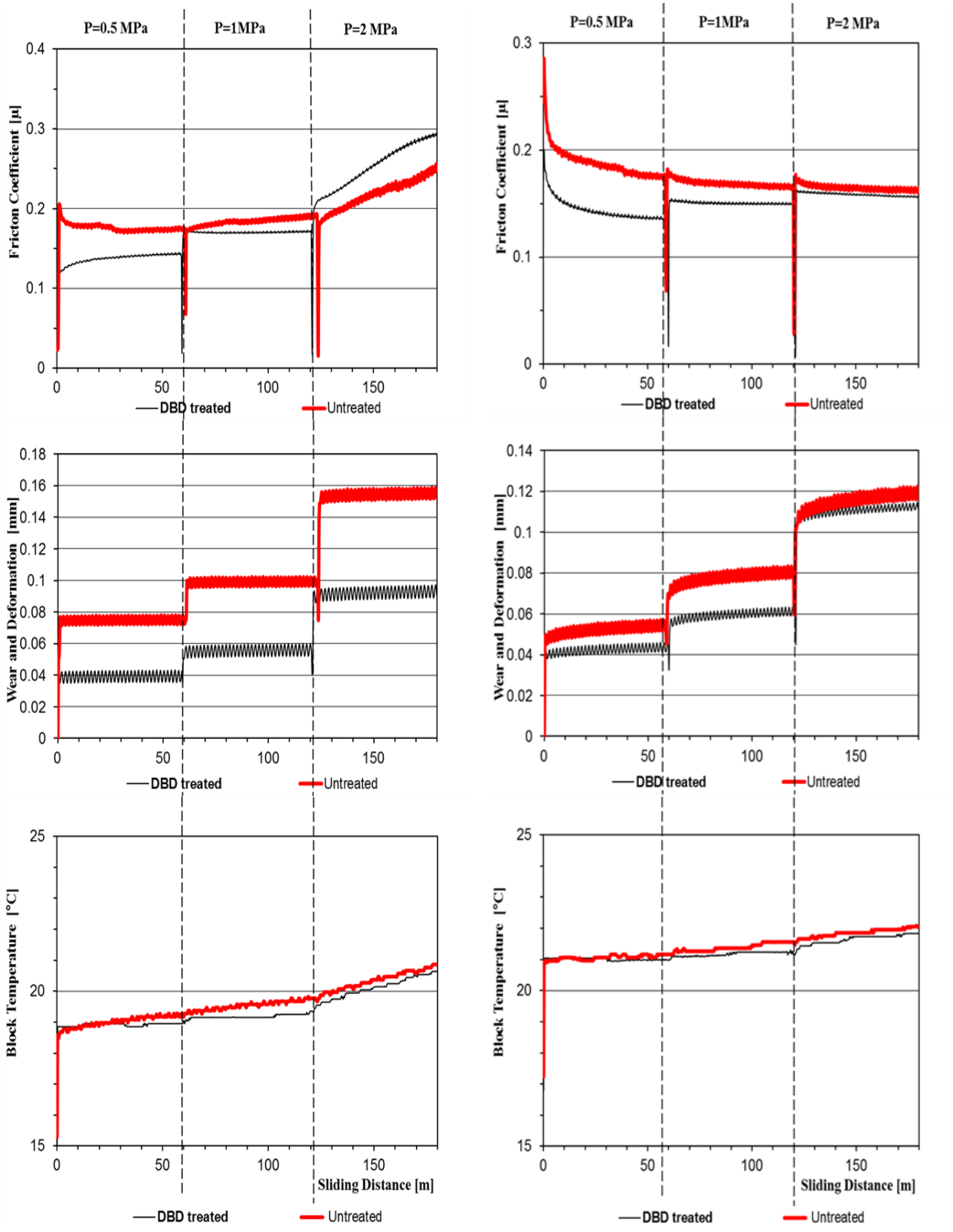

a) b) Continued

(Continued)

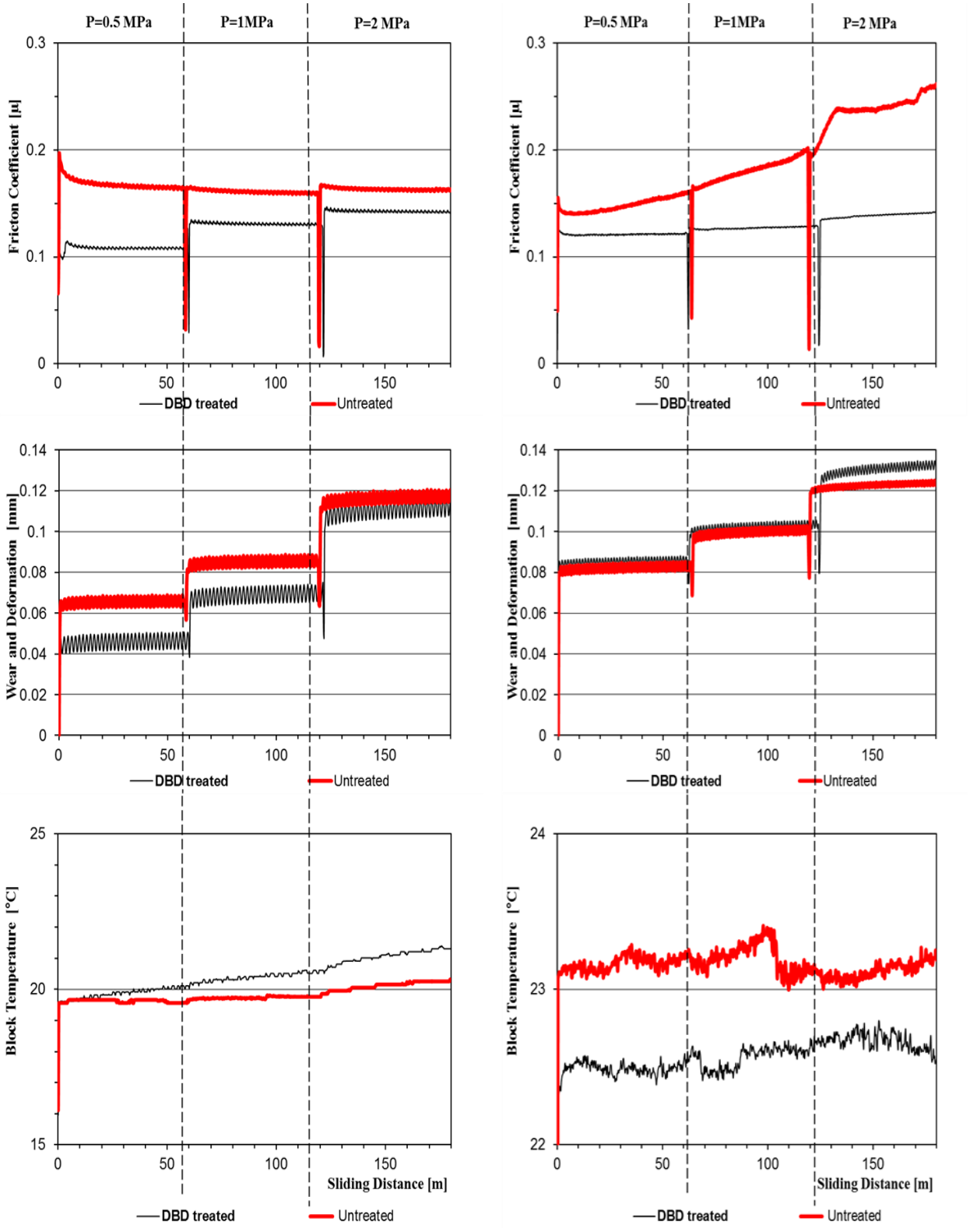

Fig. 4.19. Tribological testing under dry sliding conditions at 0.5, 1, and 2 MPa, including on-line measurements for coefficients of friction, wear and displacement Δh, temperature for a) PEEK, b) PET, c) PA6-E, and d) POM-C

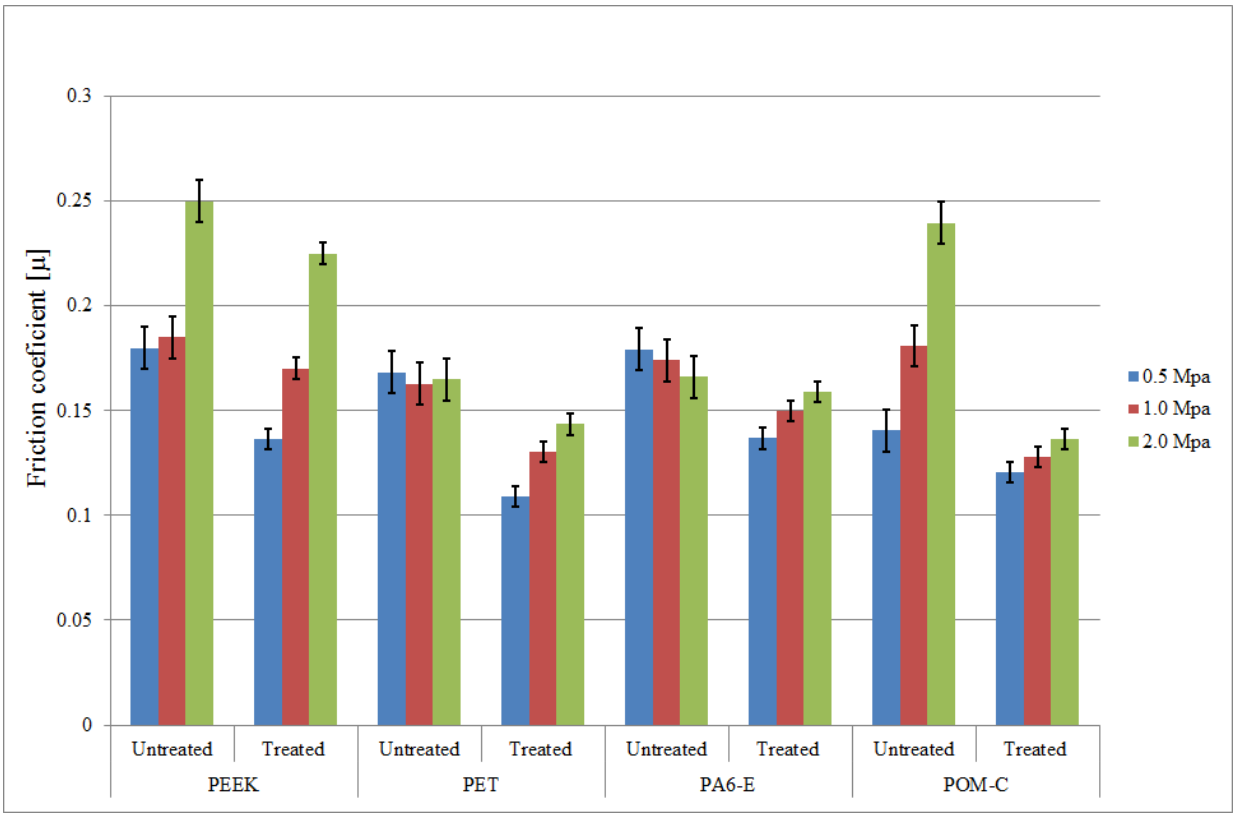

a)

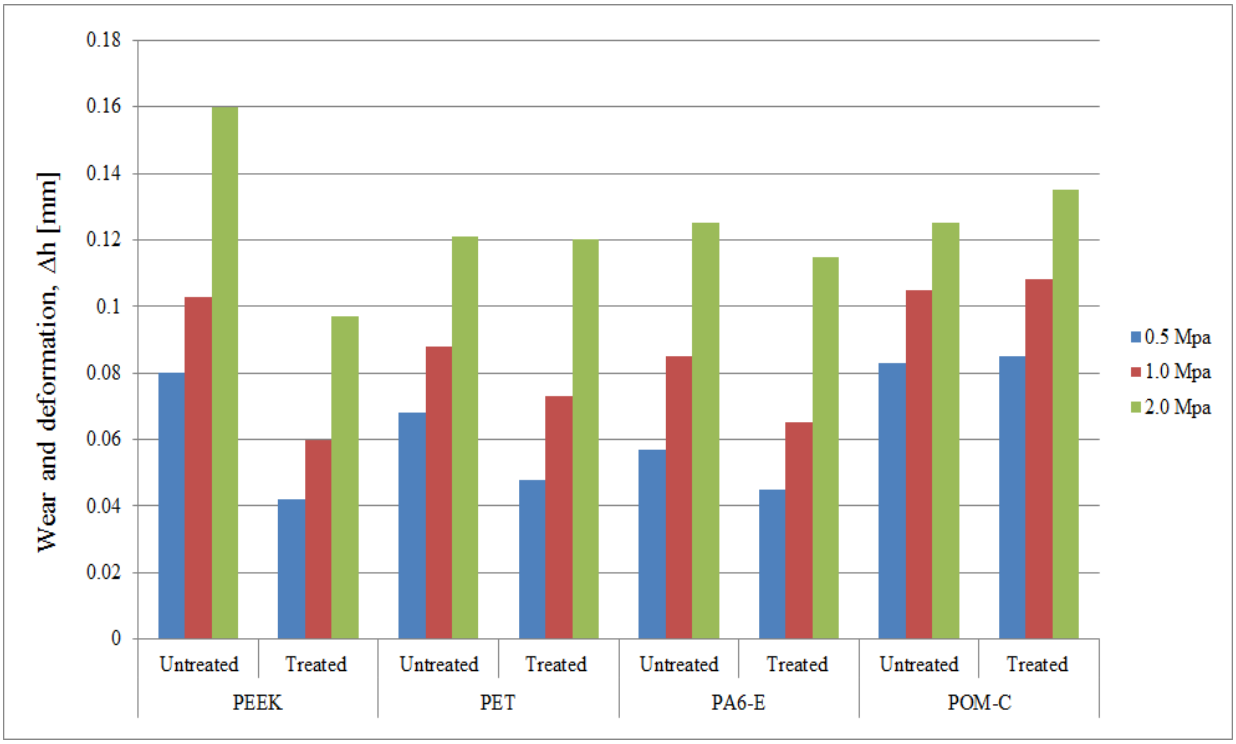

b)

Fig. 4.20. Tribological testing under dry sliding conditions at 0.5, 1, and 2 MPa: summary of tribological data with a) average coefficients of friction, b) wear and deformation Δh for engineering polymers

Lubrication run-out tests

The on-line measurements for coefficients of friction under oil-lubricated sliding and “run-out” lubrication conditions are presented in Fig. 4.21 for pristine and plasma-treated samples of engineering polymers. The maximum and average coefficients of friction (Fig. 4.22) are lower than previous tests under dry sliding at 0.5 MPa. The presence of a thin lubricating film efficiently demonstrated differences in tribological properties between untreated and treated polymer samples. After application of an oil droplet during the first period of sliding, low coefficients of friction (<0.05) with almost no differences between different samples are observed through the lubrication action of an oil film. After cleaning the sliding track, friction remains lower than under dry sliding conditions while different behaviour occurs between pristine and plasma-treated samples: the lubricating effect responsible for low friction of plasma-treated samples lasts for longer sliding times. The lower friction under “run-out” lubrication conditions can be attributed to the better retention of the oil in the sliding interface in case of plasma-treated surfaces: the surface energy (and mainly the surface polarity) of the plasma-treated polymer surfaces is significantly higher than the pristine surfaces and, therefore, favourably enhances the adsorption of the hydrophobic (polar) oil lubricant on the polymer surface and entrapment in the interface. However, more periodic fluctuations in friction occur after removal of the oil from the sliding track: the latter typically indicate friction instabilities within the mixed lubrication regime and can be attributed to dynamic changes in layer thickness of the remaining lubricant. While the coefficients of friction are lower for plasma-treated surfaces than for pristine surfaces for all polymers, the coefficients of friction for PEEK remain higher than for PET, PA-E, and POM-C, respectively, in parallel with the tendencies under dry sliding conditions, where it was stated that mechanical properties (i.e., higher stiffness of PEEK) can have an influence on the coefficients of friction.

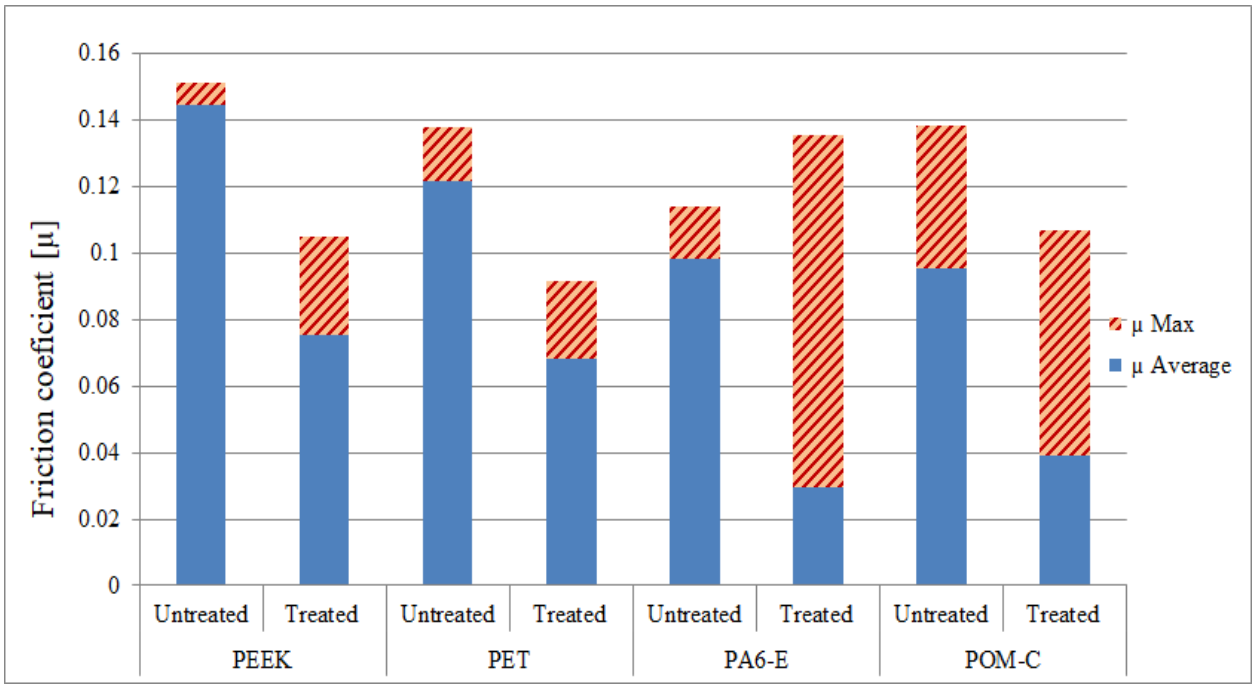

Fig. 4.22. Summary of average and maximum coefficients of friction of tribological testing under lubricated sliding and run-out conditions at 0.5 MPa for engineering polymers

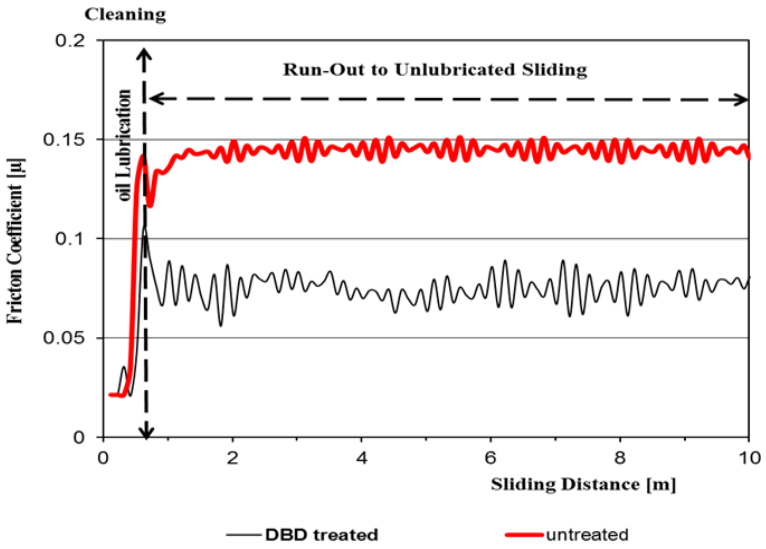

a)

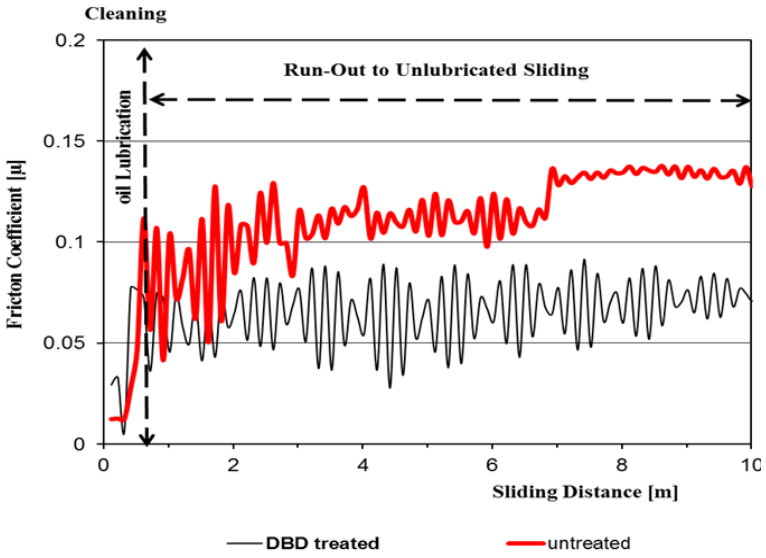

b)

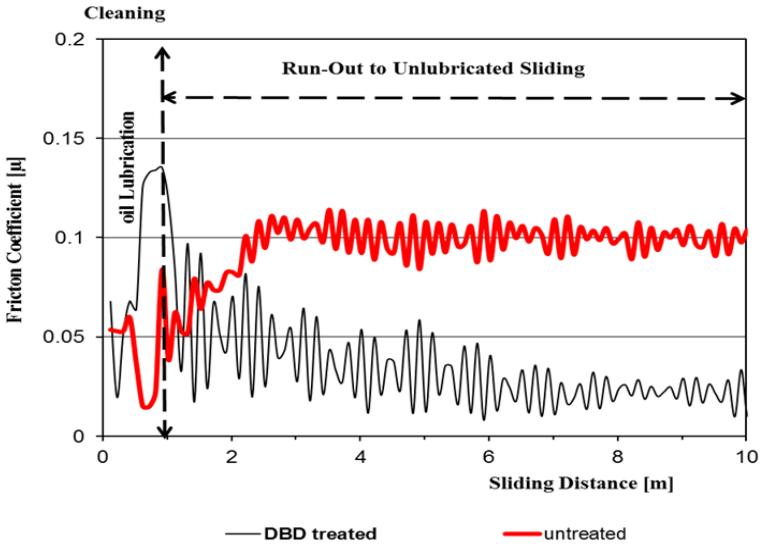

c) Continued

(Continued)

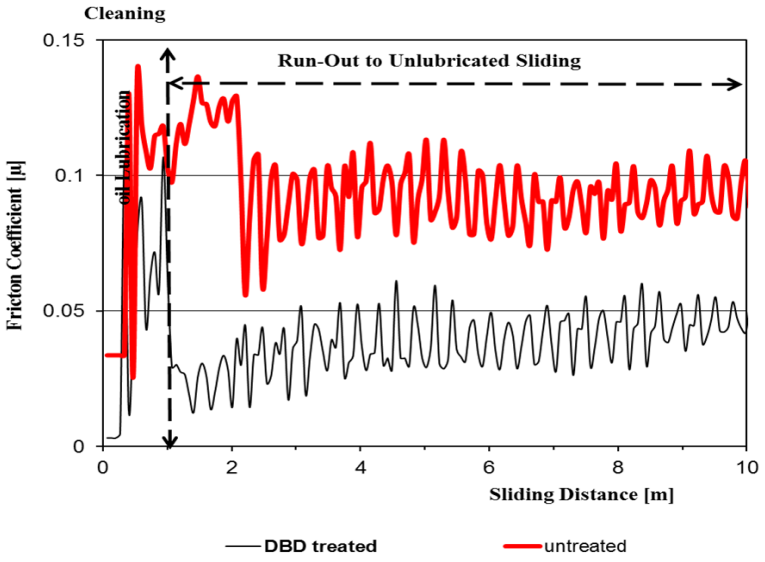

d)

Fig. 4.21. Tribological testing under lubricated sliding and run-out conditions at 0.5 MPa, with coefficients of friction of a) PEEK, b) PET, c) PA6-E, and d) POM-C

4.3.2. Effect of atmospheric DBD plasma on tribological behaviour of polyolefin polymers and PTFE

Dry sliding tests

The on-line measurements for coefficients of friction, wear, and bulk temperature during dry sliding tests on pristine and plasma-treated samples under different normal loads are shown for polyolefin polymers and PTFE in Fig. 4.23. The average values for coefficients of friction µ and vertical displacement Δh per load are summarised in Fig. 4.24. The coefficients of friction and wear were determined from three repetitions with a statistical variation of ± 2.5% on pristine and ± 1% on plasma-treated samples. Similar to engineering polymers, the coefficients of friction for all pristine surfaces show running-in phenomena with a peak value during the first couple of meters; however, the peak values are smaller compared to engineering polymers attributed to the lower mechanical properties. This phenomenon can be explained by the presence of a contaminated hydrocarbon layer on the untreated polymers. The friction coefficient of PP is higher compared to other polymers concerning the high mechanical strength and stiffness (deformation component of friction), providing higher sliding resistance. The coefficient of friction of the pristine PP and PTFE shows a similar behaviour, where it is increasing with rising the load. At low load, the friction was considerably higher after plasma treatment as compared to pristine PP and PTFE, while at higher load (1 Mpa and 2 Mpa) coefficient of friction tends to become roughly identical to coefficient of friction of pristine surface. The observed tendency can be explained by Archard's theory as mentioned before. Although plasma treatment affected the roughness of the surface, the increased surface energy and as a result, the greater adhesion of the surface has dominating effect on the friction. Due to the high wear rate for PP and PTFE increase the load causes a wear off of treated layer and the friction of the pristine and the treated surface become identical. Regardless the slight higher friction coefficient of UHMW-PE HD1000, the friction coefficient of pristine UHMW-PE HD (500 and 1000) are mostly similar. The effect of the

increased surface energy and adhesion after plasma treatment resulted in a slight increase in the friction coefficient at all load levels for UHMW-PE HD (500 and 1000). The higher friction suggests that the treated layer did not wear off even at high load, which was confirmed by the correspondent curve. Similar to friction, wear is also much less for UHMW-PE HD (500 and1000) than for PP and PTFE at all load levels which is indicated to the better mechanical strength and stiffness of UHMW-PE HD (500 and 1000). The bulk temperature of pristine polymers is pretty similar and following the trends of the coefficient of friction except for UHMW-PE HD1000, where it is showing slight opposite trends with lower temperatures for treated surface corresponding to the higher friction which can be attributed to the heat barrier properties of the DBD plasma modified layer as mentioned before. Therefore, the generated heat by friction is accumulated in the contact zone and the counter-surface somewhat better than in bulk.

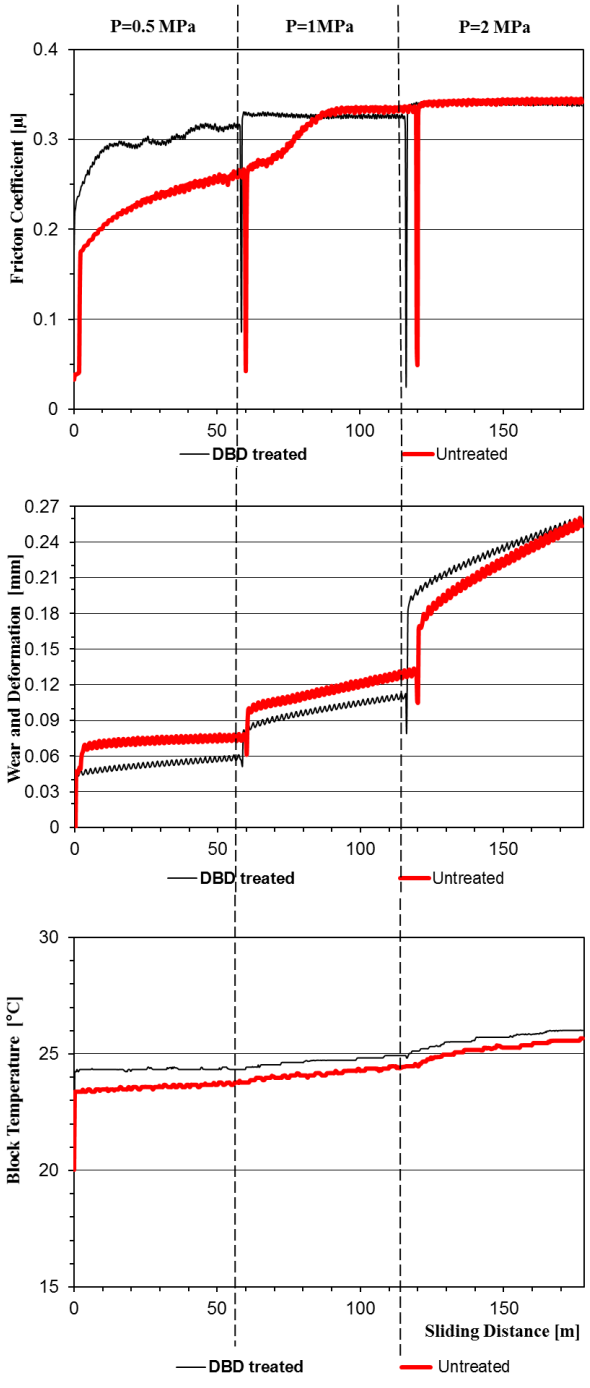

(a)

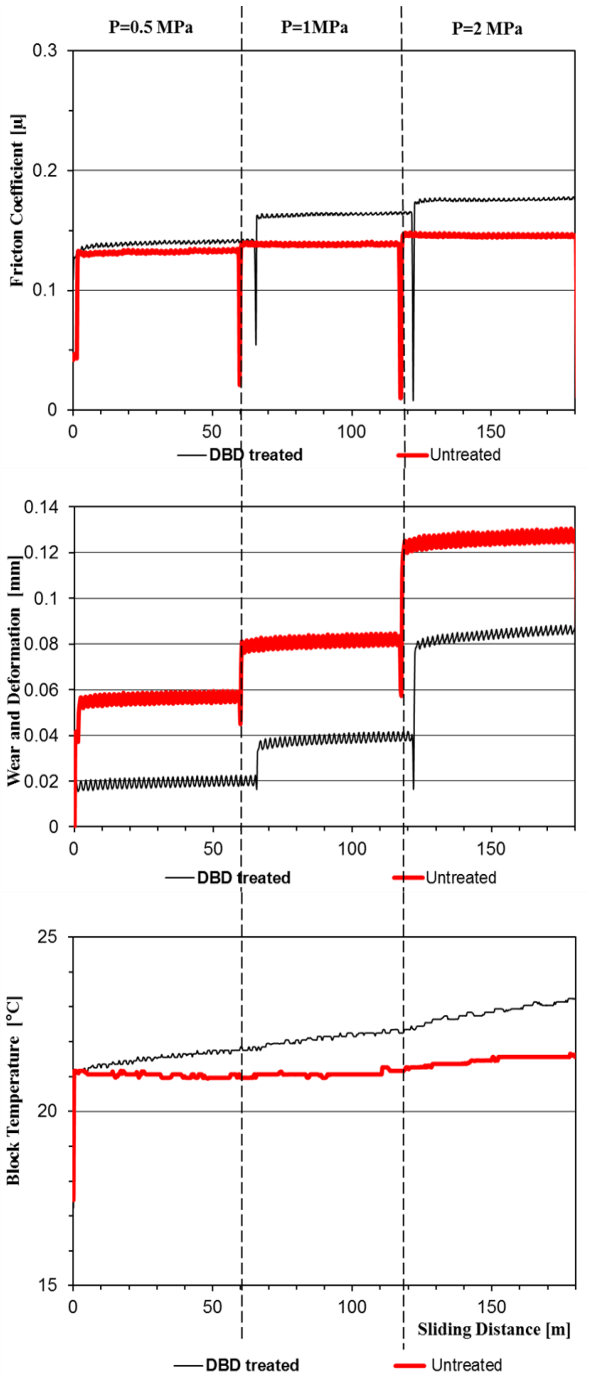

(b) Continued

(Continued)

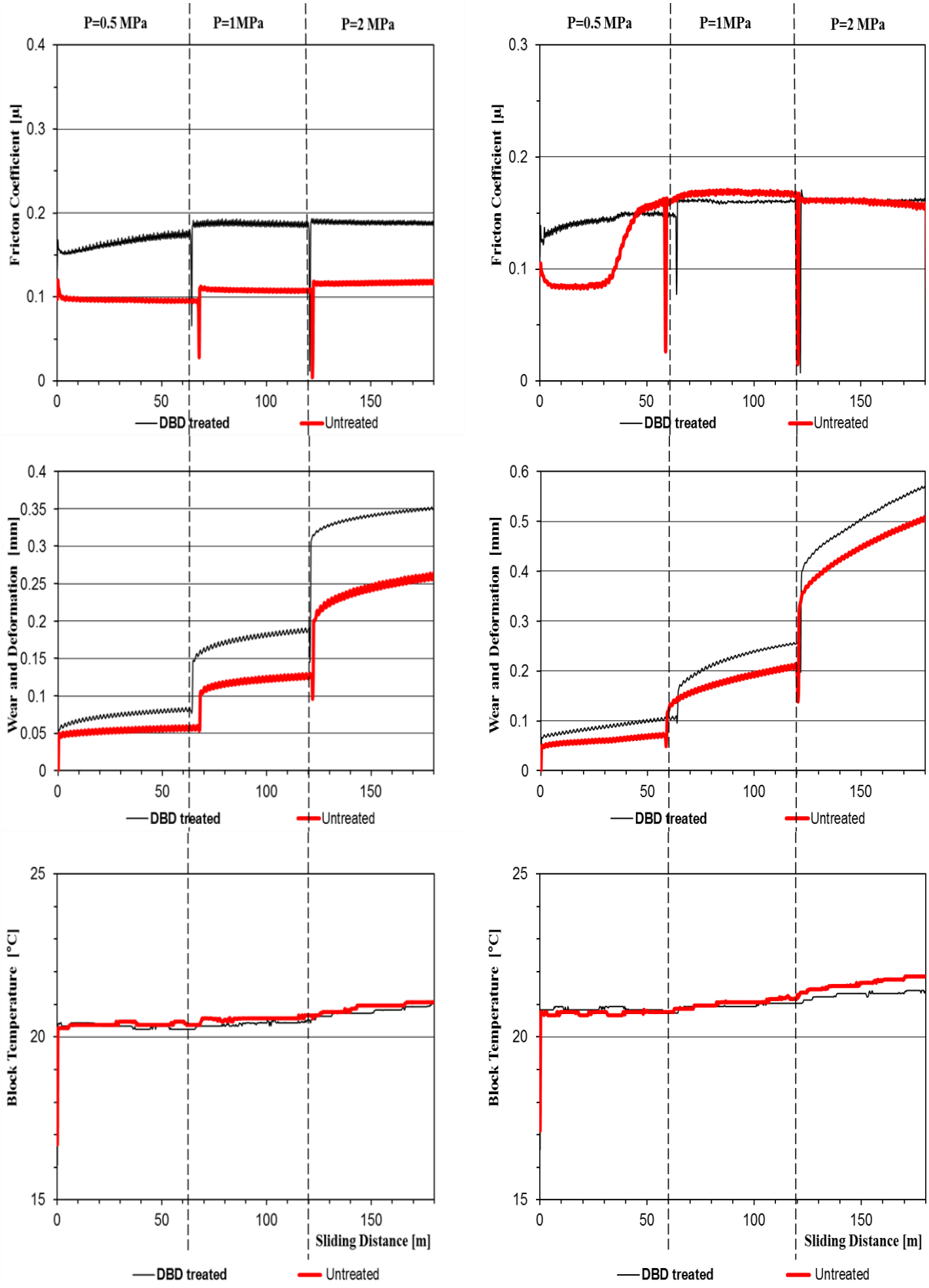

Fig. 4.23. Tribological testing under dry sliding conditions at 0.5, 1, and 2 MPa, including on-line measurements for coefficients of friction, wear and displacement Δh, temperature for a) PP, b) UHMW-PE HD500, c) UHMW-PE HD1000, and d) PTFE

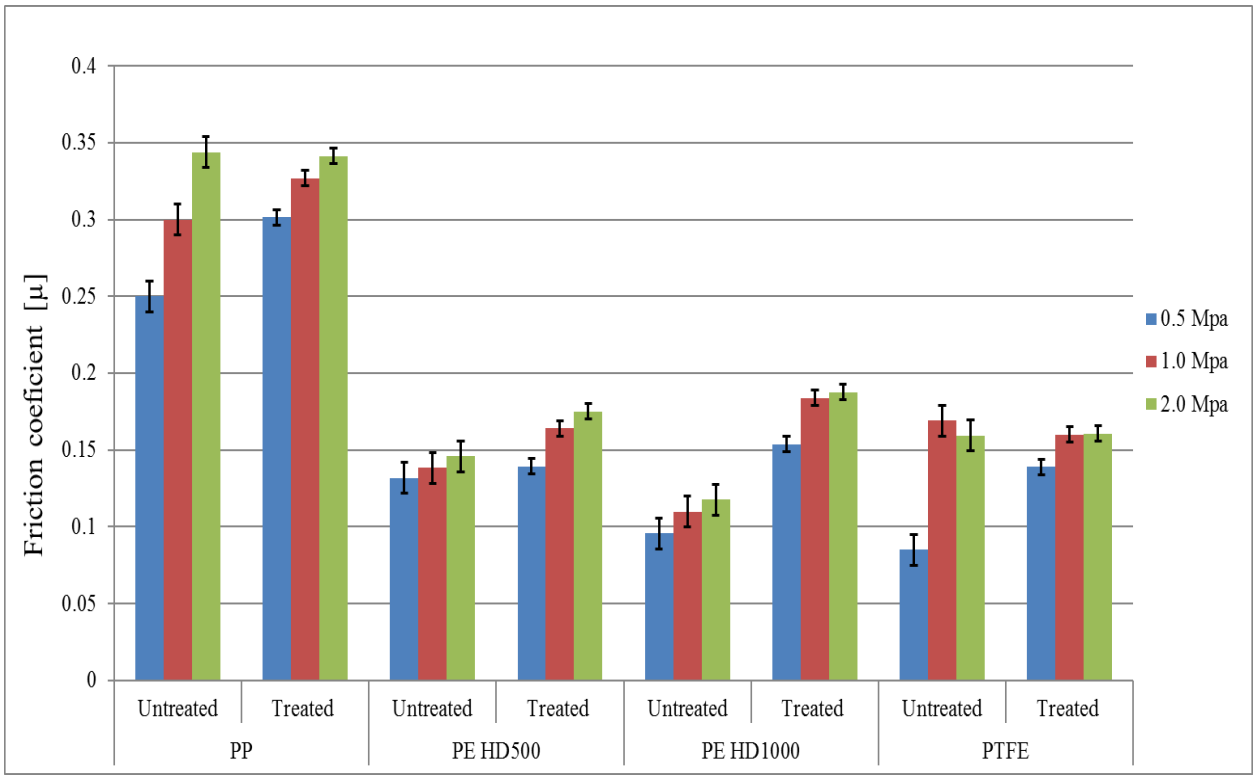

a)

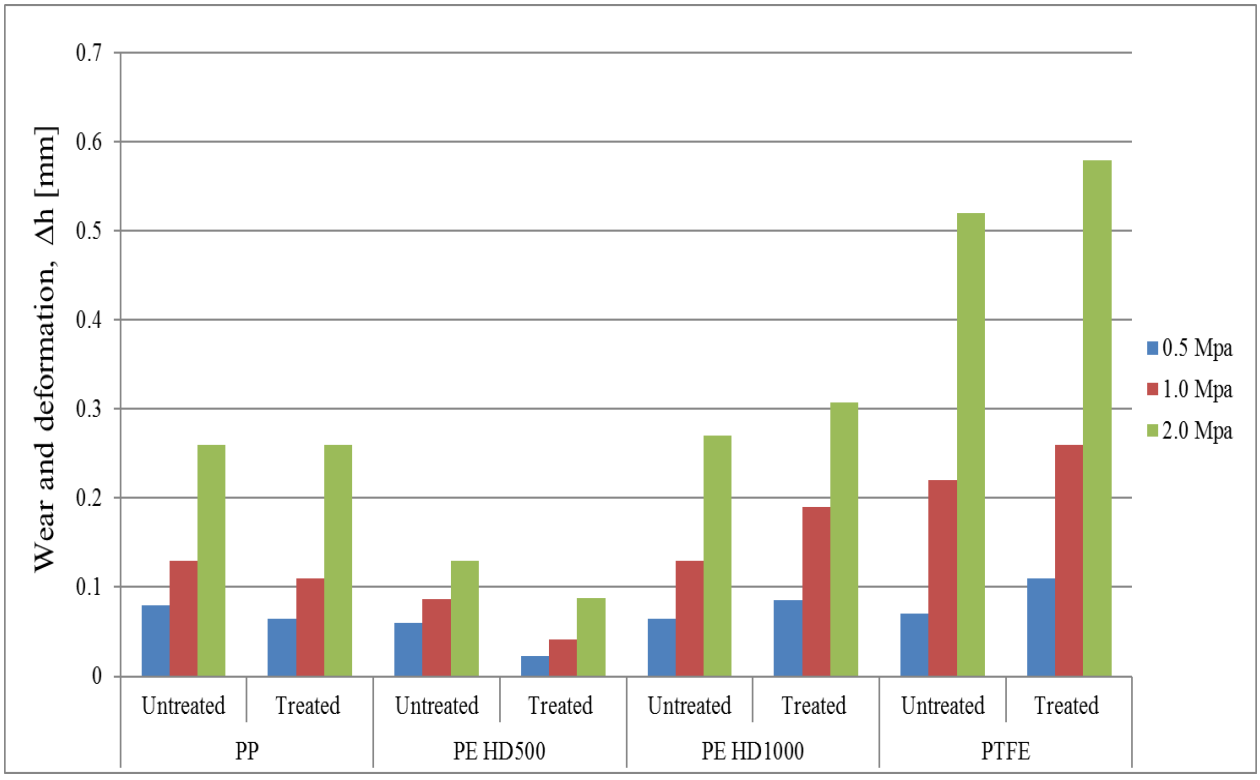

b)

Fig. 4.24. Tribological testing under dry sliding conditions at 0.5, 1, and 2 MPa: summary of tribological data with a) average coefficients of friction, b) wear and deformation Δh for polyolefin polymers and PTFE

Lubrication run-out tests

The friction coefficients in oil-lubricated sliding and run-out lubrication conditions are illustrated for the pristine and surface treated specimens of polyolefin polymers and PTFE in Fig. 4.25. The maximum and average coefficients of friction are presented in Fig. 4.26. Application of an oil droplet during the first period of sliding resulted in an identically low coefficient of friction (<0.05) irrespectively of the type of sample and treatment owing to the lubricating action of the oil film. In spite of removing the oil from the sliding track, coefficients of friction remain considerably lower than dry sliding conditions ones where friction coefficient of pristine PP remains higher than other polymers in parallel with the tendencies under dry sliding conditions, concerning the higher stiffness as mentioned earlier. The lower friction can be ascribed to the oil retention ability of the polymer surface. However, a combination of the modified microgeometry and the increased surface energy of the plasma-treated polymers favourably enhances the adsorption of the oil lubricant on the polymer surface and entrapment in the interface resulted in lower coefficient of friction for PP, PTFE, and UHMW-PE HD500. During “run-out” the mixed friction regime approaches toward the boundary lubrication, and with decreasing thickness of the lubricant layer, the friction became stabilised at a lower level as compared to the pristine sample. The oil retention ability of treated UHMW-PE HD500 surface can also be detected, but it is much less apparent as compared to PP and PTFE. However, treated surface of UHMW-PE HD1000 was observed a slightly higher friction which is in line with topographical results (see Fig. 4.14 c) indicated to increase the surface roughness of UHMW-PE HD1000 upon plasma treatment. The higher surface roughness provides higher number of naked spots within the mixed lubrication which directly engaged with the countersurface developing junctions in the interface, and this required higher shear strength thereby higher friction. The high surface roughness was noted for PP as well but did not influence the friction behaviour due to the higher wear rate of PP which led to removing the treated layer during the first period of the sliding distance, although presenting of lubrication. In parallel, the considerable fluctuations in the friction indicate the effect of the varying layer of the lubricant.

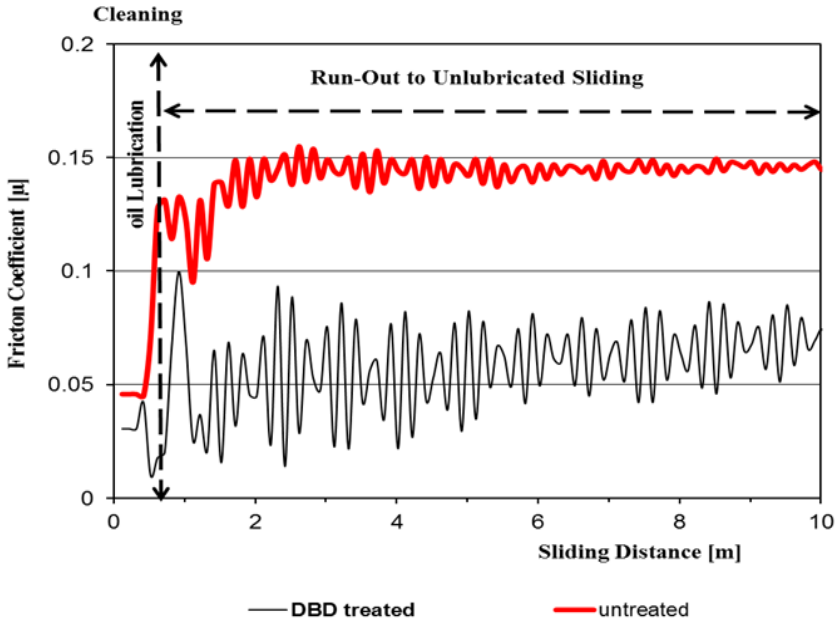

a) Continued

(Continued)

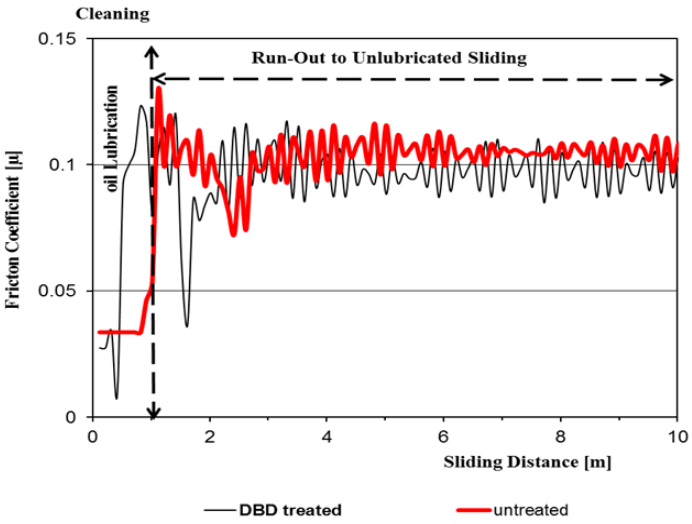

b)

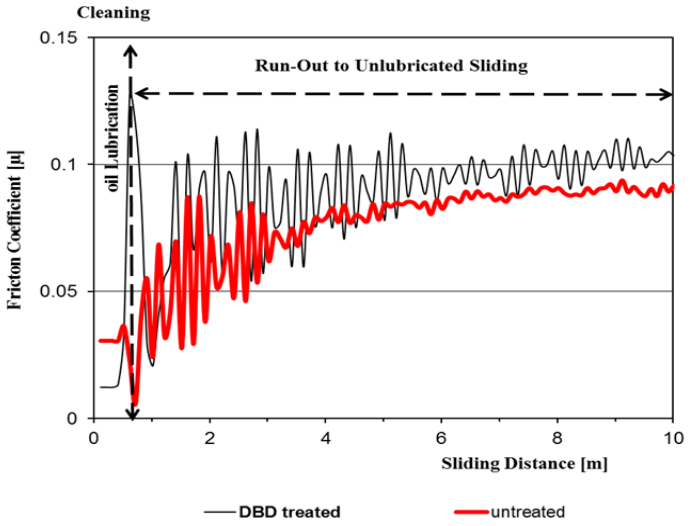

c)

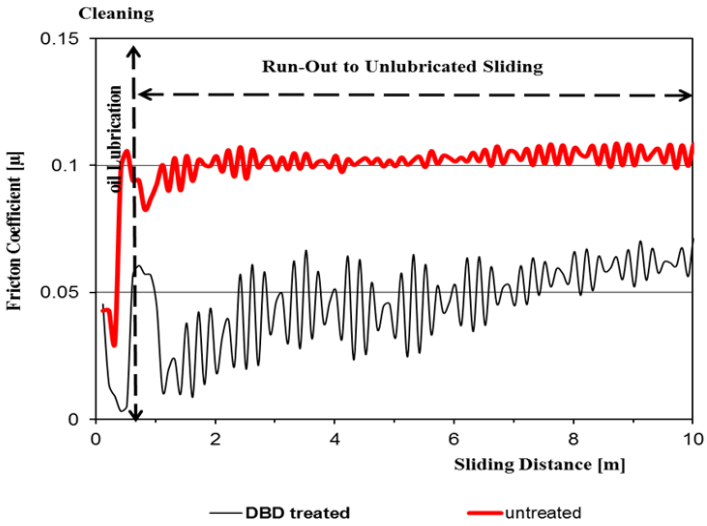

d)

Fig. 4.25. Tribological testing under lubricated sliding and run-out conditions at 0.5 MPa, with coefficients of friction of a) PP, b) UHMW-PE HD500, c) UHMW-PE HD1000, and d) PTFE

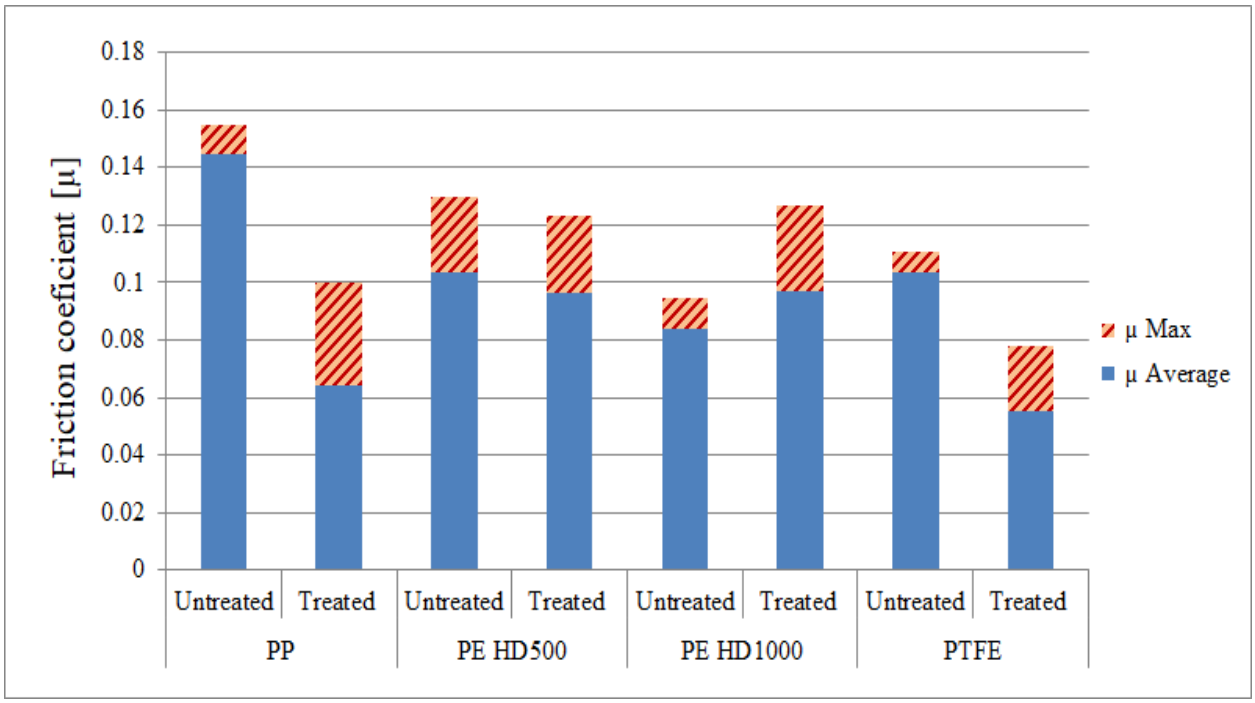

Fig. 4.26. Summary of average and maximum coefficients of friction of tribological testing under lubricated sliding and run-out conditions at 0.5 MPa for polyolefin polymers and PTFE

4.4. New scientific results

In this section the unique results investigated in my test systems are shown.

1. Surface chemical composition and wettability

Concerning the effects of DBD plasma treatment on chemical composition and wettability of polymer surfaces:

I stated that in case of PEEK, PET and PA6-E, the oxygen and nitrogen content increased while the carbon content decreased. For POM-C the oxygen content increased but no nitrogen presence was detectable besides the decreasing carbon content. The treated surfaces can be characterised by the formation of carboxylic acid and ester bonds by oxidation, especially for the aromatic PEEK and PET. Altogether I confirmed that the relative carbon content decreased with a parallel increase in overall oxygen content. The formation of polar groups containing oxygen on the surface can contribute to a hydrophilic improvement after plasma treatment. The surface energy of the treated surfaces increased, which influences both the adhesive as well as tribological behaviour.

In case of the examined polyolefin polymers and PTFE, I detected the formation of new functional groups such as hydroxyl, carbonyl and carboxylic acid, but in smaller rate compared to the examined engineering polymers.

2. Surface topography characteristics

In case of identical plasma treatments, I proved that the effect of the DBD plasma treatment on the surface topography can be bi-directional. The roughness of the original extruded smooth surfaces (R and S roughness in nano-scale) increased in parallel with the chemical modification of the surfaces following Kostov's theory, whereas the roughness of the machined and polished surfaces

(R and S roughness in micron scale) decreased because of the "melting" effects (except for UHMW-PE HD1000) following Salapare's theory.

3. Adhesive bonding response to atmospheric DBD plasma treatment

I have stated the followings on the base of shear strength tests of polymer/polymer and polymer/steel adhesively bonded overlap joints (DIN EN 1465):

In case of DBD treated polymers, the shear strength of the bonded joints increased and the statistical deviation (spread σ%) on the shear strength significantly reduced from 8-9% to around 1% for all polymers tested, regardless of the applied adhesive. In this case the technical reliability of bonded joints is significantly improved by the plasma treatment.

Concerning the DBD treated polymer surfaces the highest increase in shear strengths of the adhesive bonds were performed in case of epoxy adhesive. This is the result of the reactivity of the epoxy adhesive toward the carboxylic groups at the polymer surface after plasma treatment forming a strong adhesive bond. I stated that the untreated surfaces performed de-bonding failure on the surfaces under shear tests, while the treated polymers suffered more complex failure: de-bonding, cohesive failure in the adhesive layer and cracking in the bulk polymer occurred.

I found that among the polyolefins for the PP and UHMW-PE HD500 the increasing shear strength due to DBD plasma treatment can be concluded, however for UHMW-PE HD1000 and for PTFE the effect is barely perceptible. This phenomenon relates to the chemical composition of the surfaces and the lower mechanical strength (lower E modulus and higher strain capability) of the matrix materials, too.

4. Tribological behaviour under dry sliding conditions for engineering polymers

In my dry sliding tribology systems, I have stated that:

At low *pv* load level (*pv* 0.025 MPa x ms^{-1}) the DBD treatment can decrease the friction coefficients of engineering polymers, in spite of the increased surface energy. This can only be true in Archard's friction theory if the decrease of deformation component of friction force is more significant than the increase of the adhesive component of friction. As a result of DBD treatment of machined and polished polymer surfaces I proved the decrease of the deformation component of friction via decreased surface roughness using 3D topography.

I proved with my measurements that the increase of "*pv*" load level, i.e. the increase of the real contact area, can reach a transition "*pv*" border, when the adhesive component of friction becomes dominant in accordance with the experienced higher surface energy of treated surfaces and the resulting friction of DBD treated polymer surfaces can exceed the virgin untreated ones. That transition "*pv*" load level can be measured identically for each polymer types.

5. Tribological behaviour under dry sliding conditions for polyolefin polymers and PTFE

I stated that the phenomenon introduced in 4 is not valid for polyolefin polymers and PTFE under the applied low "*pv*" load conditions (*pv* 0.025 MPa x ms^{-1}). The friction of treated polymer surfaces was higher compared to the virgin ones. When applying Archard's theory to this phenomenon, it is explained by dominant adhesive component of friction against the decreased deformation component of friction. The normal load is low but due to minor *E* modulus of polymer matrix, the occurred real contact area is large enough for higher adhesion.

6. Tribological behaviour under "run-out" oil lubrication conditions

With oil lubricated polymer/steel sliding pairs in mixed friction systems, I proved for the tested engineering polymers, polyolefins and PTFE (except UHMW-PE HD1000) that DBD treatment can enhance the lubricant retention and can cause lower friction. This is explained by the increased surface energy (polar and dispersive components both) of the DBD treated surfaces.

I concluded in my mixed friction sliding systems that the positive oil retention effect of DBD treatment can be limited by the increased surface roughness. In case of UHMW-PE HD1000 the surface roughness increased due to plasma treatment, thus the higher deformation component of friction (dry asperity contacts) dominates over the improved lubricating effects causing higher friction of the plasma treated surface compared to the untreated one.

5. CONCLUSIONS AND SUGGESTIONS

In conclusion, cold atmospheric DBD plasma treatment of polymer surfaces may induce favourable tribological properties for precision sliding components under mild conditions, especially under oil lubrication. In addition, the adhesive bonding of DBD plasma-treated polymers can sustain higher strength, especially for engineering polymers. After the DBD treatment of studied polymer surfaces under optimised conditions in air atmosphere, comparable effects on surface characterisation, adhesion, friction, and wear have been observed as follows:

The XPS measurements indicate the effects of surface oxidation with formation of polar functional groups and carboxylic acid moieties. The contact angle measurements show a significant reduction in WCA values thereby higher surface wettability for all polymers due to the developed polar groups.

The surface morphology investigations of extruded surfaces show an increase the surface roughness of the plasma-treated polymer surfaces except for UHMW-PE where the roughness was decreased and remains almost same for POM-C. The 3D topographical measurements indicate a reduction in surface roughness of the originally polished polymer surfaces (except PP and UHMW-PE HD1000) due to flattening of the surface asperities while the machining grooves remain present.

The adhesive shear strength of polymer/polymer and polymer/ steel joints increases after plasma treatment. Epoxy-type glue system has the highest shear strength for engineering polymers. Whereas, the glues systems of polyolefin polymers and PTEF were showed a varying strength depending on the countersurface. Besides the strength improvements, the reliability of the joints could also be improved this manifested by the much smaller standard deviation of the measured values and alteration of locus failure from adhesive failure type to cohesive failure in the adhesive layers' type or pure bulk crack in some cases.

The coefficients of friction for engineering polymers under dry sliding conditions are lower than pristine samples at low "*pv*" factor, while it may become higher under more severe sliding conditions. On the other hand, the coefficients of friction of polyolefin polymers and PTEF are higher than pristine samples at low "*pv*" factor, while coefficients of friction may become identical to coefficient of friction of pristine surfaces under more severe sliding conditions due to wear off the treated layer (especially for PTFE and PP). The deformation and wear (Δh) was varied for all polymer surfaces depending on the bulk mechanical properties. The bulk temperature is following the coefficient of friction behaviour except for PA6-E due to the low heat conductivity after treatment. As a unique feature, the coefficients of friction under oil-lubricated conditions remained low during "run-out" conditions for the plasma-treated samples (except UHMW-PE HD1000), as a lubricating layer was retained in the sliding interface. UHMW-PE HD1000 was showed higher coefficient of friction due to the high surface roughness after plasma treatment.

As a follow up to this research, further investigations and activities may be required to cover the most critical effects of atmospheric DBD plasma on polymer surfaces and tribology. I suggest the following desirable points:

Investigate the effect of DBD plasma on other materials (presently are trendy) such as amorphous, polymer composites, biopolymers, 3D printed polymers. Using a dynamic specimen movement during DBD plasma treatment instead of the liner which was used. Measuring surface low-frequency modes by Raman spectroscopy and different light wavelength absorption by FTIR. In addition to single lap joints, others joint types can be utilised such as thick adherend, double lap Joint, strap Joint, and scarf Joint. Testing of special adhesives developed for polyolefin type polymers (e.g., Yparex or Plexar). Investigate the polymer tribological behaviours under constant load for dry sliding conditions, repeating the tests under water "run-out" or "continuous" lubrication conditions and "continuous" oil lubrication conditions. In addition, the oil "run-out" lubrication testes may be repeated for three normal loads similar to dry tests. Testing the effect of atmospheric DBD plasma on polymer surfaces tribological behaviour under different test configurations and standards.

6. SUMMARY

ADHESIVE AND TRIBOLOGICAL BEHAVIOUR OF COLD ATMOSPHERIC PLASMA-TREATED POLYMER SURFACES

In summary, eight commercial polymers were used in this research. Polymers were distinguished into two groups: 1) Engineering polymers including PEEK, PET, PA6-E, and POM-C, and 2) Polyolefin polymers and PTFE including PP, UHMW-PE HD500, UHMW-PE HD1000, and PTFE. Cold atmospheric DBD plasma treated the polymers for 1 min. The main objective of the research is to investigate the effect of DBD plasma on the polymers surface characterisation, adhesive bonding, and tribology. XPS was utilised to investigate the surface chemical composition. Contact angles and wettability were measured by static sessile drops, using (SEE) System apparatus. The surface morphology of polymer surfaces was analysed by SEM, AFM and 3D surface topography. The adhesive bonding was examined by lap-shear tests on single lap joints of polymer/polymer and polymer/steel pairs. The tribological tests were done by a pin-on-disc apparatus under dry (3 normal loads) and "run-out" lubrication (constant normal load) conditions.

The results show that DBD plasma can enhance the polar functional groups and carboxylic acid moieties in the polymer surfaces. The surface hydrophilicity was improved in parallel with contact angle reduction. However, polymer hydrophilicity is declined after 24 h from plasma treatment towards the initial state without reaching the original state of pristine samples. The surface morphology shows high surface roughness of extruded surfaces after treatment except for UHMW-PE and POM-C. The 3D topography is showed a reduction in the roughness parameters of plasma treated polymer surfaces due to surface flatten after melting the surface asperities except for PP and UHMW-PE HD1000 where they have a higher surface roughness after treatment.

The shear strength of polymer/polymer and polymer/steel adhesively bonded joints is improved of different adhesive systems in parallel with surface energy improvements. In general, DBD plasma treatment is favourable to improve the adhesive bonding for engineering polymers. The epoxy-type glue system was exposed the highest shear strength for engineering polymers. Whereas, the glue systems of polyolefin polymers and PTFE were varied depending on the counter surfaces. The statistical deviation of (5 repetitions) the shear strength is significantly reduced due to plasma treatment.

At low *pv* factor, the coefficients of friction for treated engineering polymers are much lower than pristine surfaces under dry sliding conditions, while the coefficient of friction may become higher under more severe sliding conditions particularly for PEEK. On the other hand, the coefficients of friction of treated polyolefin polymers and PTFE is higher than pristine ones at low *pv* due to the improvements in friction adhesive components, however, they have become identical at higher *pv* for PP, PTFE due to the wear off of treated layer. Wear was varied depending on the mechanical properties of the bulk material. The bulk temperature has almost similar behaviour to the coefficient of friction curves except for PA6-E due to the low heat conductivity after treatment.

Under lubrication "run-out" conditions the coefficients of friction of treated polymer surfaces are significantly lower than pristine samples except for UHMW-PE HD1000 due to the high surface roughness of UHMW-PE HD1000 after treatment.

7. ÖSSZEFOGLALÁS (SUMMARY IN HUNGARIAN)

NATÚR ÉS ATMOSZFÉRIKUS HIDEGPLAZMÁVAL KEZELT POLIMER FELÜLETEK ADHÉZIÓS ÉS TRIBOLÓGIAI TULAJDONSÁGAI

A kutatás során nyolc különböző, a kereskedelmi forgalomban beszerezhető polimert választottam ki a mérnöki gyakorlat szempontjai alapján. Ezek két fő csoportba sorolhatók:

1) csoport: az általános és HPM műszaki műanyagok, beleértve a PEEK, PET, PA6-E, POM-C.

2) csoport: tömegtermékek, beleértve a PP, az UHMW-PE HD500, az UHMW-PE HD1000 és PTFE.

A kiválasztott polimerek felületét 1 perces időtartamban (elő-kísérletek alapján meghatározott kezelési idő) atmoszferikus hidegplazma (DBD eljárás) hatásának tettem ki. Kutatásom fő célja, hogy a kezelt polimer felületeken bekövetkező szerkezeti-, topográfiai- és felületenergetikai változásokat együttesen elemezzem és értékeljem a mérnöki alkalmazások szempontjainak megfelelően. Ebből fakadóan a felületek ragaszthatóságát majd a súrlódó alkalmazásokban való felhasználhatóságot, a tribológiai viselkedést kutattam úgy, hogy a felületek jellemzésére használt módszereknél referenciaként kezeltem az eredeti, kezeletlen polimer felületeket. Az adhéziós (ragasztási) és tribológiai kísérletek előtt a natúr és kezelt felületek jellemzést végeztem el. XPS technikával a felületek kémiai összetétele lett meghatározva. A felületi energia számítására a cseppelemezésen (SEE) alapuló – peremszög mérés - Owens-Wendt módszert használtam. A polimer felületek felületi szerkezetének, morfológiájának elemzéséhez SEM és 3D felülettopográfiai mérések készültek. Az átlapolással összeragasztott próbatestek - polimer/polimer és polimer/acél párosítás – felületi adhéziós tapadásának kutatására a ragasztott kötések nyíróvizsgálatát végeztem szabvány szerint, szakítógép alkalmazásával. A tribológiai vizsgálatokat tű-tárcsa rendszerben (ahol a polimer próbatest képezte a tűt a forgó acéltárcsán) először száraz súrlódás esetén, három terhelési szinten végeztem el, majd olajkenéses és olajkifuttatásos méréseket is végeztem.

Az eredmények azt mutatják, hogy a DBD plazma kezelés növelheti a poláris funkciós csoportokat és a karboxil csoportok részarányát a polimer felületeken. Ezzel összhangban a felületi nedvesítőképesség javul, amit igazolt a cseppelemzés során mért érintkezési peremszögszög csökkennés. A plazmakezelés hatására a mikrogeometria átalakulása nem egyértelmű. A vizsgált rendszerben a plazma hatására a mikrogeometriai érdesség jórészt csökkent, melyet a korábbi szakirodalmak egyfajta olvadásos mechanizmussal igazolnak, de a PP és az UHMW-PE HD1000 érdessége ellenben megnőtt.

A polimer/polimer és a polimer/acél ragasztott kötések nyírószilárdsága javul a különböző ragasztórendszerekben a felületi energia növelésével, de az egyes polimereknél eltérő arányban. Méréseimmel kimutattam, hogy általában azon plazmakezelt polimer felületek esetén, ahol a felületi érdesség csökkent a kezelés hatására, és nőtt a felületi energia (poláris és diszperzív komponensek), ott a felületek képesek kenőanyagmegtartó hatást kifejteni, így kedvezőbb eredő súrlódást biztosítanak, mint a natúr polimer felületek. E jelenség nem volt érvényes az UHMW-PE HD1000 esetén, ahol a kezelés jelentősen megnövelte a felületi érdességet.

8. APPENDICES

A1: Bibliography

1. Akovali, G. (2012): The interfacial interactions in polymeric composites, Vol. 230, Ankara, Turkey, Springer Science & Business Media.
2. Akram, M., Bhowmik, S., Jansen, K. M. B., and Ernst, L. J. (2010): Surface modification of polyimide by atmospheric pressure plasma for adhesive bonding with titanium and its application to aviation and space, New materials and processes for a New Economy: 55th International SAMPE Symposium, May 17-20, 2010, Seattle, USA, p. 10.
3. Akram, M., Jansen, K.M.B., Ernst, L.J., and Bhowmik, S. (2016): Atmospheric plasma modification of polyimide sheet for joining to titanium with high temperature adhesive, International Journal of Adhesion and Adhesives, 65, pp. 63-69.
4. All Seals: The sealing specialists section 5: plastic & thermoplastic elastomer materials, online at: http://allsealsinc.com/05_Plastic-Thermoplastic.pdf, accessed on 29 November, 2017.
5. Archard, J. (1953): Contact and rubbing of flat surfaces, Journal of Applied Physics, 24(8), pp. 981-988.
6. Awajaa, F., Gilbert, M., Kelly, G., Fox, B., and Pigram, P.J. (2009): Adhesion of polymers, Progress in Polymer Science, 34(9), pp. 948-968.
7. Baldan, A. (2012): Adhesion phenomena in bonded joints, International Journal of Adhesion and Adhesives, 38, pp. 95–116.
8. Bárdos, L., and Baránková, H. (2010): Cold atmospheric plasma: Sources, processes, and applications, Thin Solid Films, 518(23), pp. 6705-6713.
9. Bartenev, G.M., and Lavrent′ev, V.V. (1981): Friction and wear of polymers, Vol. 6, Amsterdam, Elsevier; p. 212.
10. Basin, V.E. (1984): Advances in understanding the adhesion between solid substrates and organic coatings, Progress in Organic Coatings, 12(3), pp. 213-250.
11. Bely, V. A., Sviridenok, A. I., and Petrokovets, M. I. (2013): Friction and wear in polymer-based materials, Elsevier.
12. Bertóti, I., Mohai, M., and László, K. (2015): Surface modification of graphene and graphite by nitrogen plasma: Determination of chemical state alterations and assignments by quantitative X-ray photoelectron spectroscopy, Carbon, 84, pp. 185-196.
13. Bismarck, A., Brostow, W., Chiu, R., Hagg Lobland, H.E., and Ho, K.K. (2008): Effects of surface plasma treatment on tribology of thermoplastic polymers, Polymer Engineering and Science, 48(10), pp. 1971-1976.
14. Blackman, B.R.K., and Guild, F.J. (2013): Forced air plasma treatment for enhanced adhesion of polypropylene and polyethylene, Journal of Adhesion Science and Technology, 27(24), pp. 2714-2726.
15. Blau, P.J. (1989): Friction and wear transitions of materials, New York, Noyes Publication.

16. Bogaerts, A., Neyts, E., Gijbels, R., and Van der Mullen, J. (2002): Gas discharge plasmas and their applications, Spectrochimica Acta Part B: Atomic Spectroscopy, 57(4), pp. 609-658.

17. Boulos, M.I., Fauchais, P., P fender, E. (1994): Thermal plasmas: fundamental and applications, Vol. 1, New York, Plenum Press.

18. Bowden, F.P., and Tabor, D. (1964): Friction and lubrication of solids, Oxford, Clarendon Press.

19. Bowers, R.C., Clinton, W.C., and Zisman, W.A. (1953): Frictional behavior of polyethylene, polytetrafluoroethylene, and halogenated derivatives (No. NRL-4167), Naval Research Lab.

20. Briscoe, B.J. (1986): Interfacial friction of polymer composites. general fundamental principles, Chapter No 2 of Friction and Wear of Polymer Composites /ed. Friedrich, K./, Composite Materials Series, 1, Amestrdam, Elsevier, pp. 25-59.

21. Černák, M., Hudec, I., Kováčik, D., and Zahoranová, A. (2009): Diffuse coplanar surface barrier discharge and its applications for in-line processing of low-added-value materials, European Physical Journal: Applied Physics, 47(2), pp.1-6.

22. Chanda, M., and Roy, S.K. (2006): Plastics technology handbook, Fourth edition, New York, CRC press.

23. Chapman, B. (1980): Glow discharge processes, New York, Wiley.

24. Choia, Y.H., Kim, J.H., Paek, K.H., Ju, W.T., and Hwang, Y.S. (2005): Characteristics of atmospheric pressure N_2 cold plasma torch using 60-Hz AC power and its application to polymer surface modification, Surface and Coatings Technology, 193(1), pp. 319-324.

25. Conrads, H., and Schmidt, M. (2000): Plasma generation and plasma sources, Plasma Sources Science and Technology, 9(4), pp. 441-454.

26. Crawford, R. (1998): Plastics engineering, Third Edition, Amsterdam, Elsevier.

27. Deltombe, R., Kubiak, K.J., and Bigerelle, M. (2014): How to select the most relevant 3D roughness parameters of a surface, Scanning, 36(1), pp. 150-160.

28. Deryagin, B.V., Krotova, N.A., and Smilga, V.D.P. (1978): Adhesion of solids, New York, Consultant Bureau.

29. DIN EN 1465 (2009): Adhesives, Determination of tensile lap-shear strength of bonded assemblies; German version EN 1465.

30. DIN 50322 VI category (1986): Wear, Classification of categories in wear testing.

31. Dixon, D. and Meenan, B.J. (2012): Atmospheric dielectric barrier discharge treatments of polyethylene, polypropylene, polystyrene and poly (ethylene terephthalate) for enhanced adhesion, Journal of Adhesion Science and Technology, 26(20-21), pp. 2325-2337.

32. Doren, A., Genet, M.J., and Rouxhet, P.G. (1994): Analysis of poly (ethylene terephthalate) (PET) by XPS, Surface Science Spectra, 3(4), pp. 337-341.

33. Dupre´, A. (1869): The´orie me´canique de lachaleur, Paris, Gauthier-Villars, (in French).

34. Duran, M., Massines, F., Teyssedre, G., and Laurent, C. (2001): Luminescence of plasma-treated polymer surfaces at ambient temperature, Surface and Coatings Technology, 142, pp. 743-747.

35. Ebnesajjad, S., and Ebnesajjad, C. (2015): Surface treatment of fluoropolymers for adhesion, Chapter No 17 of Fluoroplastics, Second Edition, Amsterdam, Elsevier, pp. 564-588.

36. Esena, P., Riccardi, C., Zanini, S., Tontini, M., Poletti, G., and Orsini, F. (2005): Surface modification of PET film by a DBD device at atmospheric pressure, Surface and Coatings Technology, 200(1), pp. 664-667.

37. Evans, S., Pritchard, R.G., and Thomas, J.M. (1978): Relative differential subshell photoionisation cross-sections (MgKα) from lithium to uranium, Journal of Electron Spectroscopy and Related Phenomena, 14(5), pp. 341-358.

38. Field, J. (2008): David Tabor. 23 October 1913 - 26 November 2005, Biographical Memoirs of Fellows of The Royal Society, 54, pp. 425-459.

39. Flom, D.G., and Porile, N.T. (1955): Effects of temperature and high-speed sliding on the friction of 'Teflon'on 'Teflon', Nature, 175(4459). pp. 682–705.

40. Fort Jr, T. (1962): Adsorption and boundary friction on polymer surfaces, The Journal of Physical Chemistry, 66(6), pp. 1136-1143.

41. Fourche, G. (1995): An overview of the basic aspects of polymer adhesion, Part I: Fundamentals, Polymer Engineering and Science, 35 (12), pp. 957–967.

42. Frank, A, and Biederbick, K. (1984): Kunststoff kompendium, Wurzburg, Vogel-Buchverlag (in Germany).

43. Gotoh, K., Kobayashi, Y., Yasukawa, A., and Ishigami, Y. (2012): Surface modification of PET films by atmospheric pressure plasma exposure with three reactive gas sources, Colloid and Polymer Science, 290(11), pp. 1005-1014.

44. Gralben, N., and Olofsson, B. (1947): Measurement of friction between single fibers, Textile Research Journal, 17(9), pp. 488-496.

45. Griem, H. (1963): Validity of local thermal equilibrium in plasma spectroscopy, Physical Review, 131(3), pp. 1170–1176.

46. Grimblot, J., Mutel, B., Moineau, V., Colson, T., Dessaux, O., and Goudmand, P. (2000): Comparative study by XPS of nitrogen and oxygen implantation in different carbonaceous polymers using flowing nitrogen plasma, Surface and Interface Analysis, 30(1), pp. 415-419.

47. Hall, C. (1989): Polymer materials - an Introduction for technologists and scientists, Second Edition. New York, MacMillan Education Ltd.

48. Hegemann, D., Brunner, H., and Oehr, C. (2003): Plasma treatment of polymers for surface and adhesion improvement, Nuclear Instruments and Methods in Physics Research Section B: Beam Interactions with Materials and Atoms, 208, pp. 281-286.

49. Henkel: TDS Document Search, online at: http://tds.henkel.com/tds5/search.asp, accessed on 01 December, 2017.

50. Hutchinson, A.R., and Iglauer, S. (2006): Adhesion of construction sealants to polymer foam backer rod used in building construction, International Journal of Adhesion and Adhesives, 26(7), pp. 555-566.

51. Ionita, M.D., Teodorescu, M., Stancu, C., Stancu, E.C., Ionita, E.R., Moldovan, A., Acsente, T., Bazavan, M. and Dinescu, G. (2010): Surface modification of polymers at atmospheric pressure in expanding RF plasmas generated by planar dielectric barrier discharges, Journal of Optoelectronics and Advanced Materials, 12(3), pp. 777-782.

52. ISO 25178 (2012): Geometrical product specifications (GPS), Surface texture: Areal, Part 2: Terms, definitions and surface texture parameters.

53. ISO 527-1 (2012): Plastics-Determination of tensile Properties-Part 1: General principles.

54. Jost, P. (2017): Interview with Luminary Professor H. Peter Jost - The Man Who Gave Birth to the Word "Tribology". (N. C. Jim Fitch, Interviewer), online at: Machinerylubrication.com accessed on 24 May, 2017.

55. Kalácska, G., Zsidái, L., Kereszturi, K., Mohai, M., and Tóth, A. (2009): Sliding tribological properties of untreated and PIII-treated PETP, Applied Surface Science, 255(11), pp. 5847-5850.

56. Kalácska, G. (2013): An engineering approach to dry friction behaviour of numerous engineering plastics with respect to the mechanical properties, eXPRESS Polymer Letters ,7(2), pp. 199–210.

57. Kalácska, G., Károly, Z., Klébert, Sz., and András, E. (2015): NPIII treatment towards to cold atmospheric plasma as surface modification technics of engineering polymers, Scientific Bulletin Series C: Fascicle Mechanics, Tribology, Machine Manufacturing Technology, 29, pp. 51-56.

58. Kalácska, G., Keresztes, R., Földi, L., Klébert, Sz., Károly, Z., and Zsidai, L. (2016): Thermal conductivity of plasma modified polyethylene terephthalate and polyamide-6 layers, eXPRESS Polymer Letters, 10(5), p. 373.

59. Kalácska, G., Zsidai, L., Keresztes, R., Tóth, A., Mohai, M., and Szépvölgyi, J. (2012): Effect of nitrogen plasma immersion ion implantation of polyamide-6 on its sliding properties against steel surface, Wear, 290, pp. 66-73.

60. Kaplonek, W., and Lukianowicz, C. (2012): Coherence correlation interferometry in surface topography measurements, Chaper No 1 of Recent interferometry applications in topography and astronomy /ed. Padron, I./, Rijeka, Croatia, InTech, pp. 1-27.

61. Károly, Z., Klébert, Sz. (2015): Atmospheric cold plasma treatment for plastic surfaces, Workshop presentation, MTA TTK, Budapest.

62. Keresztes, R., Szakál, Z., Kári-Horváth, A., Pataki, T., and Sarankó, Á. (2016): Tensile behaviour of adhesive overlap joints with PP, UHMW-PE and PTFE polymers, Scientific Bulletin Series C: Fascicle Mechanics, Tribology, Machine Manufacturing Technology, 30, pp. 51-56.

63. Kereszturi, K., Tóth, A., Mohai, M., and Bertóti, I. (2008): Surface chemical and nanomechanical alterations in plasma immersion ion implanted PET, Surface and Interface Analysis, 40(3-4), pp. 664-667.

64. Kereszturi, K., Tóth, A., Mohai, M., Bertóti, I., and Szépvölgyi, J. (2010): Nitrogen plasma-based ion implantation of poly (tetrafluoroethylene): Effect of the main parameters on the surface properties, Applied Surface Science, 256(21), pp. 6385-6389.

65. King, R.F., and Tabor, D. (1953): The effect of temperature on the mechanical properties and the friction of plastics, Proceedings of The Physical Society, Section B, 66(9). pp. 728-737.

66. Kinloch, AJ. (1980): The science of adhesion: I. surface and interfacial aspects, Material Science, 15, pp. 2141–2166.

67. Kogelschatz, U. (2003): Dielectric-barrier discharges: their history, discharge physics, and industrial applications, Plasma Chemistry and Plasma Processing, 23(1), pp. 1-46.

68. Kostov, K.G., Hamia, Y.A.A., Mota, R.P., Dos Santos, A.L.R., and Nascente, P.A.P. (2014b): Treatment of polycarbonate by dielectric barrier discharge (DBD) at atmospheric pressure, Journal of Physics: Conference Series, 511(1), p. 012075.

69. Kostov, K.G., Nishime, T.M.C., Hein, L.R.O., and Tóth, A. (2013): Study of polypropylene surface modification by air dielectric barrier discharge operated at two different frequencies, Surface and Coatings Technology, 234, pp. 60-66.

70. Kostov, K.G., Nishime, T.M.C., Castro, A.H.R., Tóth, A., and Hein, L.R.D.O. (2014a): Surface modification of polymeric materials by cold atmospheric plasma jet, Applied Surface Science, 314, pp. 367-375.

71. Koutsos, V. (2009): Polymeric materials: an introduction, Chapter No 46 of ICE manual of Construction Materials: Vol. II: Fundamentals and theory; Concrete; Asphalts in Road Construction; Masonry, Thomas Telford Ltd, pp. 571-577.

72. Kovalev, A., Shulha, H., Lemieux, M., Myshkin, N., and Tsukruk, V.V. (2004): Nanomechanical probing of layered nanoscale polymer films with atomic force microscopy, Journal of Materials Research, 19(3), pp. 716-728.

73. Kragelskii, I. (1982): Friction and wear, Elmsford, Pergamon Press, pp. 458.

74. Kumar, A., and Gupta, R.K. (2003): Fundamentals of polymer engineering, Second Edition. New York, CRC Press.

75. Labay, C.P., Canal Arias, J.M., Navarro Sentanyes, A., and Canal Barnils, C. (2012): Comparison of the effects of corona and low pressure plasma on the release of caffeine from PA66 filaments, 51st Dornbirn Man-Made Fibers Congress Lectures CD, pp. 1-6.

76. Lancaster, J.K. (1968): Relationships between the wear of polymers and their mechanical properties, Proceedings of The Institution of Mechanical Engineers, Conference Proceedings, Sage UK: London, England: SAGE Publications, 183(16), pp. 98–106.

77. Lee, L.H. (1974): Effect of surface energetics on polymer friction and wear, Advances in Polymer Friction and Wear, 5, Boston, MA: Springer, pp. 31-68.

78. Leggett, G.J., and Beake, B.D. (1998): Development of surface morphology, local friction and adhesion in plasma treated poly (ethylene terephthalate) films, Polymer Preprints (USA), 39(2), pp. 1228-1229.

79. Lieberman, M.A., and Lichtenberg, A.J. (1994): Principles of plasma discharges and materials processing, MRS Bulletin, 30, pp. 899-901.

80. Liu, C., Brown, N.M., and Meenan, B.J. (2006): Uniformity analysis of dielectric barrier discharge (DBD) processed polyethylene terephthalate (PET) surface, Applied Surface Science, 252 (6), pp. 2297-2310.

81. Liu, C.Z., Wu, J.Q., Ren, L.Q., Tong, J., Li, J.Q., Cui, N., Brown, N.M.D. and Meenan, B.J. (2004): Comparative study on the effect of RF and DBD plasma treatment on PTFE surface modification, Materials Chemistry and Physics, 85(2), pp. 340-346.

82. Lopez, R., Sanchis, R., Garcia, D., Fenollar, O., and Balart, R. (2009): Surface characterization of hydrophilic coating obtained by low-pressure CH4-O2 plasma treatment on a polypropylene film, Journal of Applied Polymer Science, 111(6), pp. 2992-2997.

83. Louette, P., Bodino, F., and Pireaux, J.J. (2005): Poly (ether ether ketone) (PEEK) XPS reference core level and energy loss spectra, Surface Science Spectra, 12(1), pp. 149-153.

84. Ludema, K.C., and Tabor, D. (1966): The friction and visco-elastic properties of polymeric solids, Wear, 9(5), pp. 329-348.

85. Luo, H., Xiong, G., Ren, K., Raman, S.R., Liu, Z., Li, Q., Ma, C., Li, D. and Wan, Y. (2014): Air DBD plasma treatment on three-dimensional braided carbon fiber-reinforced PEEK composites for enhancement of in vitro bioactivity, Surface and Coatings Technology, 242, pp. 1-7.

86. Mandolfino, C., Lertora, E., Gambaro, C., and Bruno, M. (2014a): Improving adhesion performance of polyethylene surfaces by cold plasma treatment, Meccanica, 49(10), pp. 2299-2306.

87. Mandolfino, C., Lertora, E., and Gambaro, C. (2014b): Effect of cold plasma treatment on surface roughness and bonding strength of polymeric substrates, Key Engineering Materials, 611, pp. 1484-1493.

88. Mark, H. (1945): Molecular structure and mechanical properties of high polymers-a review, American Journal of Physics, 13(4), pp. 207-214.

89. Meyer, T., and Keurentjes, J. (2005): Handbook of polymer reaction engineering, Weinheim, Wiley-VCH Verlag GmbH & Co.

90. Milz. W.C., and Sargent, L.E. (1955): Frictional characteristic of plastics, Lubrication Engineering, 11(5), p. 313.

91. Mitchell, L. (2012): The fiction of nonfriction, Popular Science, 281 (5), p. 40.

92. Mohai, M. (2004): XPS MultiQuant: multimodel XPS quantification software, Surface and Interface Analysis, 36(8), pp. 828-832.

93. Moore, D.F. (1972): The friction and lubrication of elastomers, Oxford, Pergamon Press.

94. Myshkin, N.K., Kim, C.K., and Petrokovets, M.I. (1997): Introduction to tribology, Seoul, Cheong Moon Gak.

95. Myshkin, N.K., and Kovalev, A.V. (2009): Adhesion and friction of polymers, Chapter No 1 of Polymer Tribology /eds. Sinha, S.K. and Briscoe, J.B./, Singapore: Imperial College Press, pp. 2-37.

96. Myshkin, N.K., and Petrokovets, M.I. (2004): Mechanical behavior of plastics: surface properties and tribology, Chapter No 3 of Mechanical tribology, materials, characterization, and applications /eds. Totten G.E. and Liang H./, New York, Marcel Dekker, pp.57–94.

97. Myshkin, N.K., Petrokovets, M.I., and Kovalev, A.V. (2006): Tribology of polymers: adhesion, friction, wear, and mass-transfer, Tribology International, 38(11), pp. 910-921.

98. Naresh, K., N., Yap, S.L., Khan, M.Z., and Pattela Srinivasa, R.S. (2016): Effect of argon plasma treatment on tribological properties of UHMWPE/MWCNT nanocomposites, Polymers, 8(8), p. 295.

99. Nastuta, A.V., Rusu, G.B., Topala, I., Chiper, A.S., and Popa, G. (2008): Surface modifications of polymer induced by atmospheric DBD plasma in different configurations, Journal of Optoelectronics and Advanced Materials, 10(8), pp. 2038-2042.

100. Nishime, T.M.C., Tóth, A., Hein, L.R.O., and Kostov, K.G. (2012): Surface characteristics analysis of polypropylene treated by dielectric barrier discharge at atmospheric pressure, Journal of Physics: Conference Series, 370(1), p. 012025.

101. Noeske, M., Degenhardt, J., Strudthoff, S., and Lommatzsch, U. (2004): Plasma jet treatment of five polymers at atmospheric pressure: surface modifications and the relevance for adhesion, International Journal of Adhesion and Adhesives, 24(2), pp. 171-177.

102. Novák, I., Popelka, A., Luyt, A.S., Chehimi, M.M., Špírková, M., Janigová, I., Kleinová, A., Stopka, P., Šlouf, M., Vanko, V., Chodák, I., and Valentin M. (2013): Adhesive properties of polyester treated by cold plasma in oxygen and nitrogen atmospheres, Surface & Coatings Technology, 235, pp. 407–416.

103. Novák, I., Popelka, A., Valentín, M., Chodák, I., Špírková, M., Tóth, A., Kleinová, A., Sedliačik, J., Lehocký, M., and Marônek, M. (2014): Surface behavior of polyamide 6 modified by barrier plasma in oxygen and nitrogen, International Journal of Polymer Analysis and Characterization, 19(1), pp. 31-38.

104. Nptel: Thermoplastics and thermosets, A Project funded by MHRD, Govt. of India, online at: http://nptel.ac.in/courses/, accessed on 15 August, 2016.

105. Onsuratoom, S., Rujiravanit, R., Sreethawong, T., Tokura, S., and Chavadej, S. (2010): Silver loading on DBD plasma-modified woven PET surface for antimicrobial property improvement, Plasma Chemistry and Plasma Processing, 30(1), pp. 191-206.

106. Owens, D.K., and Wendt, R.C. (1969): Estimation of the surface free energy of polymers, Journal of Applied Polymer Science, 13(8), pp. 1741-1747.

107. Pandiyaraj, K.N., Selvarajan, V., Deshmukh, R.R., and Gao, C. (2008): Adhesive properties of polypropylene (PP) and polyethylene terephthalate (PET) film surfaces treated by DC glow discharge plasma, Vacuum, 83(2), pp. 332-339.

108. Pandiyaraj, K.K. (2016): Effect of cold atmospheric pressure plasma gas composition on the surface and cyto-compatible properties of low density polyethylene (LDPE) films, Current Applied Physics, 16(7), pp. 784-792.

109. Perni, S., Kong, M.G., and Prokopovich, P. (2012): Cold atmospheric pressure gas plasma enhances the wear performance of ultra-high molecular weight polyethylene, Acta Biomaterialia, 8(3), pp. 1357-1365.

110. Petrokovets, M.I. (1999): Effect of temperature on real contact area of rough surfaces, Journal of Friction and Wear, 20 (2), pp. 1-6.

111. Pijpers, A.P., and Meier, R.J. (2001): Adhesion behaviour of polypropylenes after flame treatment determined by XPS (ESCA) spectral analysis, Journal of Electron Spectroscopy and Related Phenomena, 121(1), pp. 299-313.

112. Poisson, C., Hervais, V., Lacrampe, M.F., and Krawczak, P. (2006): Optimization of PE/binder/PA extrusion blow-molded films. II. Adhesion properties improvement using binder/EVA blends, Journal of Applied Polymer Science, 101(1), pp. 118-127.

113. Prat, R., Koh, Y.J., Babukutty, Y., Kogoma, M., Okazaki, S., and Kodama, M. (2000): Polymer deposition using atmospheric pressure plasma glow (APG) discharge, Polymer, 41(20), pp. 7355-7360.

114. Pratt, G.C. (1986): Bearing materials, Encyclopedia of materials science and engineering /ed. Bever, M.B./, Oxford, Pergamon Press, pp. 281-288.

115. Preedy, E.C., Brousseau, E., Evans, S.L., Perni, S., and Prokopovich, P. (2014): Adhesive forces and surface properties of cold gas plasma treated UHMWPE, Colloids and Surfaces A: Physicochemical and Engineering Aspects, 460, pp. 83-89.

116. Pukánszky, B., and Fekete, E. (1999): Adhesion and surface modification, Mineral Fillers in Thermoplastics I /eds. Jancar, J., Fekete, E., Hornsby, P.R., Jancar J., Pukánszky, B., and Rothon, R.N /, Springer, Berlin, Heidelberg, pp. 109-153.

117. Qin, R.Y., and Schreiber, H.P. (1999): Adhesion at partially restructured polymer surfaces, Colloids and Surfaces A: Physicochemical and Engineering Aspects, 156(1), pp. 85-93.

118. Rashed, U.M., Ahmed, H., Al-Halwagy, A., and Garamoon, A.A. (2009): Surface characteristics and printing properties of PET fabric treated by atmospheric dielectric barrier discharge plasma, The European Physical Journal-Applied Physics, 45(1). pp. 11001.

119. Rees, B. (1957): Static friction of bulk polymers over a temperature range, Research, 10, pp. 331-338.

120. Reilman, R.F., Msezane, A., and Manson, S.T. (1976): Relative intensities in photoelectron spectroscopy of atoms and molecules, Journal of Electron Spectroscopy and Related Phenomena, 8(5), pp. 389-394.

121. Sagbas, B. (2016): Effect of argon plasma surface modification on tribological behavior of biopolymers, Industrial Lubrication and Tribology, 68(4), pp. 508-514.

122. Sakai, O., Kishimoto, Y., and Tachibana, K. (2005): Integrated coaxial-hollow micro dielectric-barrier-discharges for a large-area plasma source operating at around atmospheric pressure, Journal of Physics D: Applied Physics, 38(3), pp. 431-441.

123. Salapare, H.S., Guittard, F., Noblin, X., de Givenchy, E.T., Celestini, F., and Ramos, H.J. (2013): Stability of the hydrophilic and superhydrophobic properties of oxygen plasma-treated poly (tetrafluoroethylene) surfaces, Journal of Colloid and Interface Science, 396, pp. 287-292.

124. Samad, M.A., Satyanarayana, N., and Sinha, S.K. (2010): Tribology of UHMWPE film on air-plasma treated tool steel and the effect of PFPE overcoat, Surface and Coatings Technology, 204(9), pp. 1330-1338.

125. Samyn, P., Quintelier, J., Ost, W., De Baets, P., and Schoukens, G. (2005): Sliding behaviour of pure polyester and polyester-PTFE filled bulk composites in overload conditions, Polymer Testing, 24(5), pp. 588-603.

126. Samyn, P., Craenenbroeck, J.V., Quintelier, J., Schoukens, G. (2006): Friction induced conformational changes on large-scale and small-scale polyester sliding surfaces, Surface and Interface Analysis, 38(4), pp. 868-872.

127. Sargent, J.P. (2005): Durability studies for aerospace applications using peel and wedge tests, International Journal of Adhesion and Adhesives, 25 (3), pp. 247–256.

128. Schäfer, J., Hofmann, T., Holtmannspötter, J., Frauenhofer, M., von Czarnecki, J., and Gudladt, H. J. (2015): Atmospheric-pressure plasma treatment of polyamide 6 composites for bonding with polyurethane, Journal of Adhesion Science and Technology, 29(17), pp. 1807-1819.

129. Schallamach, A. (1952). The load dependence of rubber friction, Proceedings of The Physical Society B, 65 (393), pp. 658-661.

130. Schallamach, A. (1953): The velocity and temperature dependence of rubber friction, Proceedings of The Physical Society B, 66(5), pp. 386-393.

131. Segu, D.Z. (2016): NBR surface modification by Ar plasma and its tribological properties, Industrial Lubrication and Tribology, 68(2), pp. 227-232.

132. Sęk, D. (1988): Structural variations of liquid crystalline polymer macromolecules. Review, Acta Polymerica, 39(11), pp. 599-607.

133. Shooter, K.V., and Tabor, D. (1952): The frictional properties of plastics, Proceedings of The Physical Society, Section B, 65(9), pp. 661-672.

134. Shooter, K.V., and Thomas, P.H. (1949): Frictional properties of some plastics, Research, Journal of Science and Its Applications, 2(11), pp. 533-539.

135. Šimor, M., Ráhel', J., Vojtek, P., Černák, M., and Brablec, A. (2002): Atmospheric-pressure diffuse coplanar surface discharge for surface treatments, Applied Physics Letters, 81(15), pp. 2716-2718.

136. Singer, I.L., and Pollock, H. (2012): Fundamentals of friction: macroscopic and microscopic processes, Vol. 220, Braunlage, Harz, Germany, Springer Science & Business Media.

137. Slepička, P., Michaljaničová, I., and Švorčík, V. (2013): Controlled biopolymer roughness induced by plasma and excimer laser treatment, eXPRESS Polymer Letters, 7(11), pp. 950-958.

138. Takahashi, T., Hirano, Y., Takasawa, Y., Gowa, T., Fukutake, N., Oshima, A., Tagawa, S., and Washio, M. (2011): Change in surface morphology of polytetrafluoroethylene by reactive ion etching, Radiation Physics and Chemistry, 80(2), pp. 253-256.

139. Tanaka, K. (1984): Kinetic friction and dynamic elastic contact behaviour of polymers, Wear, 100 (1–3), pp. 243-262.

140. Tendero, C., Tixier, C., Tristant, P., Desmaison, J., and Leprince, P. (2006): Atmospheric pressure plasmas: A review, Spectrochimica Acta Part B: Atomic Spectroscopy, 61(1), pp. 2-30.

141. Thai Polymer supply: plastics-engineering, online at: http://www.thaipolymer.co.th/plastics/plastics-engineering.html, accessed on: 15 May, 2017.

142. Toshifuji, J., Katsumata, T., Takikawa, H., Sakakibara, T., and Shimizu, I. (2003): Cold arc-plasma jet under atmospheric pressure for surface modification, Surface and Coatings Technology, 171(1), pp. 302-306.

143. Tosun, K., Felekoğlu, B., and Baradan, B. (2012): Multiple cracking response of plasma treated polyethylene fiber reinforced cementitious composites under flexural loading, Cement and Concrete Composites, 34(4), pp. 508-520.

144. Tóth, A., Bertóti, I., Szilágyi, E., Dong, H., Bell, T., Juhász, A., and Nagy, P. M. (2000): Surface characterisation of ultra-high molecular weight polyethylene after nitrogen ion-implantation, Surface and Interface Analysis, 30(1), pp. 434-438.

145. Tóth, A., Mohai, M., Ujvári, T., and Bertóti, I. (2006a): Hydrogen plasma immersion ion implantation of ultra-high molecular weight polyethylene, Surface and Interface Analysis, 38(4), pp. 898-902.

146. Tóth, A., Mohai, M., Ujvári, T., and Bertóti, I. (2006b): Advanced surface modification of ultra-high molecular weight poly(ethylene) by helium plasma immersion ion implantation, Polymers for Advanced Technologies, 17(11-12), pp. 898-901.

147. Tóth, A., Bertóti, I., Mohai, M., and Ujvári, T. (2007): Surface modification of polyethylene by nitrogen PIII: Surface chemical and nanomechanical properties, Materials Science Forum, 537, pp. 255-262.

148. Tóth, A., Kereszturi, K., Mohai, M., and Bertóti, I. (2010): Plasma based ion implantation of engineering polymers, Surface and Coatings Technology, 204(18), pp. 2898-2908.

149. Tsuchiya, Y., Akutu, K., and Iwata, A. (1998): Surface modification of polymeric materials by atmospheric plasma treatment, Progress in Organic Coatings, 34(1), pp. 100-107.

150. Tutorvista: Polyethylene Terephthalate, online at: http://chemistry.tutorvista.com/analytical-chemistry/polyethylene-terephthalate.html, accessed on11 Jun, 2017.

151. Upadhyay, D.J., Cui, N.Y., Anderson, C.A., and Brown, N.M.D. (2005b): Surface recovery and degradation of air dielectric barrier discharge processed poly (methyl methacrylate) and poly (ether ether ketone) films, Polymer Degradation and Stability, 87(1). pp. 33-41.

152. Upadhyay, D.J., Cui, N.Y., Meenan, B.J., and Brown, N.M.D. (2005a): The effect of dielectric barrier discharge configuration on the surface modification of aromatic polymers, Journal of Physics D: Applied Physics, 38(6), pp. 922-929.

153. Van Deynse, A., Morent, R., and De Geyter, N. (2016): Surface modification of polymers using atmospheric pressure cold plasma technology, Polymer science: research advances, pratical applications and educational aspects / eds. Méndez-Vilas, A., Solano, A./, Formatex Research Center, pp. 506-516.

154. Vinogradov, G.V., Bartenev, G.M., El'Kin, A.I., and Mikhaylov, V.K. (1970): Effect of temperature on friction and adhesion of crystalline polymers, Wear, 16(3), pp. 213-219.

155. Wake, W.C. (1976): Adhesion and the formulation of adhesives, London, Applied Science Publishers Ltd.

156. Wei, Q.F., Gao, W.D., Hou, D.Y., and Wang, X.Q. (2005): Surface modification of polymer nanofibres by plasma treatment, Applied Surface Science, 245(1), pp. 16-20.

157. White, N.S. (1956): Small oil-free bearings, Journal of Research of The National Bureau of Standards, 57(4), pp. 185-205.

158. Wikipedia: Polymer, online at: https://en.wikipedia.org/wiki/Polymer, accessed on 05 May, 2017.

159. Wikipedia: Tribology, online at: https://en.wikipedia.org/wiki/Tribology#cite_note-12017, accessed on 27 May, 2017.

160. Williams, T.S., Yu, H., and Hicks, R.F. (2013): Atmospheric pressure plasma activation of polymers and composites for adhesive bonding, Reviews of Adhesion and Adhesives, 1(1), pp. 46-87.

161. Wilson, A., Jones, I., Salamat-Zadeh, F., and Watts, J.F. (2015): Laser surface modification of poly (etheretherketone) to enhance surface free energy; wettability and adhesion, International Journal of Adhesion and Adhesives, 62, pp. 69-77.

162. Wolf, R., and Sparavigna, A.C. (2010): Role of plasma surface treatments on wetting and adhesion, Engineering, 2(06). pp. 397-402.

163. Yamaguchi, Y. (1990): Tribology of plastic materials: their characteristics and applications to sliding components, Vol. 16, Tokyo, Japan, Elsevier.

164. Yeh, J.T., Lai, Y.C., Suen, M.C., and Chen, C.C. (2011): An improvement on the adhesion-strength of laminated ultra-high-molecular-weight polyethylene fabrics: surface-etching/modification using highly effective, Polymers for Advanced Technologies, 22(12), pp. 1971-1981.

165. ZEISS: ZEISS EVO Scanning Electron Microscope, online at: https://www.zeiss.com/microscopy/int/products/scanning-electron-microscopes/evo.html, accessed on 28 October, 2017.

166. Zhang, R., Häger, A.M., Friedrich, K., Song, Q., and Dong, Q. (1995): Study on tribological behaviour of plasma-treated PEEK and its composites, Wear, 181, pp. 613-623.

167. Zhang, S., Awaja, F., James, N., McKenzie, D.R., and Ruys, A.J. (2011): A comparison of the strength of autohesion of plasma treated amorphous and semi-crystalline PEEK films, Polymers for Advanced Technologies, 22(12), pp. 2496-2502.

168. Zsidái, L., De Baets, P., Samyn, P., Kalacska, G., Van Peteghem, A.P., and Van Parys, F. (2002): The tribological behaviour of engineering plastics during sliding friction investigated with small-scale specimens, Wear, 253, pp. 673-688.

A2: Publications related to the dissertation

Refereed papers in foreign languages:

1. **Al-Maliki, H.**, Kalácska, G., Keresztes, P., and De Baets, P. (2015): Adhesion of polymer surfaces: brief review, Mechanical Engineering Letters, SZIE, 12, pp. 43-49.
2. **Al-Maliki, H.**, Zsidai, L., Keresztes, R., and Kalácska, G. (2016): Shear strength of polypropylene bonded joints using pristine and DBD plasma treated surface, Mechanical Engineering Letters, SZIE, 14, pp. 71-77.
3. Károly, Z., Klébert, Sz., **Al-Maliki, H.**, and Pataki, T. (2016): Comparison of NPIII and DBD plasma treatment in terms of wettability of PTFE and PA6, Scientific Bulletin Series C: Fascicle Mechanics, Tribology, Machine Manufacturing Technology, 30, pp. 47-50.
4. Szakál, Z., Zsidai, L., **Al-Maliki**, **H.**, Odrobina, M., and Kári-Horváth, A. (2016): Shear strength behaviour of adhesive bonded polymer and steel surfaces, Scientific Bulletin Series C: Fascicle Mechanics, Tribology, Machine Manufacturing Technology, 30, pp. 110-115.
5. **Al-Maliki, H.**, Zsidai, L., Samyn, P., Szakál, Z., Keresztes, R., and Kalácska, G. (2017): Effects of atmospheric plasma treatment on adhesion and tribology of aromatic thermoplastic polymers, Polymer Engineering & Science. (IF= 1.449*). DOI: 10.1002/pen.24689
6. **Al-Maliki, H., and** Kalácska, G. (2017): Friction behavior of engineering polymers treated by atmospheric DBD plasma, Periodica Polytechnica Mechanical Engineering, 61(4), pp. 303-308.
7. **Al-Maliki, H., and** Kalácska, G. (2017): The effect of atmospheric DBD plasma on Surface energy and shear strength of adhesively bonded polymer, Hungarian Agriculture Engineering, 31, pp. 52-58.
8. Sukumaran, J., Keresztes, R., Kalácska, G., **Al-Maliki, H**., Neis, P. D., and De Baets, P. (2017): Extruded and injection moulded virgin PA 6/6 as abrasion resistant material, Advances in Tribology, 2017.
9. **Al-Maliki, H.,** Károly, Z., and Klébert, Sz. (2017): Surface morphology and chemical composition of PP and PETP treated by atmospheric plasma, Mechanical Engineering Letters, SZIE,15, pp. 47-55.
10. **Al-Maliki, H.**, Kalacska, A., & Sukumaran, J. (2017): 3D Topographical evaluation by using the coherence correlation interferometry (CCI) technique for engineering polymers treated by DBD plasma, Scientific Bulletin Series C: Fascicle Mechanics, Tribology, Machine Manufacturing Technology, 31, 2-6.
11. **Al-Maliki, H.,** and Kalácska, G. (2018): Tribological behaviour of polymers in term of plasma treatment: A brief review, Hungarian Journal of Industry and Chemistry. (Accepted).

12. **Al-Maliki, H.,** Károly, Z., Klébert, Sz., and Kalácska, G. (2018): Surface characterization of Polytetrafluoroethylene treated by atmospheric plasma, International Review of Applied Sciences and Engineering, 09(1). (Accepted).

Refereed papers in Hungarian language:

13. Szakál, Z., Al-Maliki, H., Odrobina, M., és Sarankó, Á. (2016): Extrudált PA6 és POM C lemezanyagok ragasztott kötésének nyíróvizsgálata, Műanyagipari Szemle, 1-10, o.

International conference proceedings:

14. **Al-Maliki, H.**, Zsidai, L., Keresztes R., Kalácska, G., and Szakál Z. (2016): Friction tests of different polymers treated with plasma technology, 4th International scientific conference on advances in mechanical engineering (ISCAME 2016), Debrecen, Hungary, October 13-15, 2016, pp. 211-216.
15. Zsidai, L., **Al-Maliki, H.**, Odrobina M., and Kári-Horváth A. (2016): Strength behaviour of joint polymer and steel surfaces with different adhesive materials, The 11th International conference of the Carpathian Euro-Region specialists in industrial systems (CEurSIS 2016), Baia Mare, Romania, June 2-4, 2016, pp. 165-170.
16. Károly, Z., Klébert, Sz., **Al-Maliki, H.**, and Pataki, T. (2016): Comparison of NPIII and DBD plasma in term of wettability of PTFE and PA6, The 11th International conference of the Carpathian Euro-Region specialists in industrial systems (CEurSIS 2016), Baia Mare, Romania, June 2-4, 2016, pp. 85-88.
17. **Al-Maliki, H.,** Károly, Z., Klébert, Sz., and Kalácska, G. Sukumaran, J., Kalácska A. (2017): Surface characterization of Polytetrafluoroethylene treated by atmospheric plasma, 5th International scientific conference on advances in mechanical engineering (ISCAME 2017), Debrecen, Hungary, October 12-14, 2017, pp. 1-8.
18. **Al-Maliki, H.**, Kalácska, G., and Sukumaran, J. (2017): 3D Topographical evaluation by using the coherence correlation interferometry (CCI) technique for engineering polymers treated by DBD plasma, 12th International multidisciplinary conference, Baia Mare-Nyíregyháza, Romania-Hungary, May 24-26, 2017. pp. 7-11.

International conference abstracts:

19. **Al-Maliki, H.**, Kalácska, G., Keresztes, R., and De Baets, P. (2015): Adhesion of polymer surfaces: brief review, IV. Synergy international conferences-engineering, Agriculture and green industry innovation, Gödöllő, Hungary, October 12-15, 2015, p. 100.
20. **Al-Maliki, H.,** Sukumaran, J., Kalácska, A., and Kalácska, G. (2017): Influence of atmospheric DBD plasma on 3D topography of polymers: 2nd Danube Vltava Sava polymer meeting, Vienna, Austria (DVSPM 2017), September 5-8, 2017, PO-31.
21. **Al-Maliki, H.,** Károly, Z., and Klébert, Sz. (2017): Surface morphology and chemical composition of PP and PETP treated by atmospheric plasma, V. Synergy international conferences-engineering, Agriculture and green industry innovation, Gödöllő, Hungary, October 16-19, 2017, p. 49.

A3: Early stage of surface energy investigations

Table 8.1. Surface energy of prisine polymer surfaces and its changes with the plasma treatment time

Sample	θ_w **(deg)**	θ_{CH2I2} **(deg)**	γ_{pol} **(mJ/m^2)**	γ_{disp} **(mJ/m^2)**	γ_{tot} **(mJ/m^2)**
PEEK-Untreated	70±1.5	30±6.4	6.1	44.3	50.4
0.5 min	30±3.4	32±1.8	26.5	43.5	70
1 min	24±2.7	17±2.1	26.4	48.8	75.1
2 min	28±0.6	26±1.1	26.1	46	72.1
3 min	29±2.2	29±3	26.4	44.9	71.3
PET-Untreated	71±3.3	32±3.1	6.1	43.4	49.5
0.5 min	33±3.1	20±0.5	23.4	47.8	71.1
1 min	33±1.3	18±2.2	23.0	48.3	71.3
2 min	26±1.2	21±2.3	26.4	47.4	73.8
3 min	30±2.7	24±0	25.3	46.6	71.9
PA6-Untreated	70±7.2	32±2.1	6.3	43.6	50.0
0.5 min	28±4.1	25±2.6	26.1	46.2	72.3
1 min	26±1	28±2.3	27.6	45	72.6
2 min	23±1.6	29±2.1	28.9	44.8	73.7
3 min	21±0.5	26±1.5	29.1	45.8	74.9
POM-Untreated	73±4.2	32±2.1	5.2	43.6	48.8
0.5 min	41±4.6	16±3.6	18.9	48.9	67.8
1 min	44±5.5	20±1.3	17.8	47.9	65.8
2 min	45±1.2	22±1.7	17.6	47.3	64.9
3 min	43±4.2	20±3.2	18.2	48	66.1
PP-Untreated	101±6.9	52±2.6	0.1	33.4	33.5
0.5 min	71±2.1	50±3.7	8.3	34.3	42.6
1 min	61±3.8	48±4.5	13.4	35.7	49.1
2 min	53±2.2	49±5.4	18.2	35.1	53.1
3 min	57±4.7	34±0	13	42.6	55.5
UHMW-PE-Untreated	74±4.3	42±3.9	5.9	38.5	44.4
0.5 min	44±1	25±1.2	18.4	46.2	64.6
1 min	43±1.7	30±4.6	19.7	44.4	64.1
2 min	44±2.2	33±2.5	19.6	42.9	62.5
3 min	44±2.1	25±3.9	18.2	46.4	64.6
PTFE-Untreated	108±1.5	73±3.2	0.2	21.2	21.5
0.5 min	101±3.4	73±4.6	1.2	21.1	22.4
1 min	105±2.5	62±3.9	0.1	27.6	27.7
2 min	91±3.1	64±3.6	2.7	26.5	29.3
3 min	75±1	56±1	7.5	30.9	38.4

A4: Adhesive bonding test results

The original measurement data of adhesive bonding tests is reviewed in this section. Where F (N) is the average of five force measurmets, F is the force deviation, σ % is the percentage of force deviation, and T (Mpa) is the avarage of shear strength.

Engineering polymers

Table 8.2. Adhesive bonding measurements for PEEK

Pair and adhesive type	F (N)	F	σ %	T (MPa)
0_PEEK_PEEK_406_00	633	137	22	1.99
0_PEEK_PEEK_9466_00	374	89	24	1.18
0_PEEK_PEEK_330_00	635	63	10	2
0_PEEK_S235_406_00	1137	124	11	3.58
0_PEEK_S235_9466_00	748	182	24	2.36
0_PEEK_S235_330_00	1133	133	12	3.57
1_PEEK_PEEK_406_00	2658	29	1	8.37
1_PEEK_PEEK_9466_00	4276	44	1	13.47
1_PEEK_PEEK_330_00	2239	35	2	7.05
1_PEEK_S235_406_00	4055	82	2	12.77
1_PEEK_S235_9466_00	4457	46	1	14.04
1_PEEK_S235_330_00	2868	20	1	9.03

Table 8.3. Adhesive bonding measurements for PET

Pair and adhesive type	F (N)	F	σ %	T (MPa)
0_PETP_PETP_406_00	2254	114	5	7.1
0_PETP_PETP_9466_00	298	3	1	0.94
0_PETP_PETP_330_00	372	16	4	1.17
0_PETP_S235_406_00	1913	34	2	6.03
0_PETP_S235_9466_00	1324	106	8	4.17
0_PETP_S235_330_00	927	69	8	2.92
1_PETP_PETP_406_00	2793	36	1	8.8
1_PETP_PETP_9466_00	2020	21	1	6.36
1_PETP_PETP_330_00	2153	25	1	6.78
1_PETP_S235_406_00	2896	82	3	9.12
1_PETP_S235_9466_00	3425	136	4	10.79
1_PETP_S235_330_00	2512	19	1	7.91

Table 8.4. Adhesive bonding measurements for PA6-E

Pair and adhesive type	F (N)	F	σ %	T (MPa)
0_PA6-E_PA6-E_406_00	1193	107	9	3.76
0_PA6-E_PA6-E_9466_00	249	25	10	0.78
0_PA6-E_PA6-E_330_00	701	64	9	2.21
0_PA6-E_S235_406_00	985	24	2	3.1
0_PA6-E_S235_9466_00	877	77	9	2.76
0_PA6-E_S235_330_00	1077	83	8	3.39
1_PA6-E_PA6-E_406_00	1241	77	6	3.91
1_PA6-E_PA6-E_9466_00	420	20	5	1.32
1_PA6-E_PA6-E_330_00	1458	48	3	4.59
1_PA6-E_S235E_406_00	1314	31	2	4.14
1_PA6-E_S235E_9466_00	1335	40	3	4.2
1_PA6-E_S235_330_00	2321	70	3	7.31

Table 8.5. Adhesive bonding measurements for POM-C

Pair and adhesive type	F (N)	F	σ %	T (MPa)
0_POM-C_POM-C_406_00	682	27	4	2.15
0_POM-C_POM-C_9466_00	181	13	7	0.57
0_POM-C_POM-C_330_00	414	20	5	1.3
0_POM-C_S235_406_00	634	83	5	2
0_POM-C_S235_9466_00	877	77	9	2.76
0_POM-C_S235_330_00	464	33	7	1.46
1_POM-C_POM-C_406_00	702	50	7	2.21
1_POM-C_POM-C_9466_00	1210	12	5	3.81
1_POM-C_POM-C_330_00	418	33	8	1.32
1_POM-C_S235_406_00	720	13	6	2.27
1_POM-C_S235_9466_00	2378	24	1	7.49
1_POM-C_S235_330_00	780	20	1	2.46

Polyolefin polymers and PTFE

Table 8.6. Adhesive bonding measurements for PP

Pair and adhesive type	F (N)	F	σ %	T (MPa)
0_PP_PP_406_11	1312	194	15	4.13
0_PP_S235_406_10	1473	121	8	4.64
0_PP_PP_3035_00	1032	20	2	3.25
0_PP_S235_3035_00	1091	21	2	3.44
1_PP_PP_406_11	1588	21	1	5
1_PP_S235_406_10	1713	16	1	5.4
1_PP_PP_3035_00	1370	35	3	4.31
1_PP_S235_3035_00	1217	17	1	3.83

Table 8.7. Adhesive bonding measurements for UHMW-PE HD500

Pair and adhesive type	F (N)	F	σ %	T (MPa)
0_PE HD500_PE HD500_406_11	1158	88	8	3.65
0_PE HD500_S235_406_10	967	31	3	3.05
0_PE HD500_PE HD500_3035_00	790	64	8	2.49
0_PE HD500_S235_3035_00	810	56	7	2.55
1_PE HD500_PE HD500_406_11	1182	11	1	3.72
1_PE HD500_S235_406_10	1265	21	2	3.98
1_PE HD500_PE HD500_3035_00	1201	16	1	3.78
1_PE HD500_S235_3035_00	1234	12	1	3.89

Table 8.8. Adhesive bonding measurements for UHMW-PE HD1000

Pair and adhesive type	F (N)	F	σ %	T (MPa)
0_PE HD1000_PE HD1000_406_11	519	34	7	1.63
0_PE HD1000_S235_406_10	1056	21	2	3.33
0_PE HD1000_S235_3035_00	855	7	1	2.1
0_PE HD1000_S235_3035_00	855	7	1	2.69
1_PE HD1000_PE HD1000_406_11	968	17	2	3.05
1_PE HD1000_S235_406_10	1067	16	2	3.36
1_PE HD1000_PE HD1000_3035_00	934	12	1	2.94
1_PE HD1000_S235_3035_00	904	7	1	2.85

Table 8.9. Adhesive bonding measurements for PTFE

Pair and adhesive type	**F (N)**	**F**	**σ %**	**T (MPa)**
0_PTFE_PTFE_406_11	488	31	6	1.54
0_PTFE_S235_406_10	521	47	9	1.64
0_PTFE_PTFE_3035_00	295	14	5	0.93
0_PTFE_S235_3035_00	533	48	9	1.68
1_PTFE_PTFE_406_11	495	9	2	1.56
1_PTFE_S235_406_10	524	16	3	1.65
1_PTFE_PTFE_3035_00	323	8	2	1.02
1_PTFE_S235_3035_00	535	10	2	1.69

9. ACKNOWLEDGEMENTS

This PhD work has been accomplished at Institute for Mechanical Engineering Technology, Faculty of Mechanical Engineering, Szent István University- Gödöllő, between February 2015 and July 2018.

The PhD program including the present research is supported by Stipendium Hungaricum Scholarship Program. Further, the experimental tests financially supported by OTKA K 113039(NKFIH).

I would like to acknowledge my most profound gratitude to my supervisors Prof. Dr. Gábor Kalácska for his valuable recommendations, advice, excellent guidance and continuous encouragement during my PhD research. This dissertation would not have been possible without his considerable academic support and it was my pleasure to work under his supervision and learn the sober scientific research ways. Additionally, I desire to extend my sincere gratitude to all the team of Institute for Mechanical Engineering Technology, especially thanks for prof. Dr. László Zsidai, prof. Dr. Zoltán Szakál, prof. Dr. Róbert Keresztes for their valuable help, in the laboratory and provide data, throughout my research.

In addition, I would like to express my thanks and gratitude to the head of Doctoral School of Mechanical Engineering prof. Dr. István Farkas for his valuable advice and fatherly dealing throughout my research years which has dramatically contributed to facilitate the completion of the doctoral degree.

Many thanks to Institute of Materials and Environmental Chemistry (AKI), Hungarian Academy of Sciences (MTA) for experimental support of plasma generating and surface characterisation measurements. Especially acknowledge for Dr. Szilvia Klébert and Dr. Zoltán Károly.

The surface 3D topography measurements were carried out in co-operation with University of Ghent, Department of Mechanical Construction and Production, Soete Laboratory with individual help and support from Adam Kalácska and Dr. Jacob Sukumaran.

My thanks go to Dr. Pieter Samyn from Hasselt University, Applied and Analytical Chemistry Research Group for his help in the relative publications to the present dissertation.

This scientific work is dedicated to my family, in particular, my father Lateef Radhi and my mother Khalidah Sabri for their financial and moral support.

Hayder Lateef Radhi Al-Maliki

Gödöllő, 2018